Characterization and Modeling of a Fiber-Reinforced Polymeric Composite Structural Beam and Bridge Structure for Use in the Tom's Creek Bridge Rehabilitation Project

by

Michael David Hayes

Thesis submitted to the Faculty of the

Virginia Polytechnic Institute and State University

in partial fulfillment of the requirements for the degree of

Master of Science

in

Engineering Mechanics

John J. Lesko, Chair

Richard E. Weyers

Brian J. Love

February 6, 1998

Blacksburg, Virginia

Keywords: Composite materials, fiber-reinforced polymer (FRP), hybrid composite beam, pultruded structural shapes, pultruded composites, bridge rehabilitation, shear deformation

Characterization and Modeling of a Fiber-Reinforced Polymeric Composite Structural Beam and Bridge Structure for Use in the Tom's Creek Bridge Rehabilitation Project

Michael D. Hayes

(ABSTRACT)

Fiber reinforced polymeric (FRP) composite materials are beginning to find use in construction and infrastructure applications. Composite members may potentially provide more durable replacements for steel and concrete in primary and secondary bridge structures, but the experience with composites in these applications is minimal. Recently, however, a number of groups in the United States have constructed short-span traffic bridges utilizing FRP members. These demonstration cases will facilitate the development of design guidelines and durability data for FRP materials. The Tom's Creek Bridge rehabilitation is one such project that utilizes a hybrid FRP composite beam in an actual field application.

This thesis details much of the experimental work conducted in conjunction with the Tom's Creek Bridge rehabilitation. All of the composite beams used in the rehabilitation were first proof tested in four-point bending. A mock-up of the bridge was then constructed in the laboratory using the actual FRP beams and timber decking. The mock-up was tested in several static loading schemes to evaluate the bridge response under HS20 loading. The lab testing indicated a deflection criterion of nearly L/200; the actual field structure was stiffer at L/450. This was attributed to the difference in boundary conditions for the girders and timber panels.

Finally, the bridge response was verified with an analytical model that treats the bridge structure as a wood beam resting upon discrete elastic springs. The model permits both bending and torsional stiffness in the composite beams, as well as shear deformation. A parametric study was conducted utilizing this model and a mechanics of laminated beam theory to provide recommendations for alternate bridge designs and modified composite beam designs.

Acknowledgments

The author would like to acknowledgment the following for their contribution and support in this work:

- **Dr. John "Jack" Lesko**, for serving as my advisor, mentor, role model, and friend over the past two years. I have had the privilege of working under Dr. Lesko as one of his first students, and I have watched him accomplish an incredible amount in a short period of time. Jack has the unique ability to motivate students through constant optimism, patience, and encouragement, and I expect great things to come out of his group in the coming years. It has been an honor and a pleasure to work for Jack, and I will always be grateful to him for giving me the opportunity to learn and grow under his guidance. It is with great reluctance that I am now getting a "real job".

- **Dr. Brian Love**, for serving on my graduate committee and for serving as my undergraduate advisor and mentor. I am extremely grateful to Dr. Love for the opportunities to work in his laboratory and for introducing me to the areas of polymers and biomaterials.

- **Dr. Richard Weyers**, for serving on my graduate committee and for assisting our group in the Tom's Creek Bridge rehabilitation. His civil engineering expertise was invaluable to our efforts.

- **Dr. Thomas Murray**, for allowing us access to the structures testing facilities in civil engineering. His assistance to Dr. Lesko and myself in designing the experiments is also greatly appreciated.

- **Dr. Scott Case**, for all of his assistance in various aspects of my work, but especially in the analytical portion. Scott's guidance and assistance was invaluable.

- **Dr. Jack Duke**, for his assistance in the Tom's Creek Bridge project with all of the non-destructive evaluation.

- **Brett Farmer and Dennis Huffman**, the technicians at the Structures and Materials Research Lab who answered our endless questions and provided assistance in all of the set-up and testing at their lab. None of the experimental work in this thesis could have been accomplished without their help. Thanks to Brett and Dennis for being so patient and helpful.

- **Joe Howard, John Haramis, Brian Carlin**, and all of the Civil Engineering students at Structure and Materials Research Lab who allowed a mere mechanics student to play with their toys. Special thanks to Joe for helping me to get acquainted with the lab equipment and procedures and for providing endless hours of assistance. Special thanks to John and Brian as well for their assistance in the latter stages of the project including the beam and bridge testing.

- **Brian Moser**, a summer intern from Penn State who assisted in the early stages of beam testing and also developed the first version of the bridge model.

- **Phil Vallance and Chris Kelley**, undergraduates in the Mechanical Engineering program who provided hours of invaluable help in strain gaging and the in-lab bridge construction.

- **Howard Halverson**, for helping me learn the ropes of 102 Norris and for his assistance in learning LabView and other aspects of data acquisition.

- **Nikhil Verghese**, for teaching me how to use the MTS equipment and for all of his assistance in the moisture absorption work, as well as the Tom's Creek Bridge project.

- **Kyle Garcia**, for his assistance in ALL of the projects that I have worked on.

- **Judy Wood**, for teaching me about strain gaging, Wheatstone bridges, and numerous other miscellaneous things.

- All of the other members of the **Materials Response Group** who have helped me out in so many ways over the past two years. The MRG is certainly a special place to work and I hope the group continues to thrive in the coming years.

- **Mac McCord**, the workhorse of the MRG who has a hand in every single experimental project that comes through the door. Thanks to Mac for his patience and dependable presence.

- **Sheila Collins**, **Paula Lee**, **Beverly Williams**, **Cindy Hopkins**, and **Pat Baker**, the staff of the Materials Response Group and the ESM Department who have provided invaluable assistance during my stay at Virginia Tech. They are the real work force at this university. Thanks for enduring the antics of the "engineering types"!

- **Bob Simonds and George Lough**, technicians in the ESM department who have helped me out in so many ways over the past 4^+ years.

- **Dan Witcher, Glen Barefoot, and Clint Smith of Strongwell Inc.**, for all of their participation in the Tom's Creek Bridge project. They have provided enormous support in the form of material donations and financial resources. Good luck in their endeavors to market the hybrid composite beam utilized in this work.

- A word of thanks to all of the other individuals and organizations who participated in the Tom's Creek Bridge rehabilitation and made it a success:
  - **Julius Volgyi, Ernesto Villalba, Mal Kerley,** and the Virginia Department of Transportation

- **José Gomez, Wally McKeel**, and the Virginia Transportation Research Council
- **Jim Stewart** and the Center for Innovative Technology
- **Randy Formica, Adele Schirmer**, and the Town of Blacksburg
- **Dr. Jim McGrath** and the National Science Foundation Science and Technology Center for High Performance Polymeric Adhesives and Composites, Virginia Tech

▪ A final word of thanks to the **Center for Composite Materials and Structures at Virginia Tech** and **Dow Chemical Company** for providing me with funding in the form of fellowships.

Finally, I want to thank my parents, Jim and Sharon Hayes, for all of their steadfast love and support (both emotional and financial). I appreciate everything you have done for me; I only wish that I could somehow repay you. Thank you for the stable and nurturing environment and for opening so many doors for me in my life. I'm positive that you all come as close to perfect parents as anyone. I also want to thank my brother Jason for his love and friendship through the years. I may be older and taller, but I want you to know that I look up to you and admire so many qualities in you.

Table of Contents

List of Tables

List of Figures

Chapter 1: Introduction and Literature Review

1.1 Introduction

Recent interests in utilizing fiber reinforced plastic (FRP) composites as structural members in infrastructure applications has brought the issue of composite durability to the forefront. Besides having high stiffness- and strength-to-weight ratios and excellent fatigue resistance, composites are often claimed to offer superior resistance to environmental degradation compared to the traditional engineering metals. However, little data is available in the literature to substantiate these claims. Long-term data documenting the effects of environment on the modulus, strength, and life of composites is scarce. Some short-term laboratory studies have addressed the issue of degradation, but these studies usually involve very specific constituents and fiber architecture, environmental conditions, and loading types. This variability in material systems and test conditions precludes any generalizations about composite durability from the existing data. Furthermore, few attempts have been made to correlate laboratory data with long-term field performance. Comprehensive, accelerated test methods for predicting long-term performance in infrastructure environments are also not available. Investigations involving actual field studies in parallel to laboratory testing are needed to develop durability data and to more accurately mimic service environments in the lab.

The current database of composite data is derived mainly from the aerospace industry where cost and durability are often of secondary importance. Carbon fiber and epoxy resins have been the materials of choice for these high performance applications. However, the composite materials that are currently most cost competitive for usage in the construction and infrastructure industries are the lower cost vinyl ester and polyester resins and glass fiber. Far less data exist for these resins and composites, and glass fiber is known to be highly sensitive to moisture, salt, acidic and alkaline solutions, and stress corrosion/creep rupture (failure under static loading well below the static strength due to environmental factors). Any confidence that has been established in using fiberglass composites has resulted mainly from marine and chemical storage applications.

Unfortunately, the success of composites in these applications has not been well documented.

Besides the lack of durability data, there exist few standards by which to guide design and repair with composite materials. The field of advanced fiber-reinforced composites is relatively new compared to the concrete and steel industries where well established practices and standards exist for designing with these materials. A few of the larger composite structure manufacturers are independently developing design guides for their own products, and efforts are underway on the academic and government sides to develop test standards and design guides, as well. Again, however, these efforts are made more difficult by the wide range of constituent materials and architectures available, and generalizations about failure modes and durability are difficult to make due to the orthotropic nature of composites. The situation is further complicated by the fact that most composite structures are deficient in modulus as compared to steel (although the stiffness-to-weight ratios are much higher for composites) and connections with composite members can be considerably more difficult. These issues, though, will likely become less critical as the cost of carbon fiber becomes more competitive with glass, and experience with composite connections grows.

In order to facilitate the utilization of FRP composites in the infrastructure and construction industries, the composites community must expand the database of durability information, further develop testing and design standards, and reduce the cost of the higher-performance materials. The only way these tasks can be accomplished, however, is through actual field applications such as demonstration projects and small-scale, low-risk projects. However, the author likens this situation to the “chicken and egg” analogy: in order to improve the acceptance of composite materials in the civil engineering community, design guides and durability data must be developed. Yet, this information cannot be developed without trial field applications in civil engineering projects.

1.2 The Tom's Creek Bridge Rehabilitation Project

The Tom's Creek Bridge rehabilitation project is one effort that should provide some useful design and durability information in a safe, controlled application. The Tom's Creek Bridge is a small structure owned by the Town of Blacksburg, Virginia (Figure 1-1). The bridge was built in 1932 and reconstructed in 1964. The original bridge was 7.32 m (24 ft) wide and spanned 5.33 m (17.5 ft), with twelve 6.10 m (20 ft) long W10 x 21 steel stringers resting on concrete abutments (see Figure 1-2). The deck was composed of 10.2 cm x 20.3 cm (4 in x 8 in) transverse wood planking and 5 to 8 cm (2 to 3 in) of asphalt. The original structure was rated at 178 kN (20 tons), but inspections of the bridge in 1990 identified significant corrosion in a number of the steel stringers; the bridge was then posted at 89.0 kN (10 tons). The Town of Blacksburg was looking for a temporary repair solution, as the road is planned for widening in 10-15 years, and they were open to exploring new technologies.

Concurrently, Strongwell Corporation of Bristol, Virginia and Dr. Abdul Zureick of Georgia Tech developed a new FRP composite structural beam as part of an Advanced Technology Program through the National Institute of Standards and Technology (NIST) [1]. The proposed beam would be a pultruded 91.4 cm (36 in) deep hybrid composite composed of glass and carbon fibers in a vinyl ester matrix that would meet AASHTO (American Association of State Highway and Transportation Officials) standards for future bridge construction. The development process involved manufacturing a 20.3 cm (8 in) deep prototype using both phenolic and vinyl ester resins (see Figure 1-3). Once the prototypes were completed, the design was then scaled up to 91.4 cm (36 in). Upon completion of the initial prototype production, Strongwell was looking for small demonstration projects that would utilize the vinyl ester prototype. Discussions between Virginia Tech, Strongwell, and the Town of Blacksburg resulted in a proposal for replacing the corroded steel members in the Tom's Creek Bridge with the 20.3 cm (8 in) deep vinyl ester beams. A team of engineers and researchers at Virginia Tech, Strongwell, the Virginia Transportation Research Council (VTRC), the Virginia Department of Transportation (VDOT), and the Town of Blacksburg, Virginia collaborated to complete the rehabilitation. Due to the town's financial constraints and the willingness of the composite manufacturer to offer the beam at a discounted cost, the rehabilitation with composites became a viable alternative.

The team opted to replace all of the twelve steel stringers in the Tom's Creek Bridge with 24 composite beams to rehabilitate the bridge to HS20-44 loading. The transverse and plan views from the design plans are illustrated in Figure 1-4 and Figure 1-5, respectively. The rub rail/guard rail design is shown in Figure 1-6. The two-for-one replacement was necessary due to the lower bending stiffness of the composites. The lower stiffness of the composite beams (relative to the steel shapes resident in the existing structure) is due not only to the lower moduli of the constituent materials, but also to the shorter geometry of the prototype (8 in versus 10 in). This repair design was certainly not optimal, and a deeper composite beam could be manufactured to perform a more efficient rehabilitation, but no other section was available at the time of this project. Still, a number of organizations have expressed interest in utilizing the 20.3 cm (8 inch) section for industrial applications, since the completion of the rehabilitation. This project then serves as a means of demonstrating and evaluating a composite structure that may soon be commercialized.

Prior to the bridge's rehabilitation in the summer of 1997, a full-scale replica of the new bridge was built and tested in the laboratory (detailed in the Chapter 2). The new bridge was also tested by Virginia Tech and the VTRC after construction. Furthermore, as this project provides a unique opportunity to track material behavior of a composite structural member in service, Virginia Tech is monitoring the bridge response under traffic loading and environmental conditions over a 10-year period. Non-destructive evaluation techniques will also be utilized to periodically monitor material condition. In addition, the VTRC and Virginia Tech will perform periodic field tests to assess changes in bridge response with time. The Town of Blacksburg anticipates having to widen Tom's Creek Road in 10 years due to nearby residential growth. At that time, the bridge will likely be replaced altogether with a new structure, and the composite beams will be extracted for testing. This situation then provides a unique opportunity to test the remaining strength and modulus of composite beams after 10 years of actual service. Several beams will also be replaced periodically to monitor stiffness and strength reduction due to loading and environment, as part of a Federal Highway Administration (FHWA) program.

To summarize, the Tom's Creek Bridge rehabilitation project entailed a number of tasks:

1) Testing the composite members to assess basic engineering design properties and manufacturing consistency
2) Developing an analytical model to predict the performance of the rehabilitated structure and to guide the design of the new structure
3) Designing the new bridge structure
4) Constructing and testing a mock-up of the bridge in the laboratory to verify the predictions and to evaluate construction needs and difficulties
5) Constructing the new bridge in the field
6) Testing the bridge in the field after installation
7) Monitoring and testing the bridge through its life for durability purposes.

The current study addresses items 1, 2, and 4, as well as some parametric investigations intended to provide recommendations for future design with this composite beam in similar short-span bridges. The results of the field testing are also briefly mentioned, but the details of that work are outside the scope of this thesis.

1.3 Literature Review

In order to gain some perspective on the condition of the civil infrastructure and the potential markets for composites, a survey of literature has been conducted. This review summarizes the first efforts of utilizing composite superstructure systems for bridge repair or replacement, as well as the state of the art in composite beam technology. Additionally, this information will provide some insight into the significance of the Tom's Creek Bridge rehabilitation.

1.3.1 Current Status of U.S. Infrastructure

The poor condition of the United States' highway infrastructure system is attracting growing concern as the turn of the century approaches. But while the severity of the problem is common knowledge, the urgency of the situation is perhaps less appreciated. Many of the bridges are long overdue for maintenance or repair, yet there are insufficient financial resources available to maintain the structures. The total number of bridges in the U.S. is reported to be between 542,000 and 600,000, and roughly 4-10% of those are considered to be in a state of advanced decay or are requiring immediate repair [2-4]. One source indicates that as many as 200,000 are either "structurally deficient" or "functionally obsolete", and the deficiency in 132,000 of those is attributed to deterioration and/or substandard bridge decks [4]. The cost per year to rehabilitate all of these bridges is enormous, estimated to be around $50 billion by the year 2000 [1], or as high as $167 billion for both bridges and highways by another source [5]. However, only $5 billion is currently available in the budget for infrastructure improvement [1].

The severity of this problem is detailed in a recent report by the Great Lakes Composites Consortium (GLCC), the Basic Industrial Research Laboratory (BIRL) at Northwestern University, and the University of Kentucky [3]. According to the report, the typical life span of a bridge is around 70 years, and the average bridge requires rehabilitation at mid-life due to deterioration. Most of this damage can be attributed to corrosion of the decks caused primarily by deicing salts [3,4]. Considering that the majority of the bridges in the U.S. were built after 1945, it is estimated that 40% of the bridges will actually require replacement in the next decade [3]. Furthermore, the average cost to a state department of transportation (DOT) to replace a bridge is reported to be $1.56 million per bridge [3]. The alternative to replacement is, of course, repair/rehabilitation to extend the service life of these structures. Still, inspection alone costs the average state DOT $1000 per bridge every two years, maintenance costs $130,000 per bridge every 40 years, and rehabilitation averages the state DOT's $1.05 million per bridge [3]. To compound the problem, the cost of rehabilitation is increasing at a rate faster than inflation due to new costs associated with environmental and health regulations [3].

1.3.2 Utilizing Composites in Infrastructure: Motivations

The financial constraints associated with immediate repair and replacement, as well as concerns for future bridge construction, are motivating civil engineers to look for new technologies in bridge design and materials. While some efforts are being made to improve existing materials by use of coatings (i.e. epoxy-coated rebar) or binders (polymer concrete), or by choosing alternative metals (aluminum bridge decks), there is growing interest in the utilization of FRP composite materials as substitutes for steel and concrete. In fact, the BIRL report estimates that the potential market share for composites in construction and civil engineering could be as high as 50%, amounting to $14 to 71 million for bridge maintenance and $3 to 15 million for pedestrian bridges [3].

One of the primary motivations for utilizing FRP composites in infrastructure environments is that composites are generally considered to be more corrosion resistant than metals [6,7]. The superior durability of composites is attributed to their relative chemical stability and resistance to fatigue crack growth. An improvement in durability would reduce maintenance costs and lengthen the service lives of bridges. The high strength to weight ratio of composites is also attractive and could potentially reduce labor costs associated with transportation and installation [6]. Furthermore, lighter-weight materials may allow for "reduced-weight bridge designs" [8]. Other significant advantages include higher damping and energy absorption, high dielectric strength, and greater suitability for prefabrication [6]. Although FRP composites are generally more expensive than concrete or metallic structures, the improved durability of the composites may also make them more cost-effective in terms of life-cycle costs [9].

1.3.3 Utilizing Composites in Infrastructure: Issues and Concerns

Usage of FRP composite members in bridge structures is hindered by a number of issues. For instance, while superior environmental durability is often cited as an advantage for composites, long-term aging data to support these claims is not conclusive. The bulk of experience with composites has been derived from the aerospace industry where the service lives are much shorter than those required in infrastructure (25-30 years vs. 70 years) [3]. Furthermore, the primary materials of choice in aerospace are graphite fiber and epoxy resin, whereas glass fiber and the lower-cost resin systems are currently most feasible for civil engineering. While glass fiber composites have found considerable use in the marine, chemical storage, and automotive industries in the past, these applications are not well documented, and often, the applications did not utilize composites as primary or critical load-carrying members [9].

Although glass-fiber composites do not degrade by the same mechanisms as metals (i.e. rust), glass-fiber composites are prone to a change in state by both physical aging and chemical aging. Physical aging refers to relaxation of the glassy state of a polymer network towards its equilibrium state, which results in a densification over time [10]. Chemical aging can also occur in infrastructure environments via various environmental factors including moisture, freeze-thaw cycling, deicing salt solutions, acidic or alkaline solutions, UV radiation, and fire. Absorbed moisture, for instance, is known to reduce the strength and/or stiffness of glass-fiber composite members by either plasticizing or hydrolyzing the matrix [11-13], degrading the glass/fiber interface [13,14], or degrading the glass fiber itself [13,15]. Freeze-thaw cycling can also induce damage, cracking the matrix and possibly damaging the fiber [16,17]. Exposure to acidic or alkaline solutions, especially under load (i.e. stress corrosion or creep rupture), can lead to premature failure of a composite structure, and repeated exposure to UV radiation can degrade the surface of a composite [13,15].

The relatively low stiffness of FRP composites is also a key obstacle to their usage in civil engineering applications, as most bridge designs are deflection-controlled [7,9]. Serviceability requirements are also difficult to meet with a composite design. For instance, with fiberglass bridge decks or even composite superstructures, the large deformations may deteriorate the concrete overlay and deck-to-support connections prematurely [7,8]. Although the introduction of carbon fiber into a fiberglass composite structure can significantly improve the bending stiffness, these hybrid composites are not yet cost-competitive.

Two additional design issues stand as significant stumbling blocks for widespread usage of FRP composites in bridge design: connection design and failure mechanisms.

Due to the tendency of a composite laminate to delaminate at its free edges, stress risers such as holes must be avoided, and care must be taken to insure that the laminates are not damaged by abrasion or crushing in the out-of-plane direction. The typically linear elastic response of a composite laminate up to failure also provides a new challenge to civil engineers who are accustomed to designing with steel, which yields prior to failure (i.e. ductility). In a composite structure, too, structural members can be designed to fail with some "pseudo-ductility" by utilizing failure modes that absorb large amounts of energy (i.e. laminate delamination, debonding of adhered members, local buckling, etc.).

1.3.4 Utilizing Composites in Infrastructure: Materials and Applications

The FRP composite members being manufactured for infrastructure applications are typically glass/polyester or glass/vinyl ester, as these systems are the most inexpensive. However, carbon fiber and epoxy resins also find limited usage in certain applications, such as steel or concrete repair or in hybrid structural beams. As composites are selected for primary load-bearing members, hybrid structures of both glass and carbon will be necessary to improve the flexural stiffness [3]. Aramid fiber is also sometimes selected for cables in cable-stay bridges and tendons in pre- or post-stressed structures.

Currently, the most popular process for manufacturing composite members for large-scale infrastructure applications is pultrusion. Pultrusion is preferable for civil engineering applications due to its simplicity, low-cost, and flexibility for utilizing various resins and fiber architectures. Pultrusion is also suited for large-scale production of structural shapes. Pultruded components typically utilize a combination of glass rovings, random fiber mats, and stitched fabrics that provide cross-ply (0/90°) and ± 45° fiber orientations. Typically, the fiber volume fractions are low in pultruded composites, between 40 and 55% [6]. Other processes such as resin infusion and Vacuum Assisted Resin Transfer Molding (VARTM, sometimes referred to as Seeman composite Resin Infusion Molding Process or SCRIMP®) are also sometimes utilized for custom applications, or for developing prototypes for future structural components [8,18,19].

FRP composites are being considered for a number of bridge applications as secondary and even primary members. Secondary members include guard rails, diaphragms, reinforcement and repair of steel truss members and splice plates, concrete beam reinforcement, column wrapping, stay-in-place forms, and handrails [3]. Composites can also be used for shielding other structural elements from the environment: expansion joints, bridge bearings, and drainage shielding systems [3]. Potentially, composites may also be utilized for primary members such as girders and bridge decks to improve the durability of a bridge in corrosive environments. Currently, a number of pedestrian bridges exist, and several traffic bridges have recently been constructed or are planned for the near future. These latter structures are mainly experimental or demonstration bridges that are serving as test cases for design and durability investigations. The following is a review of some of the more significant projects utilizing FRP in primary members; post-stressing and bonded repair applications are beyond the scope of this review.

1.3.5 Review of Bridges Utilizing a Composite Superstructure or Deck

Pedestrian Bridges

Pedestrian bridges have been identified as a viable application for introducing composite materials into the infrastructure markets. In fact, there are already over 60 composite pedestrian bridges in service in the United States [20]. A few of the more noteworthy ones in the U.S. and elsewhere are presented here.

In the fall of 1995, the Chicago Department of Transportation, Strongwell, the BIRL at Northwestern University, the GLCC, and the Kentucky Transportation Center (KTC) at the University of Kentucky renovated the LaSalle Street pedestrian walkway [21-23]. This is a lift bridge over the Chicago River that carries pedestrian and maintenance vehicle traffic only. The walkway was originally comprised of a steel and wood decking supported by steel I-beams. In the repair, two 1.22 m x 3.66 m (4 ft x 12 ft) experimental walkway sections were utilized. The deck was constructed by sandwiching 5.08 cm (2 in) DURADEK® grating with 1.91 cm (0.75 in) thick EXTREN® plate. Both products are E-glass/vinyl ester pultrusions manufactured by Strongwell.

Another pedestrian bridge that has attracted significant attention is the Antioch composite bridge at Antioch Golf Club in Illinois. This structure was built in 1995 by the Chicago DOT and E.T. Techtonics. The structure is 13.7 m long x 3.05 m wide (45 ft x 10 ft) with a 44.5 kN (5 ton) rating for pedestrian and gold cart traffic. The bridge is made of four main support girders constructed from back-to-back C-channels with square spacer tubes in between. Each girder has two segments which are connected with a splice plate. In addition, there are eight transverse beams underneath the girders that are also constructed from the C-channels and tubes; the deck is composed of wood planking. This bridge is being monitored with instrumentation for environmental conditions and changes in structural response [23,24].

E.T. Techtonics has been involved in the installation of two FRP pedestrian bridges in the Golden Gate National Recreational Area in San Francisco. FRP designs were selected for installation on the Point Bonita Lighthouse trail in the Marin Highlands because of their light weight and durability. The first bridge spans 10.7 m (35.1 ft) and utilizes an FRP truss system and a wood decking. The design consists of a standard double beam top and bottom chord connected with lateral and horizontal bracing; 15.2 cm (6 in) deep FRP channel is utilized. The second structure utilizes a deeper FRP channel (20.3 cm or 8 in) and cross bracing. Both structures were designed for an L/360 (live load) serviceability criterion [25].

The University of Kentucky and Strongwell completed the installation of a pedestrian bridge in the Daniel Boone National Forest in Bath County, Kentucky in September 1996. The bridge is 18.3 m long x 1.83 m wide (60 ft x 6 ft) and contains two cable-stayed, 61.0 cm (24 in) deep I-beams. The deck is made of a fiberglass grating, has eight post-tensioning rods made of glass/vinyl ester, and utilizes concrete abutments. The I-beams are similar to Strongwell's standard EXTREN® beams, but carbon fiber was introduced into the flanges during the pultrusion process to increase the bending modulus to 41.4 GPa (6 Msi). The deflection-to-span ratio is L/180 [26,27].

Frieder Seible at the University of California, San Diego (UCSD) is involved in a number of innovative projects to develop new design philosophies for composite bridges and has several structures in place or under development on the UCSD campus [28]. Seible's group investigated several designs for the Scripps Crossing pedestrian bridge, including one structure utilizing a carbon/glass skin and stiffener structure and foam core to be manufactured by RTM and another design utilizing a carbon shell/concrete system with a fiberglass deck. The carbon shell system would be manufactured by filament winding and the deck could have been constructed using hand lay up, RTM, or pultrusion. A steel and concrete cable stay design was eventually chosen for the Scripps Crossing bridge, but the composite designs are being developed for future applications.

Traffic Bridges

The engineering community is reluctant to accept composites for use in traffic bridges, despite the growing experience with pedestrian bridges. Again, durability and serviceability are cited as major issues. However, a number of test structures have been built since the 1980's, and recently, a new generation of bridges utilizing composites have been constructed. These newer bridges are still experimental in nature but are generally intended for normal traffic use.

The Bonds Mill Lift Bridge in Stroud, England is one such structure that has attracted attention for its unique application of fiberglass composites. This bridge utilizes pultruded glass/polyester box sections bonded together with epoxy to support traffic over a small river. The bridge is 8.23 m long and 4.57 m wide (27 ft x 15 ft) and consists of two sections that can be lifted hydraulically to allow water traffic to pass underneath. The bridge is reported to have a 391 kN (44 ton) capacity. In this case, composite materials were favored because a lighter weight structure permitted use of a smaller lift mechanism [29].

The West Virginia University (WVU)'s Constructed Facilities Center, the West Virginia DOT, the Construction Engineering Research Lab, and the Composites Institute completed two projects during the summer of 1997 that utilize 1) an all-composite design and 2) a composite deck system. The first is the Laurel Lick Bridge in Lewis County, West Virginia which was completed in May 1997 [7,30]. This project involved replacing a timber deck and steel stringer bridge with an all-composite structure consisting of a deck system and wide flange beams both made of E-glass/vinyl ester. The deck system ("Superdeck™") is manufactured by Creative Pultrusions of Alum Bank, Pennsylvania. It utilizes both hexagonal and trapezoidal shaped tubes, which run transverse to the traffic direction. This system is detailed further in Section 1.3.6. The 6.10 m long x 4.88 m wide (20 ft x 16 ft) deck is composed of two 2.44 m (8 ft) wide modules and is supported by six 6.10 m (20 ft) long, wide-flange beams (30.5 cm x 30.5 cm x 1.27 cm thick, or 12 in x 12 in x 0.5 in), and the abutment is constructed from five 3.05 m (10 ft) long, wide-flange columns having the same cross-section as the stringers but different fiber architecture. A reinforced concrete cap beam rests on top of the columns.

The Laurel Lick Bridge utilizes a two-part polyurethane adhesive to bond the deck to the stringers and to splice the deck sections together. The deck modules were also attached to the stringers using 1.27 cm (0.5 in) huck bolt blind fasteners. The stringer-abutment connection was accomplished using steel clip plates. The bridge also utilizes a 1 cm (0.394 in) polymer concrete overlay and curbs made of FRP square tube scupper blocks and continuous square tubes connected to the deck. The deflection-to-span ratio is reported to be L/300 for the deck to stringer structure and L/500 for the total bridge [7,30]. The second West Virginia project is the Wickwire Run Bridge in Taylor County, West Virginia, built in August 1997. This demonstration bridge was built utilizing the same deck system, but the deck is supported by four steel stringers spaced 1.83 m (6 ft) apart. The bridge dimensions are 9.14 m long x 6.61 m wide (30 ft x 21.7 ft) [7,30].

Two additional traffic bridges utilizing FRP composite designs have been built by a collaboration between the Idaho National Engineering and Environmental Laboratory (INEEL), FHWA, the U.S. Department of Energy, the National Oceanic and Atmospheric Administration, Martin Marietta Materials, Lockwood Jones and Beals (LJB) Engineers and Architects, and the Idaho Department of Transportation [31-33]. The first structure, named the INEEL Bridge, was designed by the Lockheed Martin Advanced Technology Center in 1994 and then constructed at the INEEL Transportation Complex (in-ground) in 1995. The structure is 9.14 m long x 5.49 m wide (30 ft x18 ft) and utilizes a square tube and flat plate deck design that is laid across a superstructure constructed of three U-shaped girders measuring 1.22 m wide x 0.610 m deep (4 ft x 2 ft). The deck is composed of pultruded E-glass tubes (with a $[0/+45/90/-45/mat/]_s$ layup) utilizing vinyl ester resin sandwiched between face sheets of glass/vinyl ester or glass/polyester laminae, while the girders contain both quasi-isotropic and unidirectional glass laminae in a polyester-vinyl ester blend resin. Both components were manufactured by hand layup and cured at room temperature. The deck was actually installed in three sections, 3.05 m wide x 5.50 m long (10 ft x 18 ft) with the tubes running transverse to the girders, and the deck was bolted to the U-girders. The overlay consists of 5 to 8 cm (2 to 3 in) asphalt, and a separate guard rail system utilizing steel beams was utilized. The abutments consist of concrete columns which support the U-girders at the joint between adjacent girders. This structure was designed to meet HS20 loading with a serviceability ratio of L/800. A similar structure was previously built and tested in 1995, and results from the testing indicated a strength of 578 kN (130 kips). The bridge is expected to carry 250 passenger buses per day.

In July 1997, the same group built an all-composite traffic bridge named the "Tech 21 Bridge" in Butler County, Ohio [31,33,34]. The project involved replacing a one-lane bridge that carried approximately 1000 vehicles per day with a 10.1 m long x 7.32 m wide x 83.8 cm deep (33 ft x 24 ft x 3 in) two-lane structure that is expected to carry 2000 vehicles per day. The bridge design is similar to the INEEL structure, but the deck is comprised of trapezoidal tubes (also pultruded). Furthermore, the deck panels were adhered to the U-girders prior to installation to form three modular sections, and these sections were then installed and joined using a “compression joint” design. These field bond lines were both bolted and bonded using an epoxy adhesive. The U-shaped girder designed was also modified slightly to a flat, box design to improve the interface between the abutment and girders. In addition, internal frames were located every 3.05 m (10 ft) along the length of the U-girders to prevent buckling. The Tech 21 bridge utilizes a 10 to 15 cm (4 to 6 in) crowned asphalt surface and a conventional guardrail design that is actually connected to the composite structure. The structure contains embedded sensors for continuous monitoring of response and moisture content, and load tests are planned four times a year to monitor changes in the bridge response.

A series of FRP composite vehicular bridges are also under development by a collaboration between the University of Delaware, Hardcore-DuPont Composites, J. Muller International, Anholt technologies, FHWA, the Delaware Department of Transportation, the Delaware River and Bay Authority, the Delaware Transportation Institute, the Delaware Research Partnership, and the Defense Advanced Research Projects Agency (DARPA) [35]. The bridges have been selected or designed to incrementally advance the service requirements and design complexity. The first bridge, completed in the summer of 1997, spans the Magazine Ditch on a private service road on the property of DARPA. This structure is a 21.3 m long x 4.88 m wide (70 ft x 16 ft) single-span bridge that replaces a two-span concrete box beam structure.

The Magazine Ditch Bridge is comprised of two post-tensioned concrete edge girders, an E-glass/vinyl ester deck, and a 4.5 cm (1.77 in) latex modified concrete overlay. The bridge is designed for HL-44 loading with L/800 deflection at service load and is intended to carry low volume, heavily-loaded maintenance traffic. The deck was manufactured using the SCRIMP® process and consists of top and bottom sheets sandwiched around a honeycomb core. The deck was bonded to the edge girders using an epoxy adhesive. Prior to installation, a deck section was tested under static and fatigue (2 million cycles) loading. The team is also planning to perform periodic load tests, as well as continuous monitoring [35].

1.3.6 Other Composite Structures Being Developed

A number of research groups in the United States are working to develop composite deck systems for replacement of concrete decks on existing bridges. The following is a brief overview of several of those systems.

The West Virginia University (WVU) group has published several papers detailing their work in the development of fiberglass decks. As part of one effort, they investigated two different deck systems: one utilizing pultruded channels as the main support beams and flat cover plates on the top and bottom flanges, and the other utilizing cellular deck sections connected using wide-flange beams and utilizing diaphragms. Both of these systems were E-glass/vinyl ester. Testing of these two systems included investigations of the transverse load transfer, joint efficiency, effective width of the deck, and degree of composite action. Results from bending tests were verified using predictions based on their Mechanics of Laminated Beam (MLB) theory [6].

More recently, the WVU group and Creative Pultrusions have developed the H-deck or Superdeck™ system mentioned in Section 1.3.5. This system is made of E-glass/vinyl ester, utilizing both multi-axial stitched fabrics and continuous strand mat (CSM). Two 20.3 cm (8 in) deep pultruded members comprise the deck system: a 30.5 cm (12 in) wide double trapezoid or truss section and a 10.2 cm (4 in) wide hexagonal shear key. The test prototypes for this system were actually manufactured by VARTM by HardCore-DuPont. The deck system is designed so that the tubes are oriented transverse to the traffic direction. The weight of the total deck is reported to be 1.03 kN/m^2 (22 lbs/ft^2) [36]. Bending tests were conducted on the deck system at different span lengths using both a patch load and a transverse line load to establish the longitudinal stiffness under cylindrical bending. The deck met the L/300 AASHTO requirement, and finite element analysis was also performed to verify the deck response. Fatigue testing was also performed by the U.S. Army Corp of Engineers [36,37].

The University of California at San Diego (UCSD), the Federal Highway Administration (FHWA), and the Advanced Research Projects Agency (ARPA) have also been working to develop a viable deck system for bridge use. This group has investigated several assemblies utilizing box or triangular truss tube sections. The various geometries have been manufactured to a 22.9 cm (9 in) depth using hand layup, resin infusion, or pultrusion, and they utilize E-glass with vinyl ester or polyester; one hybrid design containing carbon fiber was also tested. Load tests were performed on various-sized panels utilizing the different constructions. Currently, four panels are located in a field test site at the UCSD campus with continuous monitoring [38].

Hardcore DuPont Composites recently presented details regarding their progress in the development of fiberglass bridge deck systems utilizing the SCRIMP® [19]. They were investigating several different configurations for a deck to be utilized in a future bridge repair. The Hardcore DuPont group was interested in selecting a core material and geometry for a sandwich structure that would have the highest shear strength to manufactured cost ratio. Decks utilizing triangle, trapezoid, and cube elements were constructed by wrapping foam elements with fiberglass fabrics. Another deck was manufactured by using a balsa core with face skins laid up using the fiberglass fabric. Testing was performed on the decks at the University of California, San Diego and the University of Delaware. Results from the study indicate that the trapezoidal deck configuration would offer the best performance to price ratio for applications where strength in only one direction is required (end-supported), whereas the box structure would be best suited for a deck supported on all four edges [19].

The U.S. Army, also in collaboration with Hardcore DuPont Composites and the University of California, San Diego, has been working to develop a lightweight short-span assault bridging system. One of the concepts under consideration is a carbon-epoxy design consisting of two parallel treadways. Each treadway has a superstructure, deck, and wear surface composed of composites and a launch mechanism and end caps made of aluminum. Three sub-scale structures were constructed using the SCRIMP® process to manufacture the composite members, and they were tested to failure. The test results were also verified using a finite element analysis. Two full-scale treadways were to be manufactured during the summer of 1996 and then tested at UCSD and the Army's facilities [18].

The author has been involved in project at Virginia Tech to characterize a fiberglass deck system manufactured by Strongwell [39]. This system utilizes off-the-shelf pultruded shapes to accomplish L/270 deflection in a limited deck depth rehabilitation (the Schuyler Heim Bridge in Long Beach, California). The system consists of E-glass/polyester (EXTREN®) square tubes and cover plates. The tubes and plates are all bonded together with an epoxy adhesive, and the tubes are additionally joined using fiberglass bolts spaced every 30.5 cm (1 ft). The deck system is designed for 1.22 m (4 ft) stringer spacing and would run transverse to the traffic direction. Patch loading tests were conducted to characterize the deflection and strain response under service loading (92.4 kN or 20.8 kips), and a test to failure indicated an ultimate load roughly 3 times the service load. Fatigue cycling (with a maximum load of 111 kN or 25 kips at a nominal frequency of 2 Hz) up to 3 million cycles indicated no reduction in stiffness or strength.

1.3.7 Characteristics of FRP Structural Beams

Design Considerations

Fiberglass structural beams have been used for many years in industrial applications involving corrosive environments or weight-driven designs. Wide-flange beams, channels, and box beams made of glass/polyester or glass/vinyl ester are readily available as standard, commercial items from pultrusion companies. More recently, triangular, hexagonal, and trapezoidal beam sections have been developed for use in bridge decks or superstructures. The basic design methodology for these fiberglass beams is fairly universal. Although most of the off-the-shelf products utilize a constant layup of unidirectional roving and random fiber continuous strand mat (CSM) in the flanges and web, custom designs concentrate unidirectional fiber in the flanges and utilize ±45° fabric in the webs to improve the bending and shear properties [40]. The use of woven or stitched fabrics in place of CSM can also improve the transverse tensile strength of a beam, which can be a dominant failure mode [41].

Laminated Beam Theories for Beam Design and Model Predictions

Design of laminated composite beams is complicated by the anisotropic nature of the constituent composite plates. Furthermore, because the bending modulus of a fiberglass beam is typically 10 to 30 times greater than the shear modulus, shear deformation becomes significant at relatively short span lengths [40]. The usual assumptions of Euler beam theory no longer hold for fiberglass beams, and beam deflection equations must be re-derived using Timoshenko beam theory. Design of laminated composite beams or predictive modeling requires the use of some type of laminated beam theory to establish the global stiffnesses of the beam as a function of the properties of the individual laminated plates which constitute the beam (i.e. flange and web panels). Various models have been formulated to determine bending and shear stiffnesses, the degree of warping, hygrothermal or dynamic effects, and different assumptions regarding the treatment of stresses in the laminates composing the composite beam. A review of the development of such theories is discussed in References [42,43].

Typical Failure Mechanisms

While design with fiberglass structural beams is often deflection-controlled and the factors of safety on strength are often high, consideration of the failure mechanisms is still important as these mechanisms may occur prematurely or change during the life of the structure due to environmental degradation or local stresses associated with connections. There are several common forms of structural instability in fiberglass beams that may occur prior to the ultimate strength of the constituent materials: lateral torsional buckling, warping, local flange buckling due to compression, or local web buckling due to shear [44].

Due to the relatively high elongation of the matrix and glass compared to metals, the response of a laminate may be nearly linear elastic up to failure. In a beam, however, local buckling of the compression flange will usually occur prior to ultimate failure of the flange. The buckling will introduce much larger strains which can then fail the flange [44,45]. Furthermore, the damage usually initiates under a loading point [44]. Failure of the compressive flange has been demonstrated for a number of fiberglass I-beams and box-beams utilizing different resin systems under both three- and four-point bending [41,44,46]. Similar behavior was observed in carbon fiber/epoxy I-beams under four-point bending and a carbon/thermoplastic I-beam under three-point loading. In the latter case, failure in the compressive flange could be suppressed by bonding reinforcement caps to the flanges. Failure then occurred due to either shear in the web or delamination of the flange cap [44]. In one study, the shear failure at the web-flange interface was also reported as a mechanism of failure in fiberglass I-beams [41].

1.3.8 Testing of FRP Beams

Monotonic bending/flexure

The general test method for evaluating the bending response of an FRP composite beam involves testing the beam in either three- or four-point bending using a simply supported geometry where steel structural beams are used as supports. Load is applied using a hydraulic actuator to representative wheel patches. Often the tests are run for various span lengths to determine the shear stiffness, since the percentage of shear deformation increases with decreasing span length. In the case of three-point bending with simple boundary conditions, for example, the total midspan deflection is a function of both the bending stiffness and the shear deformation:

$$y_{\max} = \frac{PL^3}{48EI} + \frac{PL}{4KGA} \tag{1.1}$$

where *EI* is the bending stiffness, *KGA* is the shear stiffness that depends upon the shear modulus *G*, the cross-sectional area *A*, and a shear correction factor *K*. *P* is the applied load and *L* is the span length. If y_{max}/PL^3 is plotted versus $1/L^2$ for each span length, the slope of the line is then related to the bending stiffness, *EI*, and the *y*-axis intercept is related to shear stiffness, *GA*, assuming shear deformation. If the shear correction factor has been calculated, then the shear stiffness of the section can then be calculated. A number of researchers have obtained section properties for glass/polyester or glass/vinyl ester beams through bending tests, utilizing the above method to determine the contribution of shear deformation to total deflections for I- or wide-flange beams [45-48] or box sections [45,46,49].

In one study, Bank et al. [41] investigated the effect of the resin type and the addition of a fillet to the web/flange interface on the response of both glass/vinyl ester and glass/polyester I-beams manufactured by pultrusion. The beams were tested in bending and lateral constraints were utilized to prevent lateral-torsional buckling and local failure of the web. The fillets were added by hand layup using glass roving and epoxy, or by bonding fiberglass angles to the interface region. The results indicated that failure of the standard vinyl ester beams (no fillet) occurred by flange-web separation, whereas the polyester beams failed by compressive failure of the top flange. However, the modified vinyl ester beams (fillet added) exhibited no buckling prior to failure, and failure occurred at a load that was 1.5 times that of the unmodified vinyl ester beams. The authors concluded that the buckling capacity of the beams is affected by the torsional stiffness, which in turn depends upon both the transverse flexural stiffness of the web and the torsional stiffness of the flange-web junction. Local buckling of the flange promotes shear failure of web-flange interface, but the addition of a fillet increases the strength and stiffness of the junction and prevents shear failure. It was also noted that an increase in the thickness of the beam walls could change the failure mode from shear to compressive failure of the flange.

Gilchrist et al. [44] tested both glass/epoxy and carbon fiber/epoxy I-beams that were fabricated by hand layup. The beams were tested in four-point bending using loading pads that were adhesively bonded to web and the inside of the flanges. Beams that were both notched in the web and flanges and un-notched were tested. They found that the pads act as stiffneners and increase the buckling load. They also observed anti-symmetric (across width) buckling of compressive flange. Mottram [50] tested 23 square tubes made of E-glass/vinyl ester in three-point bending. They also monitored acoustic emission. Their results indicated that for long spans (span-to-depth ratio of 17.7), compressive failure of the top flange occurred under the load, although for thicker walls, the failure was sudden. For short spans, progressive punch-through failure occurred.

While the contribution of shear to overall beam response and failure mechanisms have been investigated, the out-of-plane buckling response is less understood. However, flexural-torsional stability can be just as important to design as bending stiffness and failure strength. Many studies have considered local buckling and lateral buckling of isotropic beams, but few have considered orthotropic (i.e. composite) beams. Mottram [51], Barbero [52], and others [53,54] are among the few who have investigated the buckling response of orthotropic, thin-walled beams.

Bending Fatigue

Reports of fatigue testing are rare in the literature, perhaps due to the time requirements involved with testing in fatigue, since the large scale test systems are usually limited to slower frequencies (1-3 Hz). A few fatigue studies have been published [36-39,55], and the general test procedure involves loading at a maximum/minimum load ratio of R = 0.1 with a maximum load near the service value. Changes in stiffness are most commonly characterized be performing static service load tests at periodic increments of cycles. Normally, tests are run for no more than 2 to 3 million cycles, even though, for many infrastructure applications, this may only represent a few years of actual service. However, it is simply not feasible to test these structures for a quantity of cycles equivalent to 50-75 years of service. Sometimes then researchers will attempt to "accelerate" fatigue damage by testing at loads much higher than the service load. However, this approach is inadequate as different damage mechanisms may dominate under different load levels.

Creep

Time-dependent deformation under sustained load is, of course, another major concern for utilizing fiberglass composites in bridge applications due to the dead weight of the deck and asphalt system. However, little work has been done to characterize the creep response of composite structural elements. Bank and Mosallam [56] tested a plane portal frame consisting of a girder supported by columns with fiberglass angles and FRP threaded rods and nuts used in the connection details. The girder and columns were pultruded glass/vinyl ester 20.3 cm x 20.3 cm x 9.53 mm (8 in x 8 in x 3/8 in) wide-flange sections. The frame was 2.74 m wide x 1.83 m tall (9 ft x 6 ft). The frame was loaded at quarter points with a total load of 7.56 kN (1700 lbs). This load was determined to be 25% of the failure load from previous tests to failure. The test was conducted for 3500 hours (almost 5 months) at room conditions.

The strain data was fit to a Findley power law expression, as recommended by the ASCE Plastics Design Manual [57]. This model has found extensive use in modeling linear viscoelastic materials and was shown to fit this particular data fairly well. The majority of creep was found to occur in the first 2000 hours, at which point the creep rate leveled off. The total deflection after 3500 hours increased 12.8% from the initial deflection. Calculations for the time-dependent axial and shear moduli indicated that the viscoelastic axial modulus would decrease by 35% over a 10-year time period, whereas the viscoelastic shear modulus would decrease by 46% [56].

Hoa [58] subjected glass/vinyl ester box beams to a static load for a three-month period. The beam was manufactured using hand lay-up and contained roving and mat. The beam was loaded under four-point bending using a pulley device to utilize a gravity load. Deflection and strains were measured, and strains were temperature-compensated. Three different loading schemes were utilized so that a controlled amount of initial strain was induced in each loading for approximately one month. At the end of each loading, the strain was allowed to relax for four days. At the end of the three-month period, the beam was then tested to failure.

Mottram [59] also conducted creep testing on a fiberglass structural system for potential use in bridge deck replacement. The structure tested was a small section of this deck system, consisting of two I-sections sandwiched with flat sheet and bonded adhesively. The sections were standard Strongwell glass/polyester members containing both unidirectional roving and continuous strand mat. Two assemblies were loaded in three-point bending: one aligned so that the roving direction of the flat sheets was parallel to the I- and channel beams and one with the sheets aligned transverse to the beams. These sections had a depth of 9 cm (3.54 in) and flange width of 7.60 mm (3 in). A relatively short span length of 70 cm (27.6 in) was utilized, and the sections were loaded to 22.8 kN (5.13 kip). These values corresponded to anticipated service conditions in a lightweight floor design. The tests were only conducted for 24 hours, and the data was shown to fit Findley's expression quite well. Shear deflection was reported to account for 40% of the initial deflection. Predictions using Findley's model indicate that the section would deflect to 100% of its initial value after 10 years.

1.3.9 Summary

The potential market for FRP composite structures in the civil engineering industry is significant. Composites may offer specific economic advantages over steel and concrete in terms of life-cycle costs due to superior durability and lower installation costs. The use of FRP composites as primary structural members appears to be one of the most promising applications for these materials. Experience in testing FRP beams is growing, as a number of investigators have utilized standard test methods to evaluate beam stiffnesses and strength, as well as stability issues. Some fatigue and creep data also exists, although the time scales for these experiments is usually inadequate to predict the durability of FRP structures for the long design lives required of civil engineering structures. Furthermore, the effect of environmental conditions on the durability of these materials has not been sufficiently examined. Nevertheless, several traffic bridges utilizing FRP composites for primary load-bearing structures are either under development or have been recently constructed in the United States. These applications represent first generation, low-risk projects aimed at demonstrating successful bridge design with FRP composites.

1.4 Problem Statement

To this date, only a handful of bridge designs have incorporated composite members as primary components. The Tom’s Creek Bridge rehabilitation project is the first application of composite beams in a bridge in the State of Virginia and one of the first in the United States. This project is unique as it utilizes a hybrid composite beam manufactured by pultrusion to directly replace steel members in a short-span, traffic bridge. The design used in the Tom’s Creek Bridge allows for conventional decking and railing systems to be used in conjunction with the composites; more sophisticated composite deck and rail systems are not necessarily required.

While the design and testing efforts that were undertaken as part of the ATP development program established the potentiality of utilizing the beam in such a project, the durability and fatigue resistance of this beam still remain significant concerns. While some work has been done to characterize fiberglass beams and structures, the data is scarce, and data involving hybrid structures incorporating both glass and carbon fibers is virtually non-existent. This study attempts to provide such data for one hybrid composite beam. Quasi-static four-point bending tests were performed to characterize the low-load stiffness of all 24 beams utilized in the Tom's Creek Bridge repair. This information provided a guide for the bridge design, as well as an indicator of manufacturing consistency. Short-term creep and fatigue tests were also initiated to provide some preliminary durability data.

To evaluate the design of the new bridge structure, a full-scale mock-up of the bridge was constructed in the laboratory using the actual composite beams, wood decking, and bridge geometry, with simulated abutments. The mock-up was tested in several static loading schemes to evaluate the bridge response and the amount of composite action. The effect of connections was also investigated using two different connection sets. The bridge response was then verified with an analytical model that treats the bridge structure as a wood beam resting upon discrete elastic springs. The model permits both bending and torsional stiffness in the composite beams, as well as shear deformation. A parametric study was conducted utilizing this model and a mechanics of laminated beam theory to provide recommendations for alternate bridge designs and modified composite beam designs.

1.5 Figures and Tables

Figure 1-1. Side view of the old Tom's Creek Bridge.

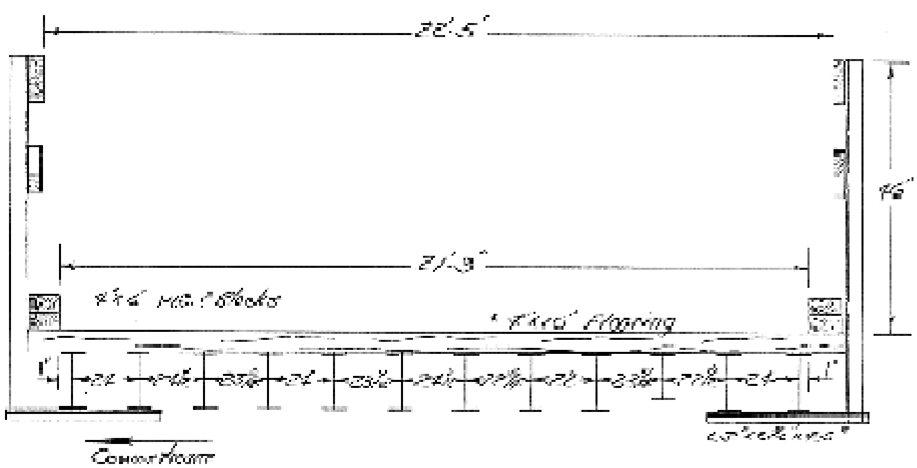

Figure 1-2. Transverse view schematic of the old bridge structure, showing steel stringer spacing.

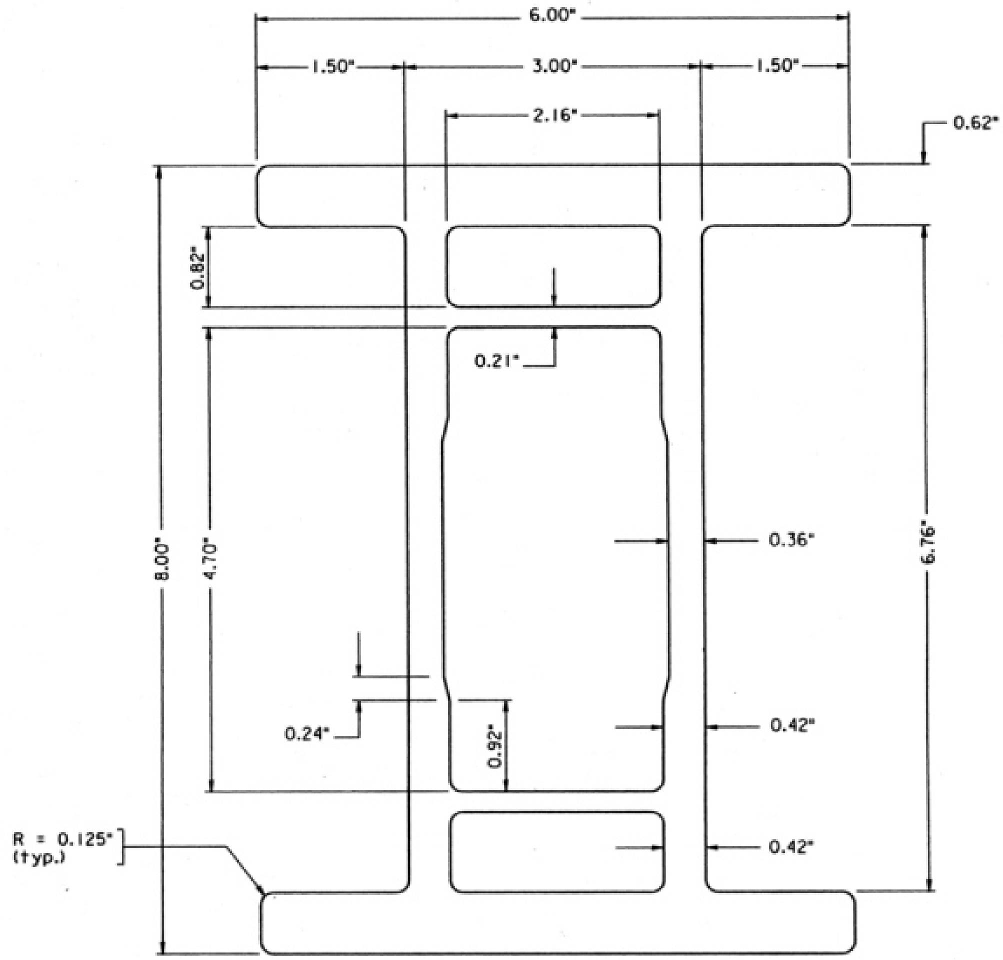

Figure 1-3. Cross-section of the 20.3 cm (8 in) ATP prototype.

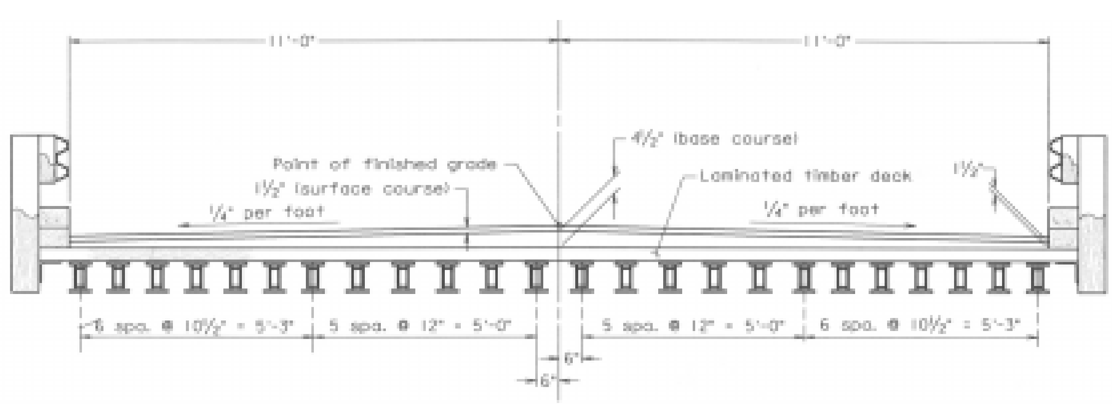

Figure 1-4. Transverse view from design plans for rehabilitated bridge structure showing placement of composite beams [60].

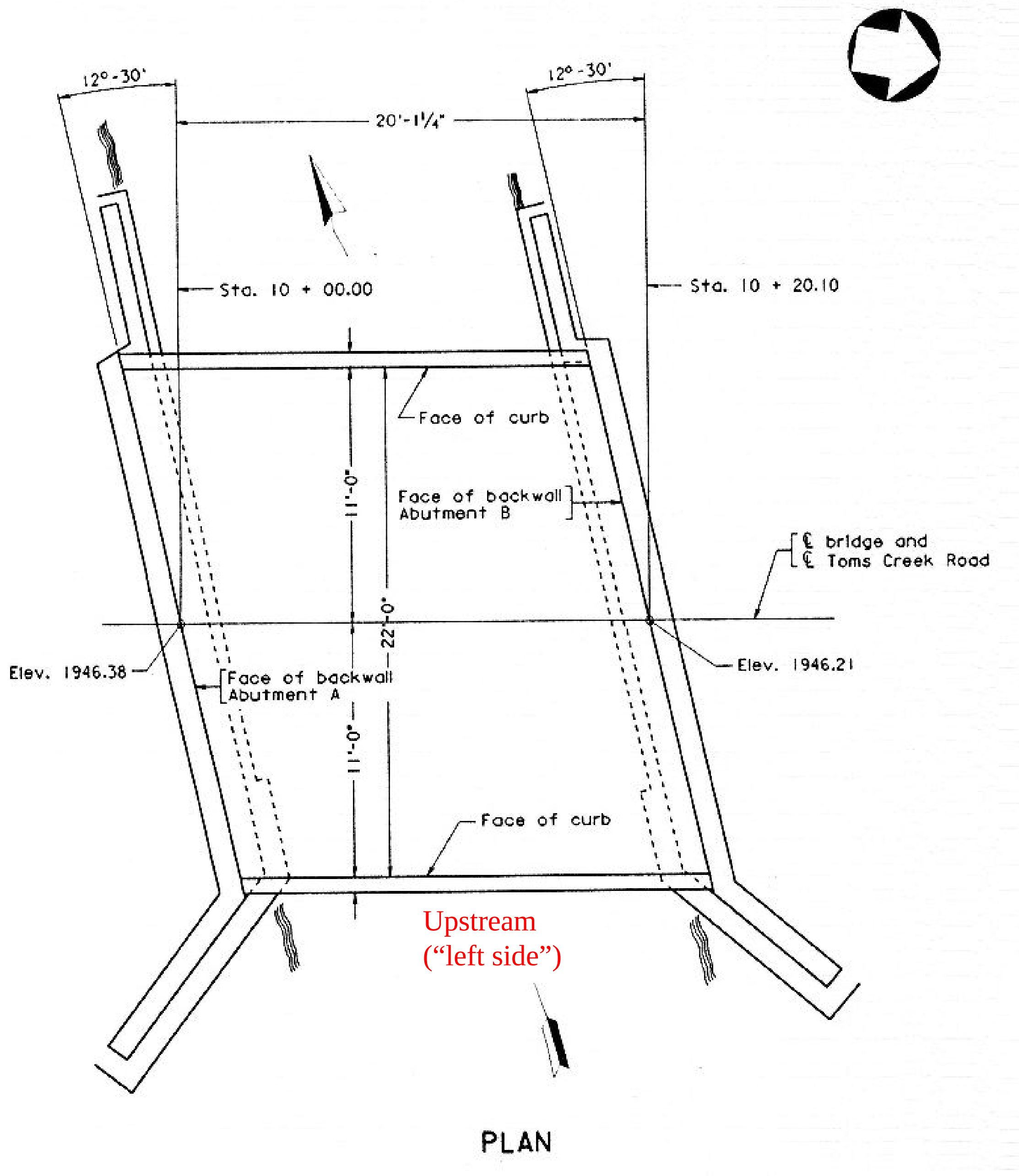

Figure 1-5. Plan view of design schematics for rehabilitated bridge structure [60].

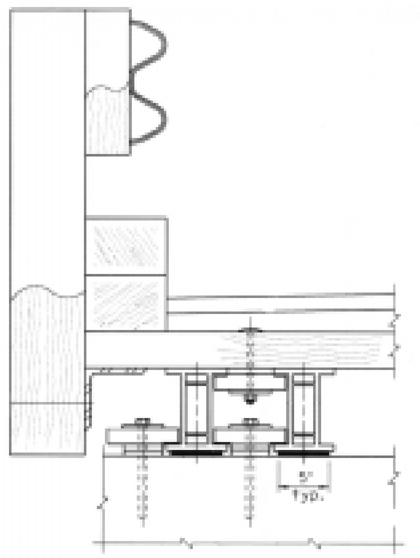

Figure 1-6. Guard rail/rub rail design [60].

Chapter 2: Experimental Procedures

2.1 Material System: Composite Beam

The composite beam utilized in the Tom's Creek Bridge rehabilitation was manufactured by pultrusion. The beam (Figure 1-3) has a double-web design with sub-flanges and is composed of glass and carbon fibers in a vinyl ester matrix. The resin system being utilized is Dow Chemical's Derakane 411-350; the manufacturer typically adds at least 10% styrene by weight, as well as some additional filler, during the pultrusion process. Glass roving, 0/90° and ±45° fabric, and continuous strand mat (CSM) are utilized throughout the section, while carbon fiber tows are dispersed in the flanges to provide greater flexural rigidity. The carbon fiber type is either Hercules AS4 36k or AKZO 50k tow, while the glass fiber is E-glass (various manufacturers). The targeted fiber volume fraction (both carbon and glass) is around 55% by weight. The fiber architecture (layup) is proprietary, but the web and flange sections are essentially quasi-isotropic in lay-up with the flanges also containing carbon fiber laminae. The double-web design and sub-flanges provide increased resistance to buckling, torsion, and shear deformation. Beams measuring 6.10 m (20 ft) long were provided for this project, and the manufacturer quoted a weight of 163 N/m (11.2 lbs/ft) [61]. The beam's geometric details are summarized in Table 2-1.

The ATP objectives called for production and marketing of a commercially viable beam manufactured with phenolic resin, rather than vinyl ester, to provide fire retardance. The vinyl ester beam was simply a first effort at refining the manufacturing process. Strongwell also provided several of the early phenolic resin beams for testing, although the manufacturing process had not been finalized. The vinyl ester resin does not provide the fire retardance desired for many infrastructure or industrial applications, but the cost is less than the phenolic resins and the mechanical properties are usually much better as compared to phenolic resin composites. The vinyl ester beams do not contain any UV inhibitors like most of Strongwell's standard structural shapes (EXTREN® products), but the beams do contain carbon black filler which should provide some protection against UV radiation.

2.2 Beam Testing

2.2.1 Strength Tests

Both a vinyl ester and a phenolic resin beam were tested in a four-point bending geometry to failure in order to determine the failure mode(s) and ultimate strength of each type of beam for the 5.33 m (17.5 ft) span length to be utilized in the Tom's Creek Bridge (Figure 2-1 and Figure 2-2). Four-point loading was chosen to provide a region of constant moment under the loading. Steel support and test frames were constructed in the Civil Engineering Structures and Materials Research Laboratory at Virginia Tech. The composite beam was supported at the ends by rollers (pin-roller boundary conditions) spaced at a width of 5.33 m (17.5 ft), so that the beams extended 38.1 cm (15.0 in) beyond the support rollers at each end. A short steel spreader beam was utilized to apply a load at the mid-span. The spreader beam was supported by the composite beam via two steel rollers to apply load at two points 30.5 cm (1 ft) off-center. Ball-and-joint restraining arms were utilized to prevent lateral movement of the composite. The arms were attached near the quarter-point locations by clamping to the top and bottom flanges; neoprene pads were placed between the steel and composite to prevent wearing of the composite. The other ends of the restraining arms were bolted to the rigid load frame. Identical restraining arms were also used to stabilize the steel spreader beam (see Figure 2-1). These restraints were utilized to prevent out-of-plane buckling and to force local material failure.

Load was applied at the mid-span using an 890 kN (200 kip) manual hydraulic actuator, and load data was measured using a 2220 kN (500 kip) load cell. Deflections were monitored at the center, left quarter, and left and right ends (7.60 cm from the support rollers) using wire potentiometers, which were attached to the top flange of the beam. Bending strains on the top and bottom flanges at the mid-span were measured with a pair of strain gages located 1.90 cm (0.750 in) from the edges of the flanges. Shear strains in the middle of the web were measured 223 cm (89.0 in) from the left roller support just outside the region of constant moment and 17.8 cm (7 in) from the left support (see Figure 2-2). Shear strains were measured on both sides of the web section and then averaged[1]. Data was collected using an Optim Electronics MEGADAC 3108 AC acquisition system. The vinyl ester beam was loaded to 53.3 kN (12 kips) and unloaded, and then this was repeated for progressively higher loads: 67.0 kN (15 kips), 116 kN (16 kips), and to failure (130 kN or 29.2 kips). The third loading cycling was stopped at 116 kN (16 kips) when an unusual AE event was detected. The phenolic beam was similarly loaded to 53.3 kN (12 kips), 67 kN (15 kips), 71 kN (16 kips), and then to failure (107 kN or 24 kips).

2.2.2 Low-Load Proof Tests

The 24 beams to be utilized in the bridge repair, plus two additional beams, were tested to between 22.2 and 31.1 kN (5 and 7 kips) in the elastic region only, in order to obtain effective bending stiffness values. This information was desired to both evaluate the quality control of the manufacturing process and to optimize the bridge design (by strategically placing the stiffest beams at the predicted locations of highest stress). For these tests, the same four-point bend setup (as used for the strength tests) was utilized, but lateral restraints on the composite and steel spreader beams were not employed. The roller supports for the spreader beam were also replaced with rubber bearing pads. Roller supports were again used at the ends, and all other geometric dimensions remained the same. A single strain gage was placed in the middle of the flange on both the top and bottom sides of the beams. Shear gages were also placed near one end support, on only one side of the web. Deflections were monitored at the left end, left quarter, and center locations. Acoustic emission was not monitored for these tests. The beams were loaded for two or three cycles only.

[1] Members of the Non-Destructive Testing Laboratory at Virginia Tech also monitored acoustic emission (AE) at key locations.

2.2.3 Fatigue Testing

Traffic monitoring at the Tom's Creek Bridge indicates that some 1000 vehicles, 95% of which are primarily cars, cross the bridge each day [62]. In the planned 10-year life of this structure then, the bridge should carry 3 to 4 million vehicles. In order to evaluate the fatigue resistance of the composite beams for the bridge's predicted service life, a dynamic loading test was initiated. Using a four-point bend set-up similar to that used in the monotonic testing, a beam was cycled between loads of 147 and 14.7 kN (3300 and 330 lbs) at slightly over 1 Hz (64 cycles per minute). This is the maximum mid-span load originally predicted for HS20-44 loading[2].

The beam was supported by a pin-roller configuration with 3.18 mm (0.125 in) thick neoprene pads between the beam and the roller plates at a span width of 5.33 m (17.5 ft). Load was applied using an MTS servo-hydraulic actuator and an MTS 458 controller and measured using an in-line 222 kN (50 kip) load cell. The load was applied to a steel spreader beam resting upon 2.54 cm (1 in) thick rubber pads spaced 61.0 cm (2 ft) apart or 30.5 cm (1 ft) off-center on the top flange. Again, the spreader beam was prevented from moving laterally using restraining arms and the ends are restrained using steel angles clamped to the steel support beams. 6.35 mm (0.25 in) thick polyethylene plates were inserted between the angles and the beam to prevent wearing of the outer flange edges (see Figure 2-3).

Fatigue loading was conducted to 3 million cycles, with periodic interruptions for inspection by an acousto-ultrasonic technique and to perform a low-load, quasi-static test. This test provided a measure of the remaining stiffness of the beam. Here, the beam was loaded to 13.3 kN (3 kips) and center and quarter deflections were monitored using LVDT's. Bending strains were also monitored at the top and bottom flanges and shearing strains were monitored in the web just outside one loading point.

[2] The analytical model utilized in these predictions is discussed in detail in Chapter 4.

2.2.4 Creep Test

A distributed load creep test was initiated to determine the rate of deformation under sustained loading at room conditions. The setup involved a load of 7.87 kN (1770 lbs) distributed over the length of a vinyl ester beam using sandbags; this was near the estimated dead weight of the deck and asphalt overlay system. The ends of the beam were supported at a span of 5.33 m (17.5 ft). Deflections at the center and quarter points and near the ends were measured periodically with dial gages (Figure 2-4). The laboratory environment was not strictly controlled, so that the temperature and humidity varied somewhat with the ambient weather; the experiment was conducted from October to April for a total of 178 days.

2.3 Bridge Mock-up Testing

A full-scale mock-up of the Tom's Creek Bridge structure was constructed in the Civil Engineering Structures and Materials Research Laboratory. A loading frame was built around the bridge structure to provide a means to simulate axle load and provide a simulated foundation for the bridge[3]. Steel W27 x 84 beams were used to simulate the existing concrete abutments. These foundation beams were spaced to provide an unsupported span length of 5.33 m (17.5 ft) and skewed at an angle of 12.5°. Steps were taken to constrain the foundation beams using the structural floor and the steel load frame (see Figure 2-5 and Figure 2-6), and a 6.35 mm (0.25 in) thick rubber pad was laid along the top flange of the foundation beam to prevent abrasion of the composites. The 24 composite beams were then spanned across the foundation beams, spaced according to Figure 1-4. The outer 7 beams of both sides (14 total) were spaced 26.7 cm (10.5 in) apart, while the central 10 beams were spaced 30.5 cm (12 in) apart. The beams were arranged so that the stiffest beams were closest to the outer edges (see Section 3.5). The bridge structure was designed as such, since the distribution of load over the beams is

[3] Dr. Jack Lesko (committee chairperson for the author) and Dr. Thomas Murray of the Department of Civil Engineering designed the steel load frame, and Dennis Huffman and Brett Farmer, technicians in the Department of Civil Engineering, assembled the frame in the lab.

smaller when the load is applied near either side edge. (The distribution of load is essentially truncated near the outer edges of the bridge). The load distribution can be improved at the edges by decreasing the spacing between the beams (effectively increasing the number of beams per unit width).

The same glulam deck employed in the rehabilitation was also utilized in the laboratory test. The seven timber deck sections (7.47 m long x 86.4 cm wide x 13 cm thick, or 240 in x 33.3 in x 5.13 in) were secured to the composite superstructure at the skew angle of 12.5°, so that they ran parallel to the foundation beams (Figure 2-7). The decking was secured to the composite beams using 17.8 or 21.6 cm long (7 or 8.5 in, depending upon the beam spacing) 2 x 4 lumber and lag bolts (1.59 cm diameter x 15.2 cm long, or 0.625 in x 6 in) as shown in Figure 2-8. The actual connections in the field were to be through-bolt connections, so the lag bolts were used in the lab to minimize the number and depth of holes put in the deck prior to construction. Not all of the deck-to-beam connections were made in the test, but were varied in two connection sets to assess the effect of connections on composite action. These connections are positioned according to Figure 2-9.

The steel test frame constructed over the bridge mock-up allowed for the placement of actuators to complete various loading scenarios. Five different types of loading were performed (illustrated in Figure 2-10 and Figure 2-11):

- HS20-44 loading (42 kips total axle load = 32 kips + impact factor of 1.3) distributed to two wheel loading patches (93.4 kN or 21 kips) positioned 61.0 cm (24 in) from the right edge and centered on the right half of the bridge. A 1.83 m (6 ft) long steel spreader beam was utilized to distribute the load to the two (50.8 cm long x 30.5 cm wide, or 20 in x 12 in) wheel patches (Figure 2-12) and was oriented perpendicular to the underlying composite beams. (both connection sets)
- Two tandem HS20-44 loads (both 42 kips for a total of 84 kips, or 4 wheel loads at 21 kips each) with the second loading applied to the left side of the bridge mock-up in-line with the original load. (connection set 1 only)

- A single HS20-44 load centered in the middle of the bridge. Again, two wheel loads of 21 kips were applied. (connection set 2 only)
- Single 21 kip patch load at the center of the bridge (connection set 2 only)
- Single 21 kip patch load located 152 cm (60 in) from the right side of the bridge (connection set 2 only). This load was applied in-line with the previous load, rather than being centered on the right portion of the bridge.

The last two loading types were performed for verification of the analytical bridge model (Chapter 4).

Hydraulic actuators with capacities of 445 kN (100 kips) were used to apply the load and load cells with a 222 kN (50 kips) capacity located at each actuator measured load. Strain gages were mounted at several locations to measure bending strains on the flanges of the composite beams:

- Mid-span (2.67 m or 8.75 ft) on the bottom flange of all 24 beams (referred to *as center bending strains*)
- 86.4 cm (34 in) off-center on the bottom flange of beams 1 through 12 to measure strains directly under the second/tandem loading (*tandem bending strains*)

For the single patch load tests, only center bending strains were recorded.

Strains on the top surface of the middle timber deck section were also monitored using extensometers rigidly mounted to the wood. These extensometers were oriented directly above and parallel to composite beams 14, 16, 18, 20, and 24. Another pair of extensometers was mounted on both the top and bottom surfaces of the deck between composite beams 20 and 21. The extensometers were attached to aluminum posts that were anchored to the wood surface (Figure 2-13). The timber deck deflections along the centerline of the deck (i.e. in-line with the center bending strain gages) were measured using wire potentiometers positioned as described for each of the cases (see the results). In addition, for select cases, the deflections at the gap between the two deck panels nearest the loading were monitored to determine the relative panel deflections. This data was recorded to investigate the potential for damage to the overlay caused by large relative panel deflections. The load, strain, and deflection signals were all input and balanced in the data acquisition system.

2.4 Figures and Tables

Table 2-1. Summary of dimensional information for composite beam.

	SI	English
Total depth height	20.3 cm	8 in
Flange width	15.2 cm	6 in
Flange thickness	1.57 cm	0.620 in
Outer width of web box section	7.62 cm	3 in
Web thickness	0.914 to 1.07 cm	0.360 to 0.420 in
Area	88.4 cm^2	13.7 in^2
Moments of inertia	I_{zz} = 5350 cm^4 I_{yy} = 1320 cm^4	I_{zz} = 129 in^4 I_{yy} = 31.7 in^4

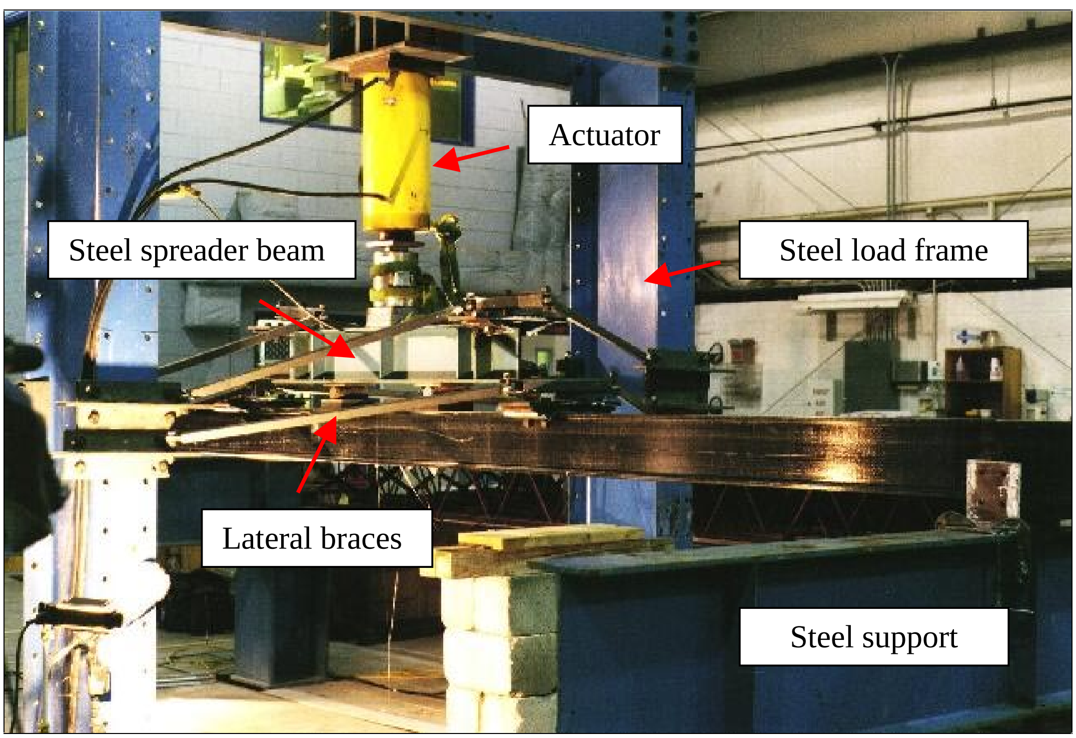

Figure 2-1. Four-point bending test on composite beam.

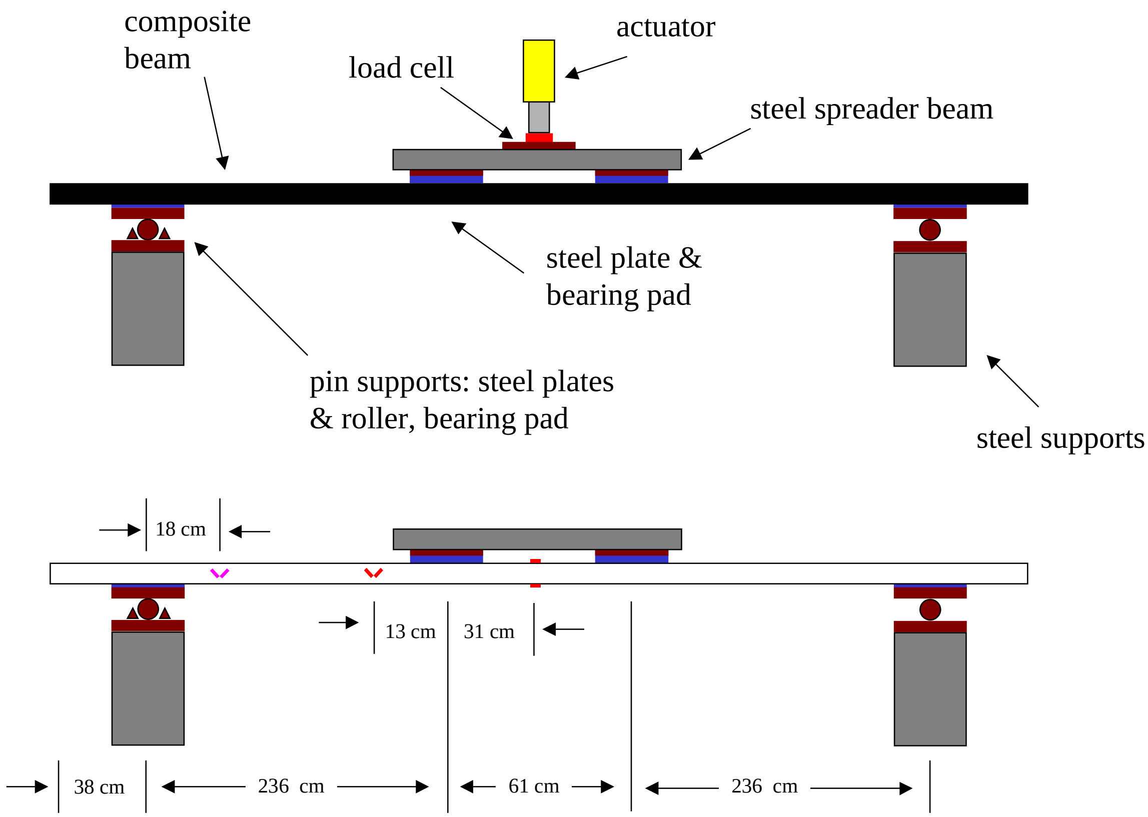

Figure 2-2. Schematic of four-point bend geometry. Strain gages are shown in red and pink (failure tests only). Note that the pin supports were also used under the spreader beam for the tests to failure; they are not shown here. The lateral restraints are also not shown.

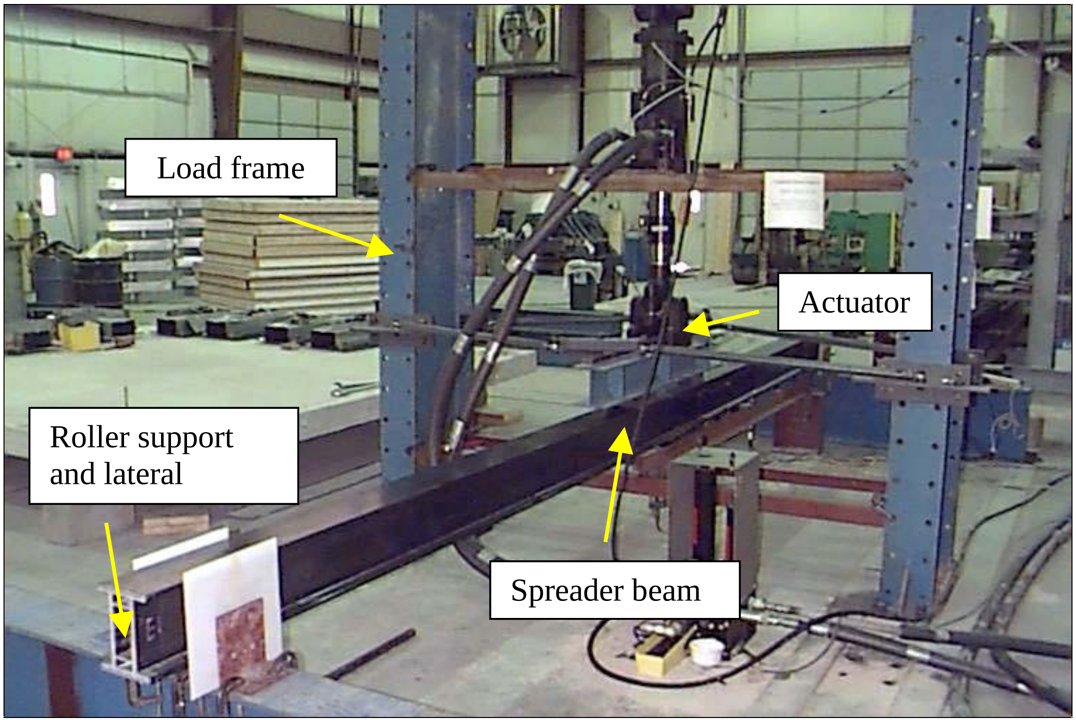

Figure 2-3. Bending fatigue set-up.

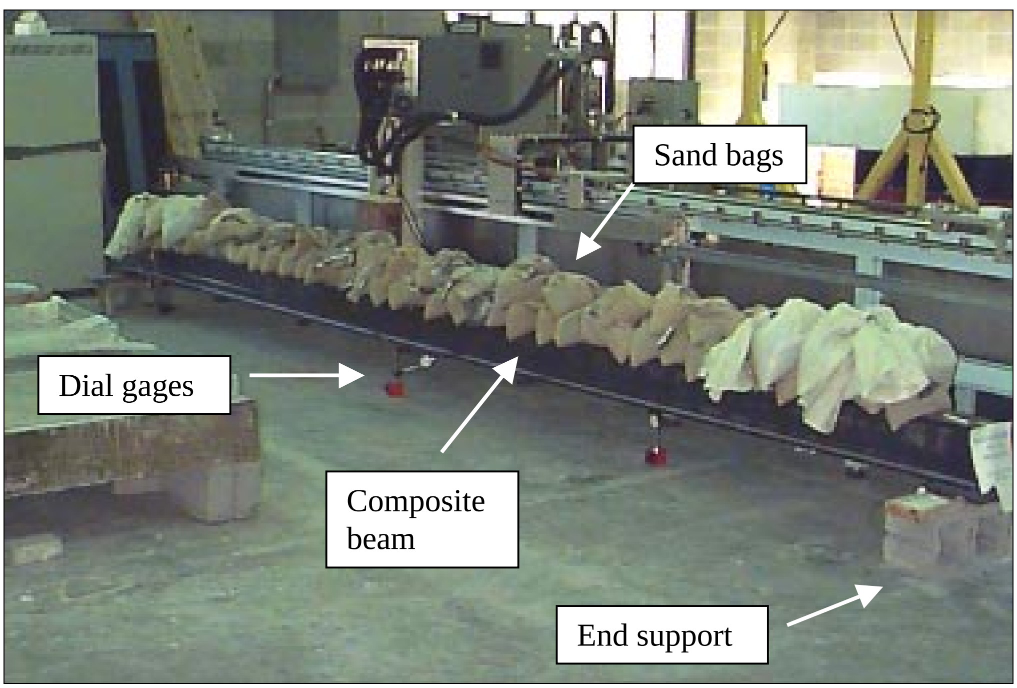

Figure 2-4. Distributed load creep test set-up.

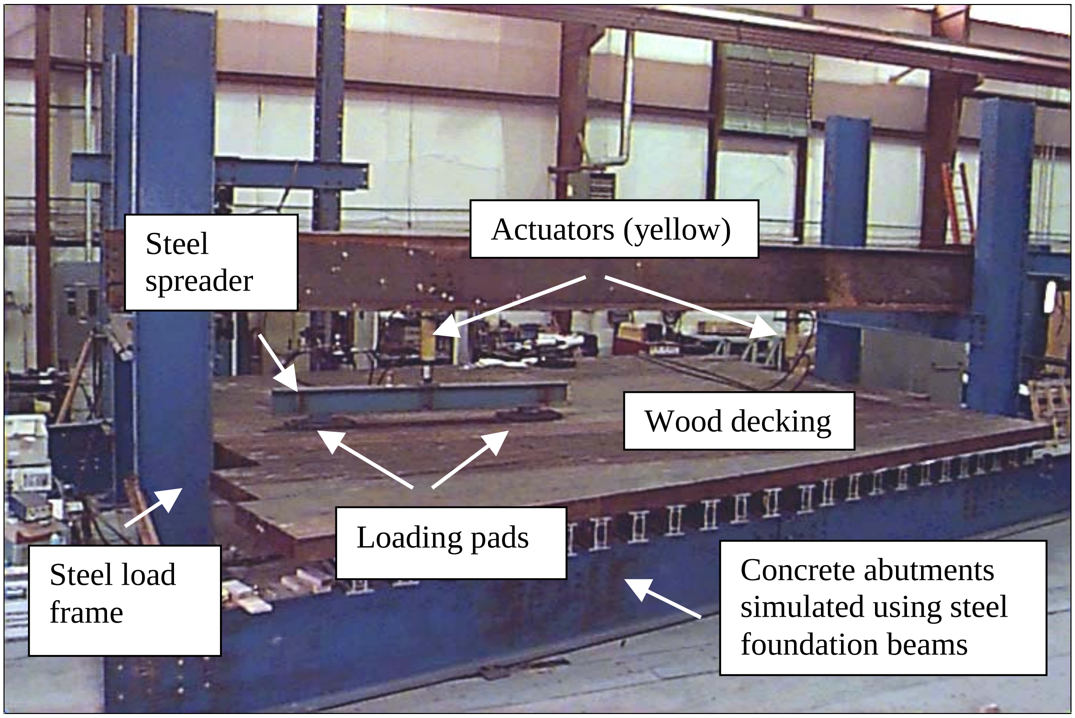

Figure 2-5. Laboratory mock-up test set up.

Figure 2-6. Overhead view of test set up.

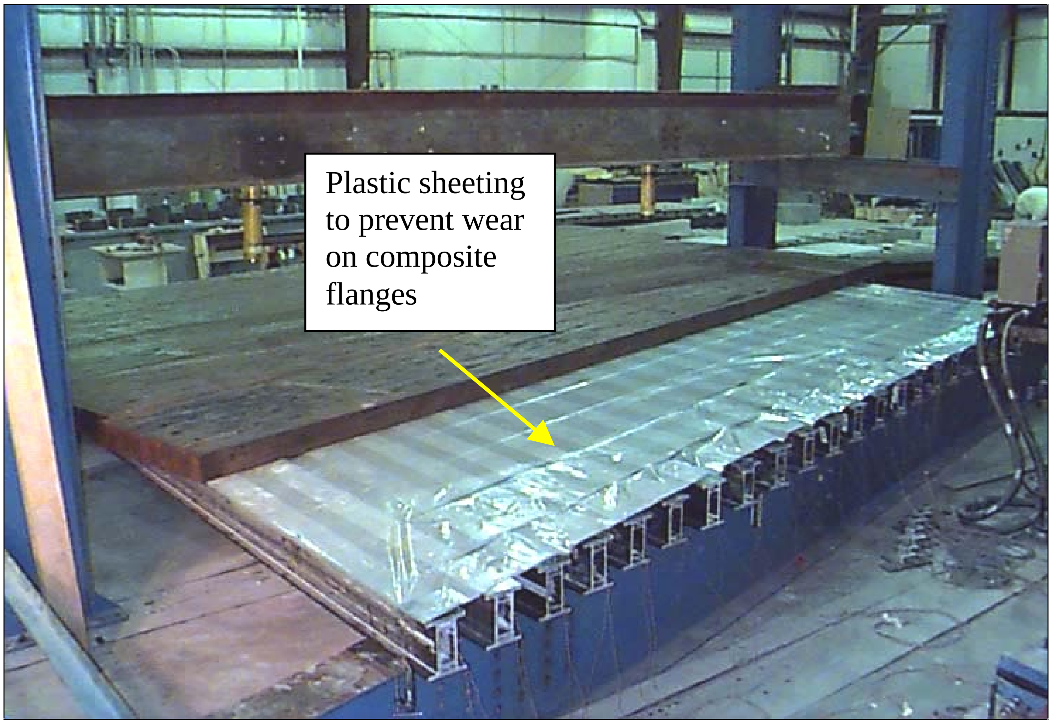

Figure 2-7. Assembly of bridge mock-up in the laboratory.

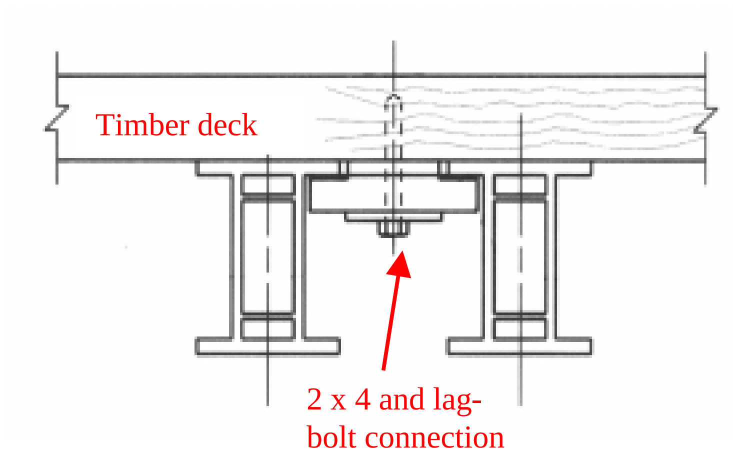

Figure 2-8. Schematic of beam-deck connection.

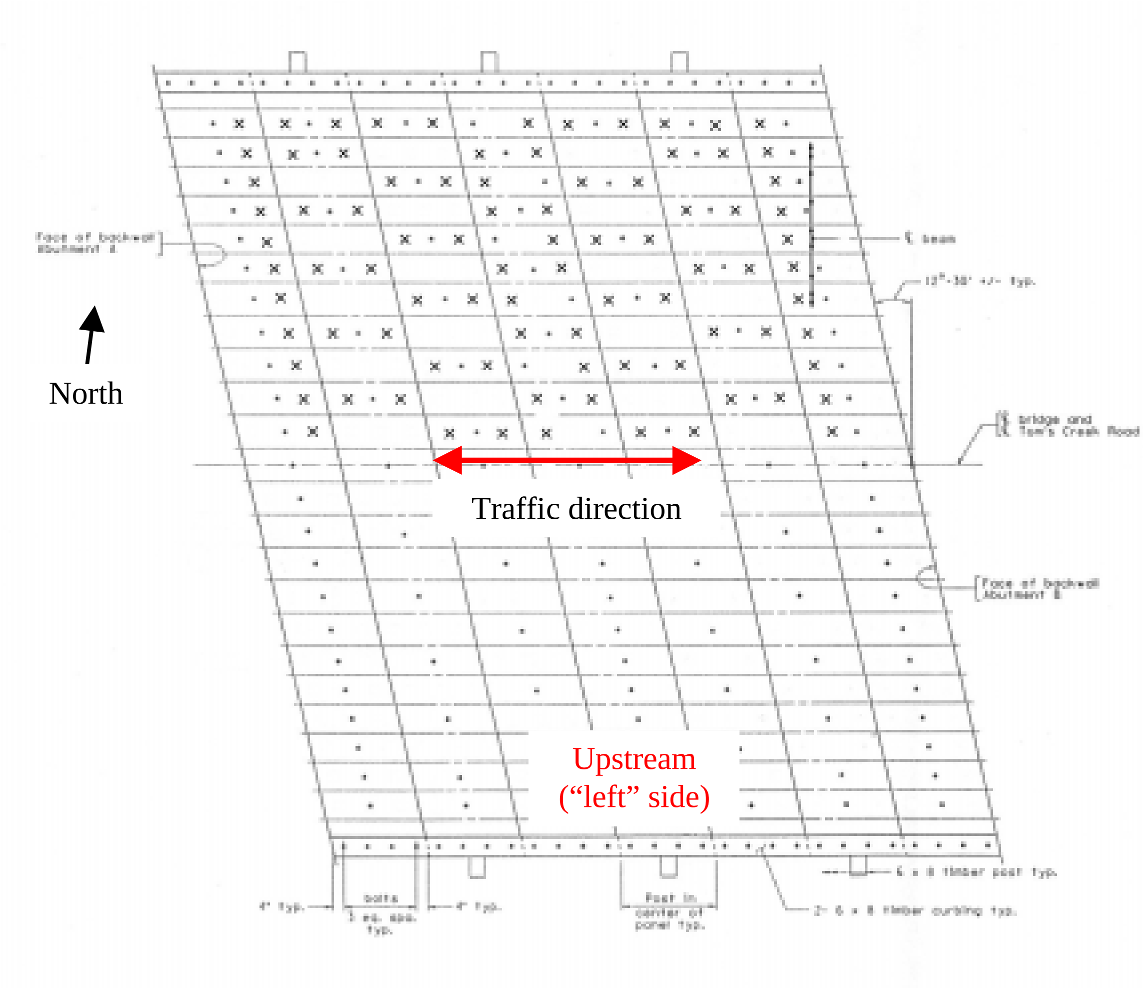

Figure 2-9. Two different connection sets utilized in the laboratory bridge testing. The first (single) connections are designated by dots; the additional connections (forming the second connection set) are designated by X's. (Also, refer to Figure 1-5.)

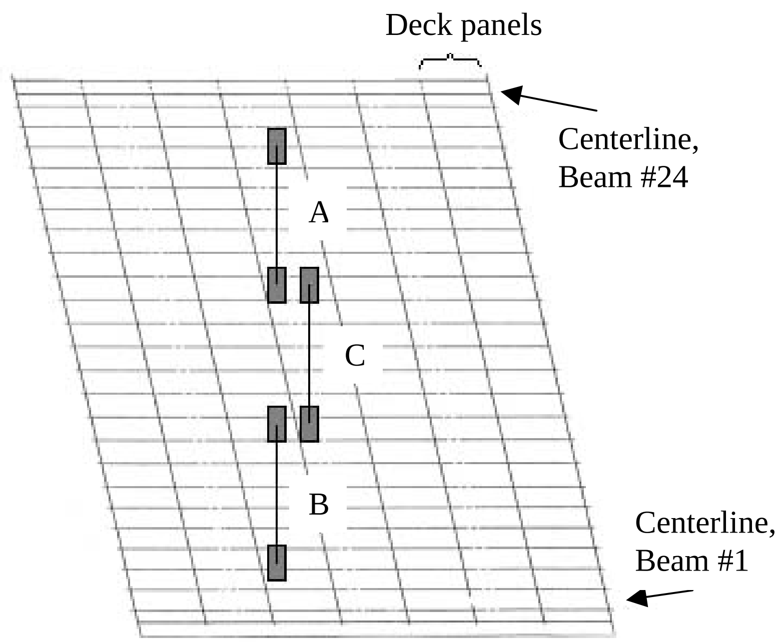

Figure 2-10. Loading scenarios applied for the HS20 loading tests

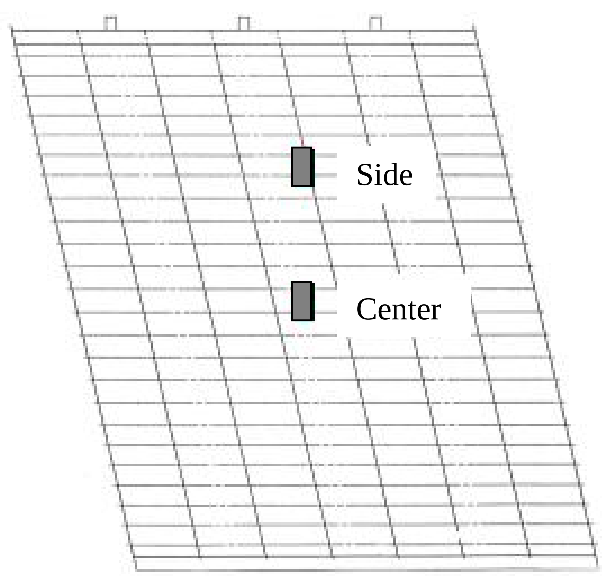

Figure 2-11. Loading scenarios for single patch load tests.

Figure 2-12. Close-up of wheel patch underneath spreader beam.

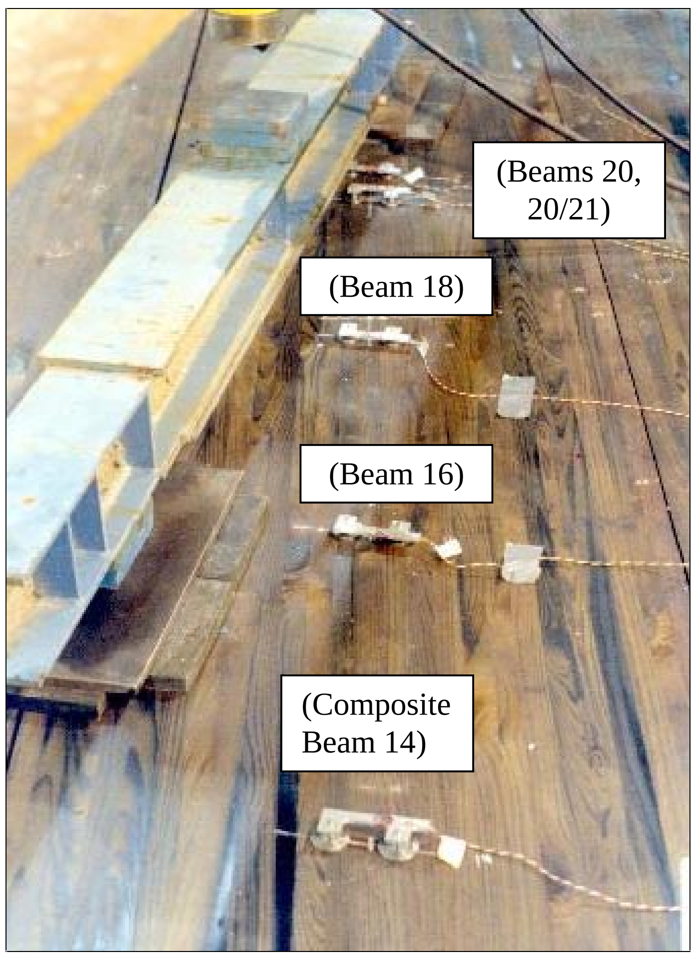

Figure 2-13. Arrangement of deck extensometers relative to loading patches.

Chapter 3: Experimental Results and Discussion

3.1 Strength Tests

Both the vinyl ester and phenolic beams exhibited fairly linear behavior up to failure, although the vinyl ester beam had both a higher stiffness and strength. The progressive loading cycles up to failure for the vinyl ester composite beam are shown in Figure 3-1. The response is very linear with little hysteresis upon unloading. Some audible noise was detected at 116 kN (26 kips), and upon unloading there was some slight hysteresis that was, perhaps, indicative of damage. However, the final loading to failure indicated no loss in stiffness. Failure of the vinyl ester beam occurred at 130 kN (29.2 kips). The phenolic beam demonstrated a similar linear response up to failure with a strength of 107 kN (24.0 kips).

Center/mid-span and quarter-point (1.8 m from support, 1/3 of span) deflections with load are shown for both beams up to failure in Figure 3-2. Mid-span bending strains from the top flange and center web shear strains are compared for both beams in Figure 3-3. The data indicate higher stiffness, strength, and strain to failure for the vinyl ester beam. To calculate an effective bending modulus for each beam, the modulus at each increment of load was calculated using the mid-span strain data and Euler beam theory (assuming no shear deformation):

$$E = \frac{Mc}{I\varepsilon} \tag{3.1}$$

where ε is the strain at the outer surface of the beam due to an applied moment M. E is the bending modulus and I is the area moment of inertia. An average bending strain was calculated using the top and bottom readings and this value was utilized in Equation (3.1). It is noted that the bottom flange strains were consistently (although only slightly) larger than the top flange strains, possibly indicating some upward shift in the neutral axis.

This calculated modulus value represents the actual bending modulus due only to bending deformation, since there is no shear between the loading points in a four-point geometry with simple boundary conditions. A similar calculation could be performed using deflection data instead, but this deflection would include both bending and shear deformation. The effective modulus versus load for both beams is plotted in Figure 3-4. An approximate value for the modulus was calculated by performing a linear regression on the data between 22.2 and 111 kN (5 and 25 kips) and then utilizing the fit to determine the modulus at 66.7 kN (15 kips). The properties of the two beams are summarized in Table 3-1.

For both beams, failure occurred by a delamination in the top (compressive) flange underneath one loading point (Figure 3-5 and Figure 3-6). The delamination occurred not at the interface of the flange and web, as is often observed for pultruded fiberglass beams, but rather within the flange. The delamination actually occurred at the interface between the lower, all-glass section of the top flange and the upper section which contains the carbon fiber; this failure mechanism can be attributed to high interlaminar stresses between the glass and carbon laminae. The delamination was followed by web buckling and compression failure of the carbon flange section, similar to that observed by others for all-glass beams [41,44,46]. The response was linear-elastic up to failure, and while the failure was sudden, the bottom flange remained intact and the beam was capable of carrying further load. This behavior may be considered to be favorable for civil engineering designs, as the failure was not truly catastrophic (i.e. resulting in total collapse of the beam). However, it is important to recall that these tests were performed using lateral constraints to prevent lateral-torsional instability; the buckling load may be lower than this ultimate strength load.

3.2 Proof Tests

The 26 vinyl ester beams that were proof tested were actually manufactured and shipped to Virginia Tech in two different batches. Beams 1-10 and 26 are referred to as "Batch 1" and 11-25 are referred to as "Batch 2". Effective bending moduli were calculated for each beam using the procedure outlined in the previous section, except that the regression was performed between 13 and 22 kN (3 and 5 kips), and the 18 kN (4 kips) value was utilized. The Batch 1 beams were noticeably stiffer than the second batch. This variation was attributed to a change in the manufacturing process in which carbon fiber with a slightly lower modulus (purchased from a different vendor) was utilized to manufacture the beams[4]. Weibull statistics for each batch were determined, and these calculations are summarized in Appendix A. The Weibull modulus values and other statistics, including A and B allowables, are summarized in Table 3-2. The Weibull modulus for the two different batches were 48.1 GPa (6.98 Msi) and 44.3 GPa (6.43 Msi), with Batch 1 demonstrating a 9% higher average modulus. The average over the 25 beams is 48.9 GPa (6.65 Msi). The Weibull cumulative probability is in shown in Figure 3-7 for the two different batches to demonstrate the difference in modulus values. Results from a student's two-sample t-test assuming equal variances indicate that the mean modulus for the two different batches are in fact significantly different: t (8.36), $p<0.05$.

3.3 Fatigue Testing

The response of the composite beam subjected to fatigue cycling showed no appreciable change in stiffness through 3 million cycles. The load-deflection response at each increment of fatigue cycles is shown in Figure 3-8. A similar plot for strains is shown in Figure 3-9. As in the previous testing, an effective bending modulus was calculated for each quasi-static test using bending strains. Here, the regression was performed between loads of 4.45 and 13.3 kN (1 and 3 kips) and the calculated value at 11.1 kN (2.5 kips) was utilized. These effective bending modulus values are plotted against the number of fatigue cycles in Figure 3-10. Again, this plot indicates no real loss in modulus with cycling up to 3 million cycles.

[4] AKZO 50k fiber with a modulus of 193 GPa (28 Msi) was substituted for Hercules AS4 36k fiber with a modulus of 234 GPa (34 Msi).

3.4 Creep Test

Deflection data for the distributed load (7.87 kN or 1770 lbs) creep test was recorded for 178 days. The near-end beam deflections were subtracted from the mid-span deflections to exclude the deflection of the end supports from the data. After the 178 days, the beam deflected 0.043 cm (0.170 in) from an initial deflection of 0.743 cm (0.293 in), and the rate of change of the deflection was nearly zero.

In the absence of strain data, it is difficult to draw any conclusions regarding the type of response that this particular composite beam demonstrates. As a simple exercise in characterizing the shape of the deflection response, a three-parameter viscoelastic solid type model was utilized to fit the deflection data:

$$\delta(t) = \delta_0 + b\left(1 - e^{-t/\tau}\right) \tag{3.2}$$

where b and τ are constant parameters and δ_o is the initial deflection upon application of the load. The parameter τ is referred to as the relaxation time constant and characterizes the time at which the deflection has reached 63% of its total/final deflection. Values of 1.08 cm (0.427 in) and 65.1 days were obtained for b and τ, respectively, by fitting the model to the data. The data and fit are plotted together in Figure 3-11. The same plot is shown again in Figure 3-12 using a logarithmic time scale in order to observe the apparent plateau in the deflection at about 200 days.

3.5 Bridge Mock-Up Testing

As mentioned in Section 2.3, the composite beams were arranged in the bridge design according to their effective bending modulus values. The stiffest beams (Batch 1), were positioned as the five outer beams on each side, with the Batch 2 beams positioned between the Batch 1 beams. The beams were then renumbered according to their position from the upstream side of the bridge (in the actual design). The upstream side of the bridge is referred to as the left side for the lab mock-up testing (see Figure 1-5). The positioning and modulus of each beam utilized in the bridge design is summarized in Table 3-3. Prior to the selection of beams for the bridge design, all of the proof-tested beams were evaluated using infrared thermography and acoustic emission in order to detect any manufacturing defects[5]. Based on this screening, Beams 1 and 16 were excluded from the bridge design. Beam 16 had an obvious "dry patch" on one flange, where the resin had not completely wet-out the fibers. Beam 1 was found to have a small delamination within one flange. Beams 2-15 and 17-26 were thus selected for use in the bridge. It is noted that beam 26 was utilized in the creep test (detailed previously); this beam was positioned near the upstream edge of the bridge (beam 2 location) for easy removal in the future as part of the long-term durability study.

For each particular investigation detailed below (different loading scenarios, different connection sets, etc.), a number of tests were conducted in order to obtain multiple data sets. In addition, the acquisition system was limited to eight input channels for full Wheatstone bridge transducers (1-2 for load and 6-7 for deflection or deck extensometers) and 36 channels for quarter-bridge transducers (strain gages). Therefore, in order to obtain all of the necessary data, multiple runs with different input signals were required. Data was recorded continuously for loading up to 187 kN (42 kips) and unloading, but only data at the peak 187 ± 4 kN load is presented below. In cases where more than 6 or 7 deflection points or 36 strain readings are presented together (e.g. in order to construct a plot showing data across all 24 composite beams), data from several tests were combined.

3.5.1 Single Patch Loads

The single patch load tests were actually performed after all of the other tests, but these results are presented here first for convenience. Note that the triple connection set was utilized (see Figure 2-9). Center bending strains only (no deflections) were recorded

[5] Non-destructive screening was performed by Michael Horne, Ph.D. candidate in Engineering Science and Mechanics, and John Haramis, Ph.D candidate in Civil Engineering, under the direction of Dr. Jack Duke, Professor in Engineering Science and Mechanics.

for these tests. Under the 50.8 cm x 30.5 cm (20.0 in x 12.0 in) single loading patch in the center location, the maximum bending strain on a composite beam (average value on bottom flange) was measured to be 657 microstrain (657 x 10^{-6} cm/cm) on beam 13 at the 93.4 kN (21.0 kips) load. Under the side loading, a maximum value of 485 microstrain on beam 18 was measured. The strains on all of the composite beams for both loads are plotted in Figure 3-13. Here, the strains are plotted versus the position of the beam across the width of the bridge (measured from the centerline of Beam 1), along the centerline of the composite beams and the centerline of deck panel 4. The load patches for the center and side cases were located at composite beams 12/13 (over both beams) and 18/19, at 336 cm (132 in) and 518 cm (204 in), respectively. It is noted that the position of the deck beam along the length of each girder is different for the center and side loadings.

The distribution of the center patch load appeared to be concentrated over a small region (beams 10-15) indicating a low degree of load distribution, while the side load was distributed more evenly over a larger number of beams. It is also noted that the strains on beams 1 and 24 were slightly negative for the center loading indicating uplift of the outer edges of the bridge structure. This behavior can also be observed on beam 1 for the right side loading.

3.5.2 HS20 Loading at Side of Bridge

For this test scenario, loading case A (Figure 2-10) with single connections only, the wheel loads were positioned above composite beams 15/16 and 21/22, at 427 cm (168 in) and 610 cm (240 in) respectively, and the largest deflection and strain values were observed at beam 22. Deflections and strains for loading case A with the single connections are shown in Figure 3-14 and Figure 3-15. Notice the positive deflections and strains between composite beams 1 and 4 (0 to 82.0 cm/32.3 in). Again, this indicates uplift at the structure’s edges. The maximum strain level at the 187 kN (42 kips) axle load was under 1000 microstrain. This value is only 15.9% of the strain to failure measured for the vinyl ester beam (6300 microstrain) tested to failure. A maximum deflection of 2.74 cm (1.08) inches was measured at 187 kN. This indicates an L/195 deflection response, L/255 if the impact factor is excluded.

For the purposes of comparison, it is noted that field testing of the rehabilitated structure conducted in October 1997 indicated a much stiffer response at L/450 (including impact factor) [63]. Deflection data under the HS20 side loading from the field testing is also shown in Figure 3-14. The increased stiffness of the actual bridge as compared to the lab mock-up may be attributed to the use of more deck-girder connections, as well as differences in boundary conditions for both the composite beams and timber deck panels. For instance, the field structure utilizes girder-to-abutment connections, so that the composite girders are effectively clamped to the abutments, thereby increasing the effective stiffness of each beam. The curb rails should also provide some additional stiffness by tying the individual deck sections together, as illustrated in Figure 1-6.

While little or no composite action was expected in this design, it is useful to consider the deck panel strains that were measured on the top of the deck (recall Figure 2-13). These strains are plotted along with the composite bending strains in Figure 3-15. Strains of about 200 microstrain were recorded near the left loading patch indicating some load transfer to the deck. It is also interesting to note that the strains are mainly tensile; this may be due to twisting of the deck panel, as the loads were applied on a line skewed compared to the deck panels and the loads were not centered on the deck panels.

3.5.3 Tandem HS20 Loads

Deflections and strains were measured for the tandem loading situation (loading locations A and B, in Figure 2-10) to evaluate the effect of loading with two HS20 truck axles. The wheel loading patches were positioned over composite beams 3/4 (61.2 cm or 24 in), 9/10 (244 cm or 96 in), 15/16 (427 cm or 168 in), and 21/22 (610 cm or 240 in). Under this loading (93.4 kN or 21 kips at each wheel patch, 374 kN or 84 kips total), the maximum deflection was just under 2.54 cm (1 in) between composite beams 22 and 23 at a location of about 635 cm (250 in) (see Figure 3-16) . The deflections under the B-axle wheel loads were somewhat less (1.91 to 2.16 cm), because the B-axle was located closer to one end of the composite beams due to the bridge's skew. The maximum strain recorded was 923 microstrain on composite beam 22 (Figure 3-17). Again, the center bending strains are less on beams 1-12 due to the relative location of the loading caused by the bridge's skew. The deck strain response was nearly indentical to that observed with the HS20 side loading with a maximum tensile strain over 200 microstrain measured.

3.5.4 HS20 Side Loading: Effect of Connections

In order to determine the effect of the connections on the degree of composite action, additional connections (as illustrated in Figure 2-9) were added. On the right half of the structure (nearest the loading), two more spanner connections were added at nearly all of the connection sites for a total of three. Thus, the number of connections on that half of the structure was nearly the same as what is being utilized in the actual bridge. The structure was then loaded according to scenario A. The deflections and strains decreased slightly due to the additional connections (Figure 3-20 and Figure 3-21). For instance, the deflections decreased as much as 6% and the strains decreased as much as 8% at some locations. These improvements are better demonstrated by plotting the data in column charts, as in Figure 3-22 and Figure 3-23. The addition of connections appears to have improved the overall stiffness of the bridge structure, but the distribution of load did not seem to improve since the reduction in strains and deflections under the load were not accompanied by increases in these values on the opposite side of the structure.

3.5.5 HS20 Loading in Center of Bridge

Loading in the center of the bridge was next performed using connection set 2. The two wheel loads were located above beams 9/10 (244 cm) and 15/16 (427 cm), and the largest deflections at 187 kN (42.0 kips) were 2.01 cm (0.791 in) (see Figure 3-24). The largest strain value recorded was 760 microstrain on composite beam 15 (Figure

3-25). Both the deflection and strain profiles were fairly symmetric. Any differences from one side of the bridge to the other may be attributed to the additional connections on the right side or slight differences in the beam properties from one side to the other. The deflections and center bending strains for all three HS20 loading cases are compared in Figure 3-26 and Figure 3-27, respectively. These results demonstrate that loading away from an edge of the bridge (i.e. center loading) allows for a greater load distribution, and thus, lower deflections. It is also interesting to note that the addition of a second side load in the tandem loading case did not significantly affect the maximum deflection.

3.5.6 Displacement of Foundation Beams and Interpanel Differential Deflection

The relative motion of the deck to the abutments was a concern, as excessive relative displacement can damage the overlay. The deck panel deflections previously reported also included deflection associated with the foundation beams. Therefore, the displacement of one foundation beam on the side nearest the loads in load case A was monitored using dial gages. The maximum displacement was approximately 0.127 cm (0.05 in) at the edge of the top flange. Uplift at the ends of the beams were also measured and recorded to be approximately 0.1778 cm (0.07 in). This amount of deflection can be absorbed by the asphalt design which incorporates a fiber reinforced rubber membrane placed between the course base and the finish grade as noted by Howard et al. [64]. Thus, reflective cracking even in the presence of this degree of deflection should not present a problem for the long-term performance of the bridge. The reader is reminded that the traffic on this structure is low, and 95% of the traffic is two-axle commuter traffic.

The interpanel differential deflection (relative displacement between deck panels) was also measured between 1) panels 4 and 5 for the side loading (case A, with triple connections) and 2) panels 4 and 5, as well as 3 and 4, for the center loading (case C, triple connections). For both loading cases, the spreader beam and wheel patches were rotated around the axis of the actuator to investigate deflections when the load axle was both parallel and skewed relative to the deck panels. Of the two HS20 loading situations, the side loading was most severe. With the wheel patches (simulated axle) aligned perpendicular to the composite girders, in the traffic direction, the maximum interpanel differential deflection was 0.120 cm (0.0472 in). Here, the two load patches were applied to two different deck panels. The work by Howard et al. indicated that a maximum interpanel differential deflection of 0.127 cm (0.05 in) could be accommodated with this particular wearing surface design [64].

For the unlikely case where the axle is aligned with the skew or parallel to the decking so that both wheel loads are applied to the center deck panel (#5), the maximum relative displacement measured was 0.283 cm (0.111 in). This again is for the HS20 side loading case. The centerline of the spreader beam was located 22.9 cm (9 in) away from the edge of panel 5.

3.6 Figures and Tables

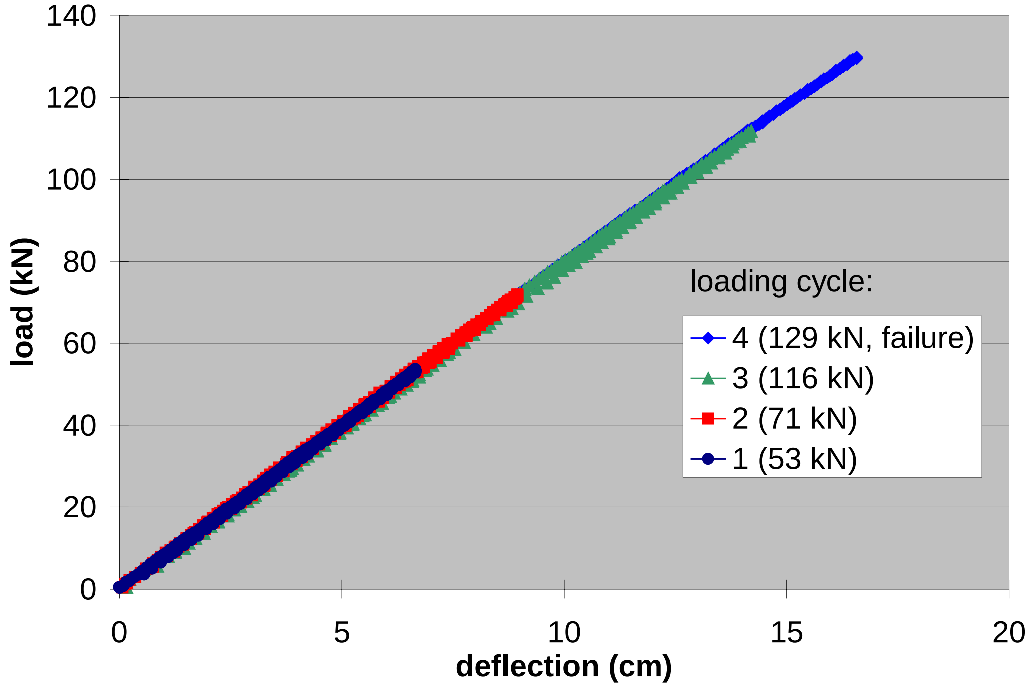

Figure 3-1. Progressive loading cycles up to failure on the vinyl ester beam.

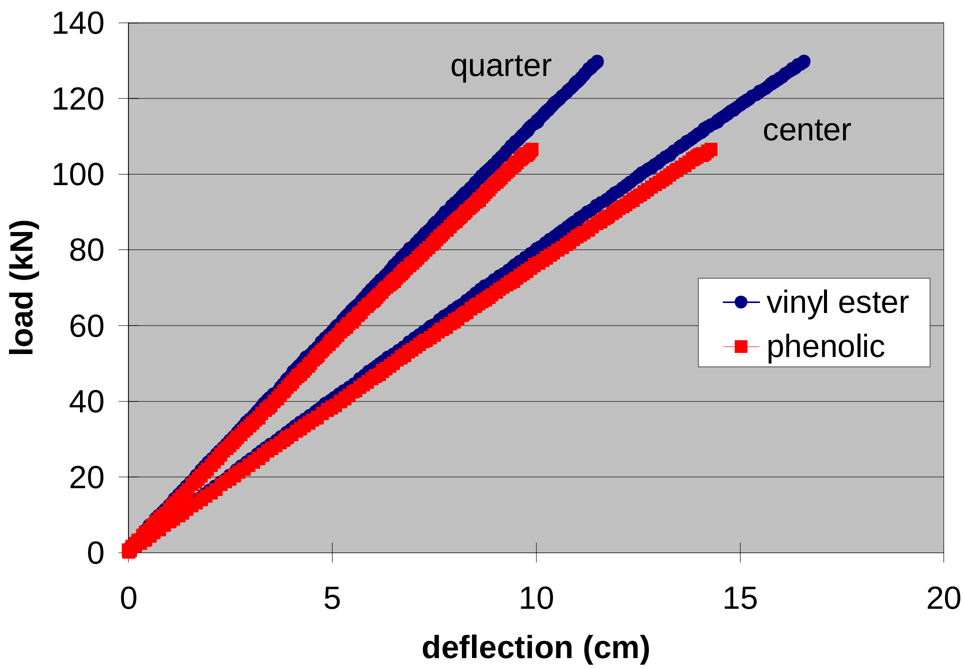

Figure 3-2. Comparison of deflection data for vinyl ester and phenolic beams.

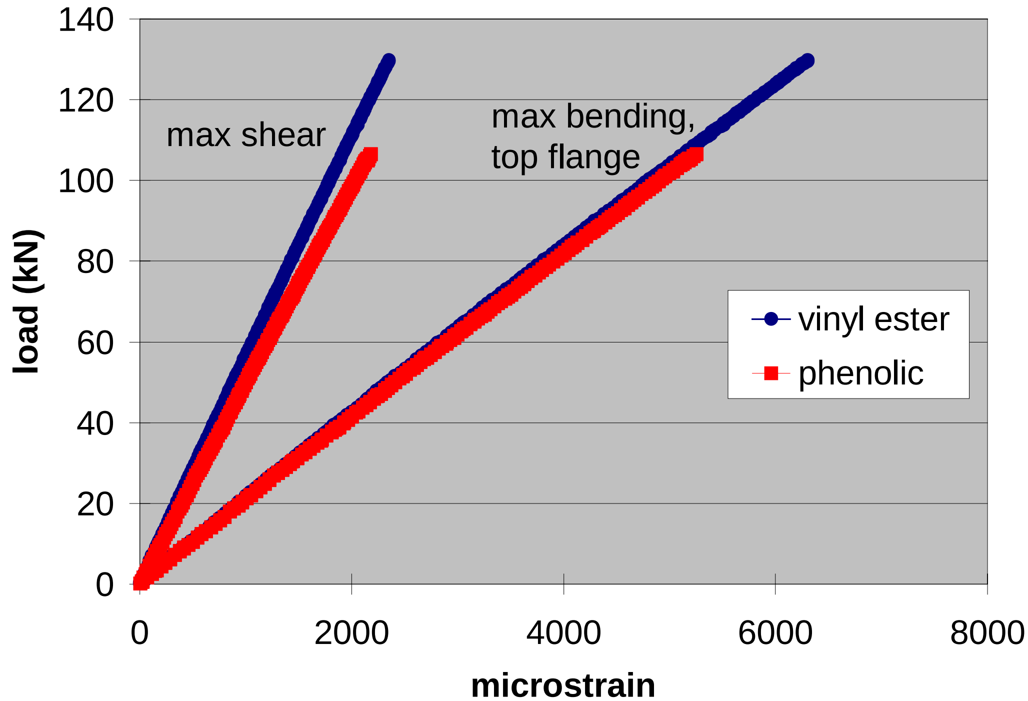

Figure 3-3. Comparison of shear and bending strains for vinyl ester and phenolic resin beams. (1 microstrain = 10^{-6} cm/cm)

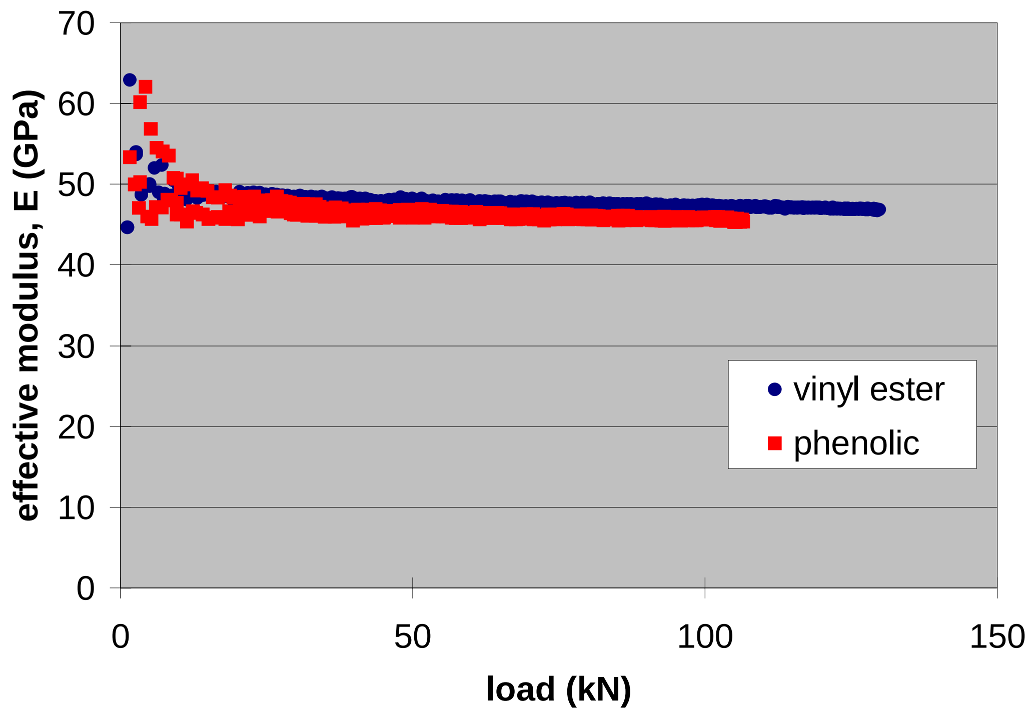

Figure 3-4. Effective bending modulus for both beams calculated using average bending strain data.

Table 3-1. Summary of basic beam properties under four-point bending for the two different resin types.

Resin type:	**Vinyl ester**	**Phenolic**
Effective bending modulus	47.8 GPa (6.93 Msi)	46.1 GPa (6.69 Msi)
Ultimate strength	130 kN (29.2 kips)	107 kN (24.0 kips)
Strain to failure	6210 microstrain (0.621%)	5270 microstrain (0.527%)

Figure 3-5. Failure of vinyl ester beam under four-point bending.

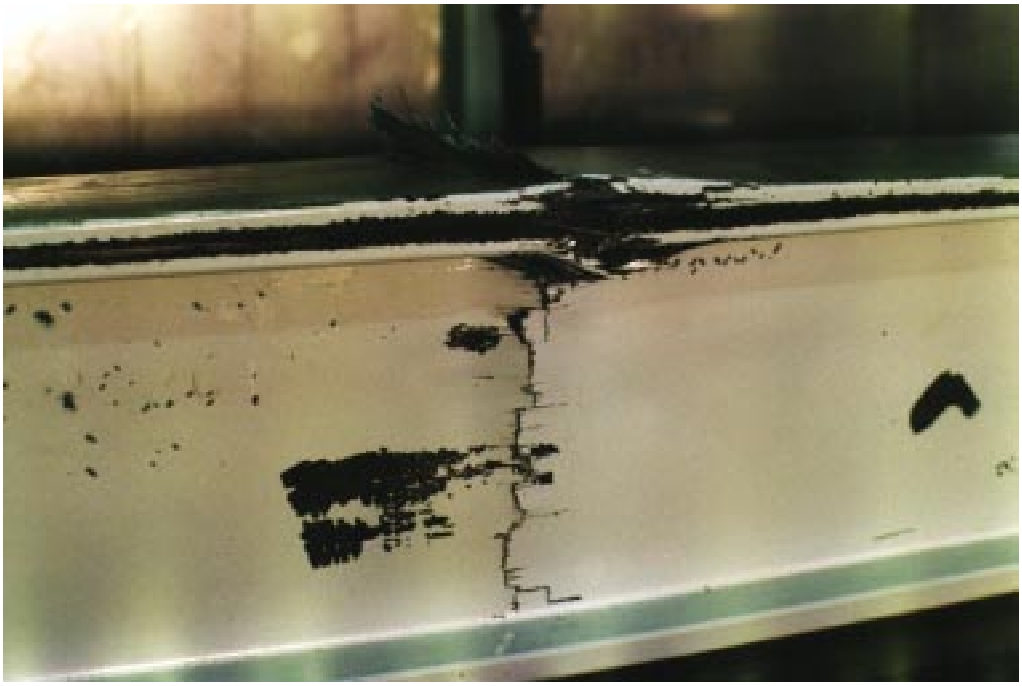

Figure 3-6. Close-up of failure site on vinyl ester beam showing delamination in flange and buckling of web.

Table 3-2. Summary of modulus values for beams 1-26.

Beam #	Modulus		Beam #	Modulus	
	GPa	**Msi**		**GPa**	**Msi**
1	48.7	7.07	**11**	42.7	6.20
2	48.4	7.02	**12**	44.2	6.41
3	45.6	6.62	**13**	44.0	6.38
4	48.7	7.06	**14**	44.0	6.38
5	49.1	7.12	**15**	44.4	6.45
6	46.5	6.74	**16**	42.9	6.22
7	48.1	6.97	**17**	43.6	6.33
8	47.8	6.94	**18**	45.6	6.62
9	48.2	6.99	**19**	46.1	6.69
10	49.2	7.14	**20**	46.7	6.77
26	47.6	6.90	**21**	44.3	6.43
			22	44.3	6.43
			23	45.1	6.54
			24	43.0	6.23
			25	44.7	6.48
Weibull mean*:	48.1 GPa	6.98 Msi		44.3 GPa	6.43 Msi
Weibull standard deviation:	1.19	0.173		1.33	0.193
A-allowable:	44.1	6.39		39.9	5.79
B-allowable:	46.2	6.70		42.2	6.12

*Weibull statistics were applied only to Beams 1-10 in batch 1; Beam 26 was not included.

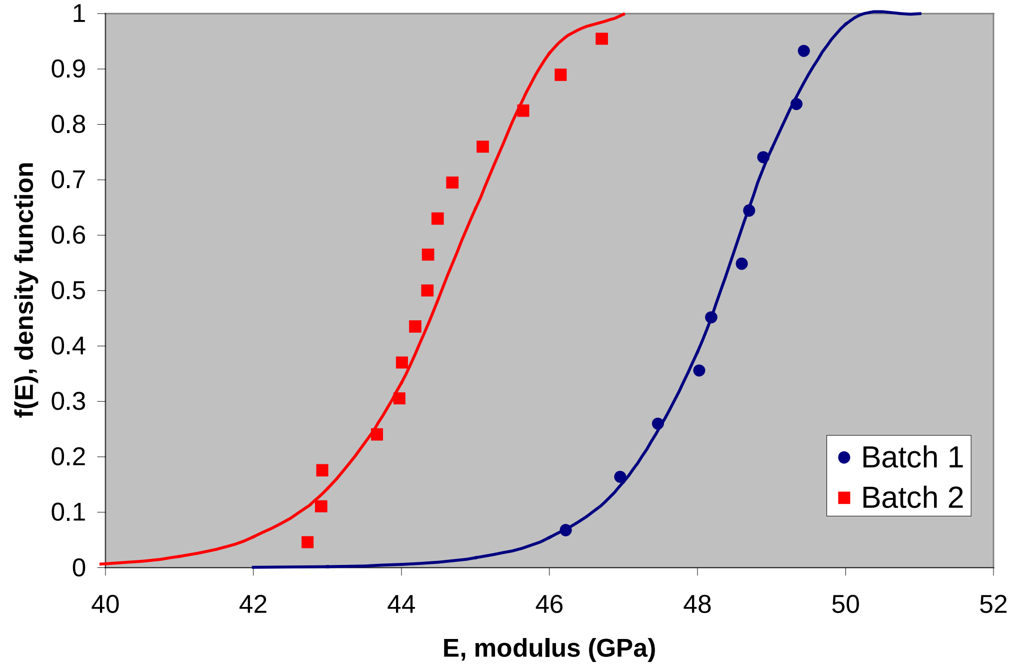

Figure 3-7. Weibull density function plot comparing modulus values for two different manufacturing batches.

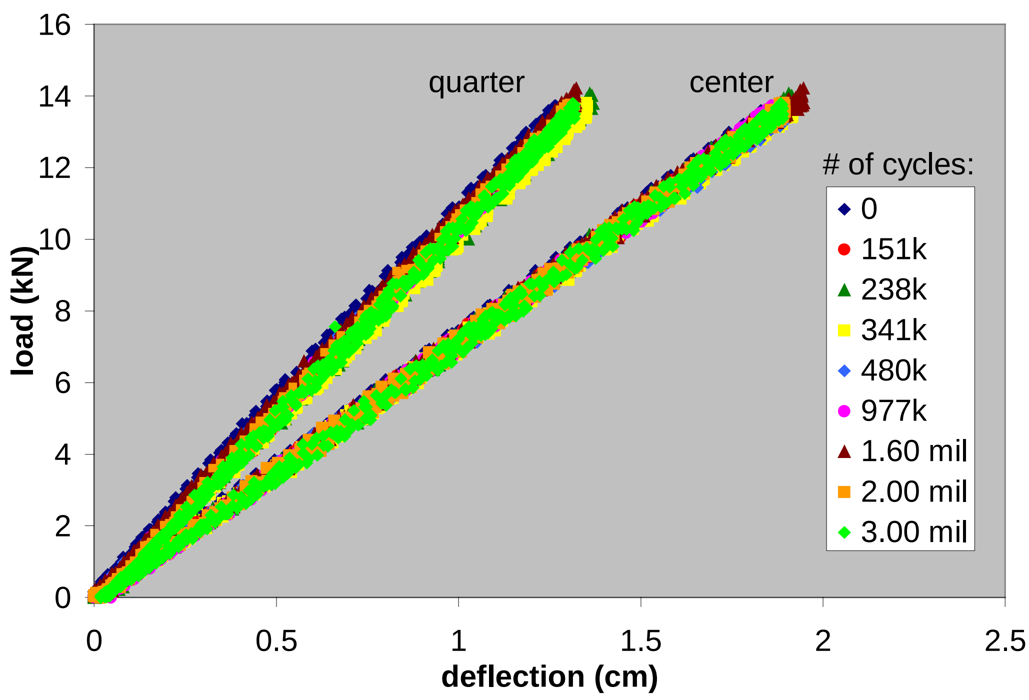

Figure 3-8. Load-deflection curves for mid-span and quarter-point locations for progressive increments of fatigue cycles up to 3 million cycles.

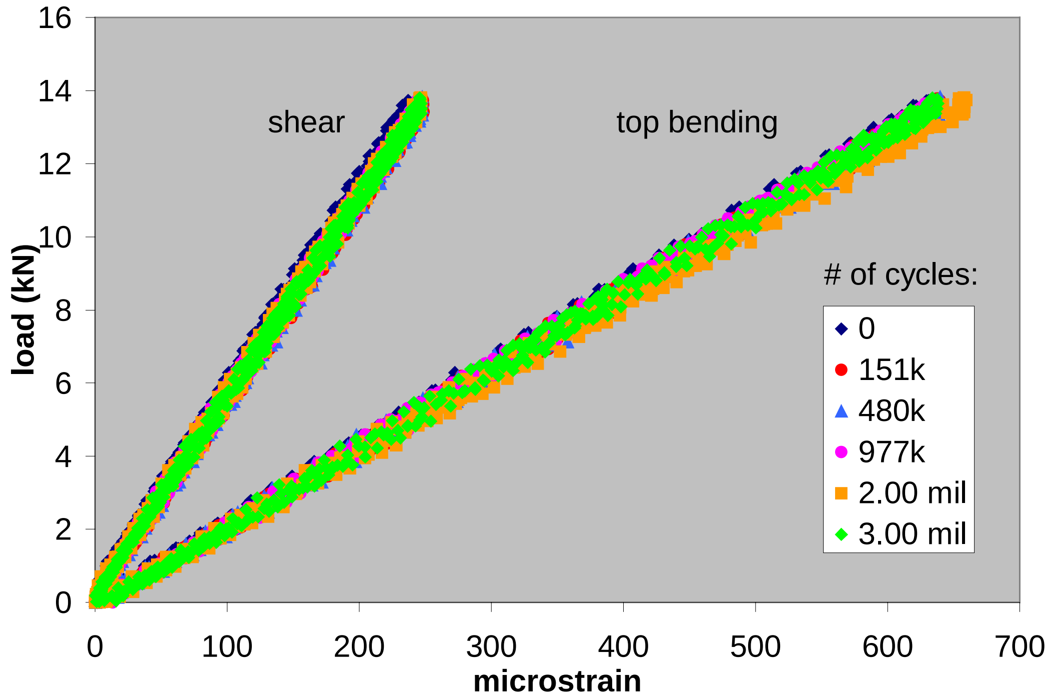

Figure 3-9. Load-strain curves for maximum bending and shear for progressive increments of fatigue cycles up to 3 million cycles.

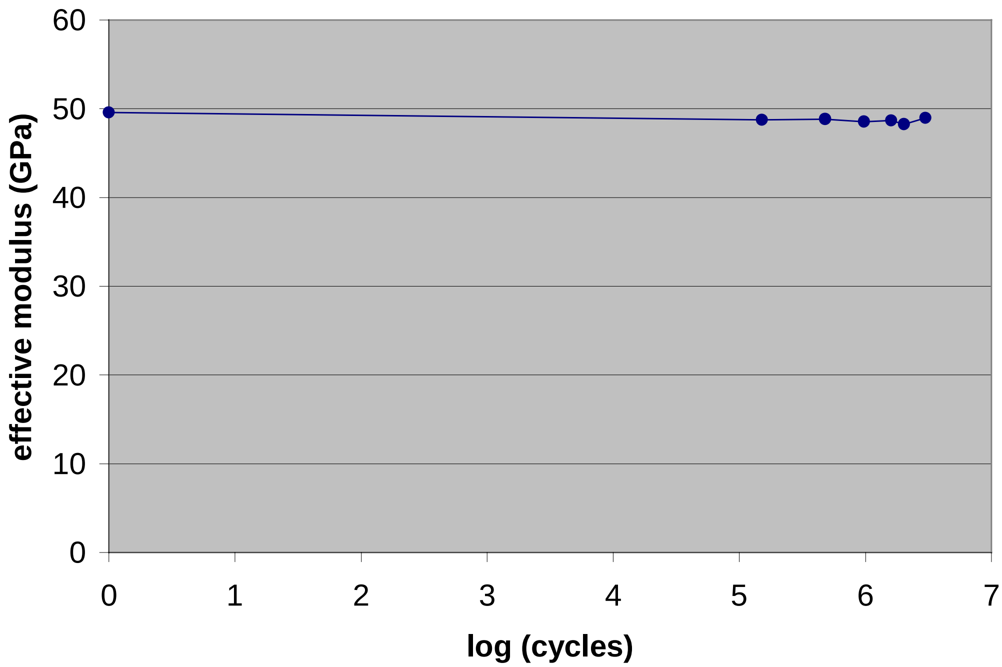

Figure 3-10. Effective bending modulus versus fatigue cycles calculated from strain data.

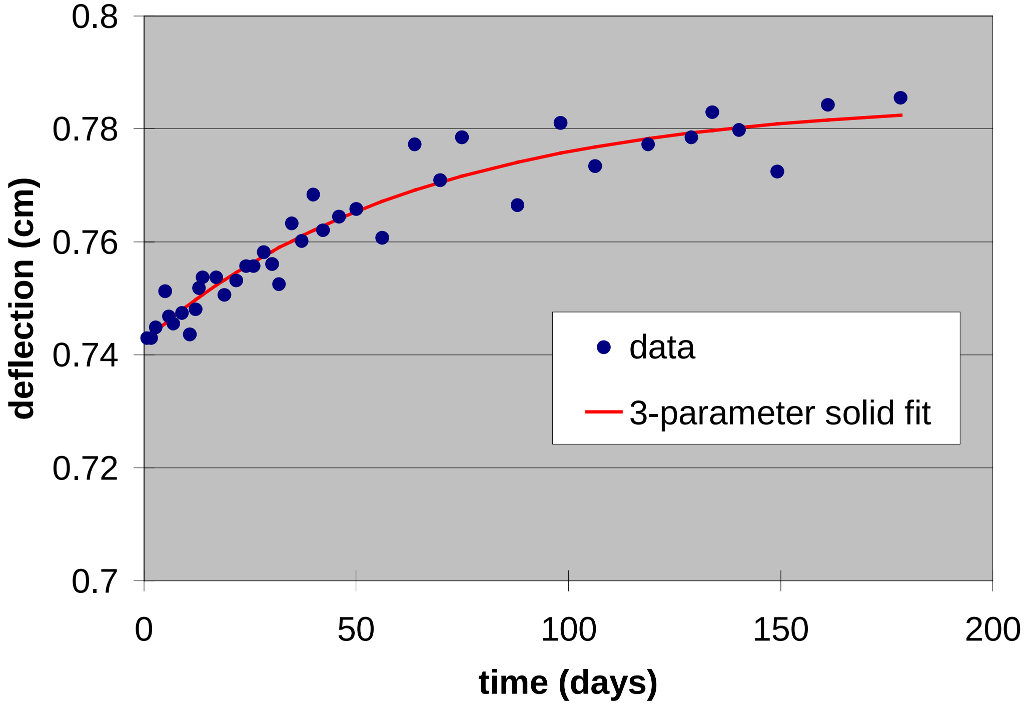

Figure 3-11. Creep data and fits plotted on a normal time axis.

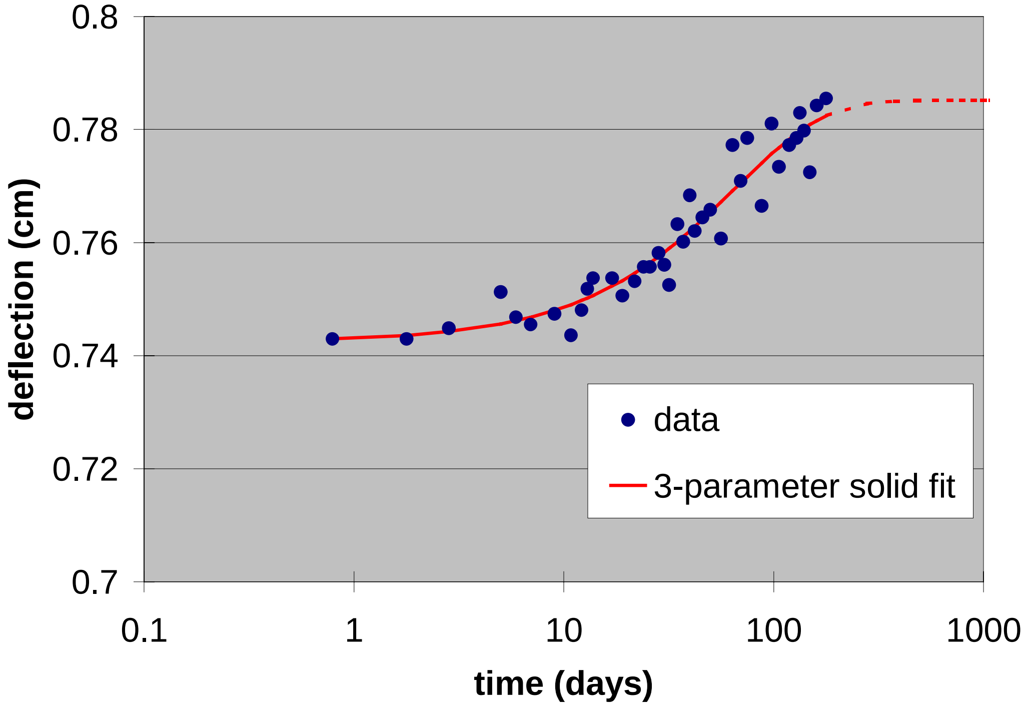

Figure 3-12. Creep data and fits plotted on a logarithmic time scale.

Table 3-3. Location of each composite beam across width of bridge along skewed centerline of beams and modulus.

numbering		location		modulus	
Bridge #	Test #	**cm**	**inches**	**GPa**	**Msi**
1	10	0	0	49.4	7.17
2	26	27.3	10.7	47.6	6.90
3	8	54.6	21.5	48.6	7.05
4	6	82.0	32.3	48.2	6.99
5	5	109	42.9	47.0	6.81
6	4	137	53.9	46.2	6.70
7	18	164	64.6	45.6	6.62
8	23	195	76.8	45.1	6.54
9	21	226	89.0	44.3	6.43
10	22	258	102	44.3	6.43
11	17	289	114	43.6	6.33
12	24	320	126	42.9	6.22
13	11	351	138	42.7	6.20
14	13	382	150	44.0	6.38
15	14	414	163	44.0	6.38
16	12	445	175	44.2	6.41
17	15	476	187	44.5	6.45
18	25	507	200	44.7	6.48
19	19	535	211	46.1	6.69
20	20	562	221	46.7	6.77
21	7	589	232	47.5	6.89
22	3	617	243	48.1	6.97
23	9	644	253	48.7	7.06
24	2	671	264	49.4	7.16

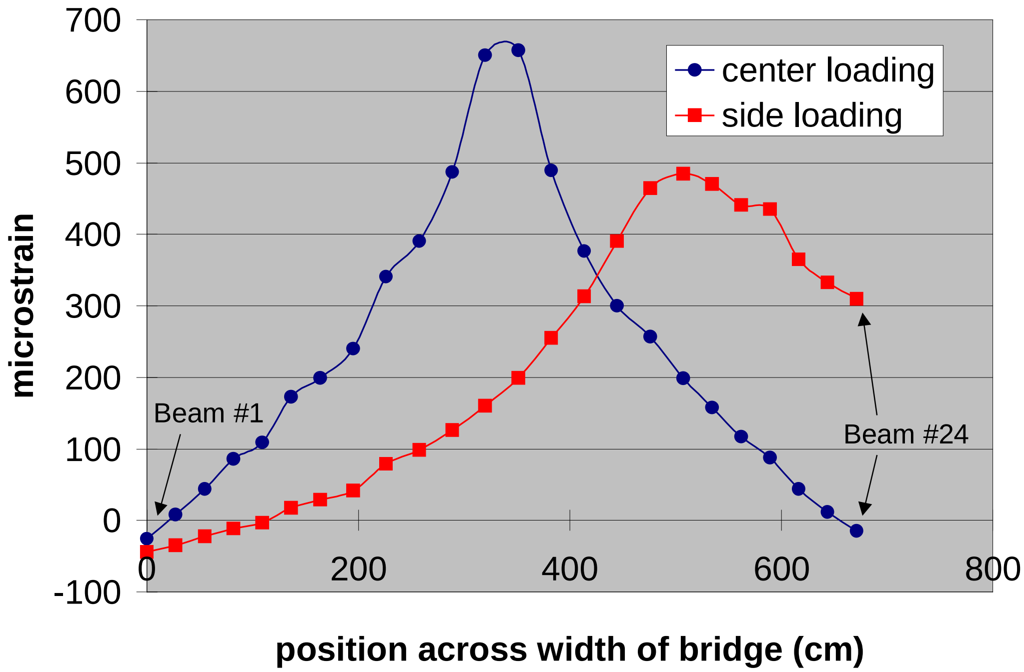

Figure 3-13. Center bending strains under single patch loading at center and side positions.

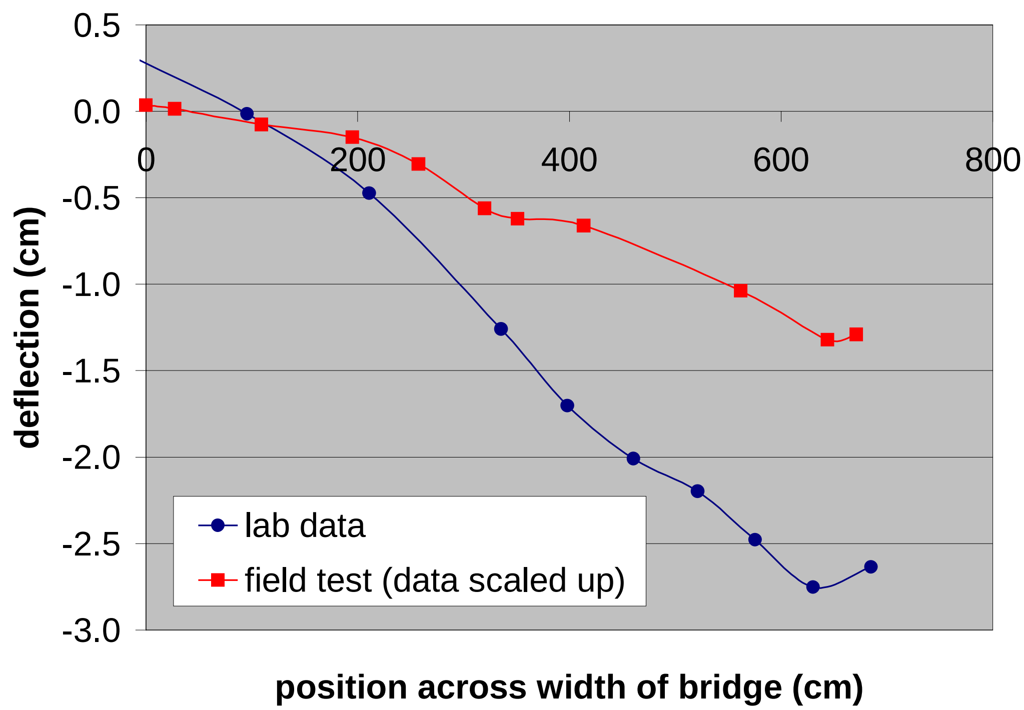

Figure 3-14. Center deck panel deflections under HS20-44 side loading (single connections).

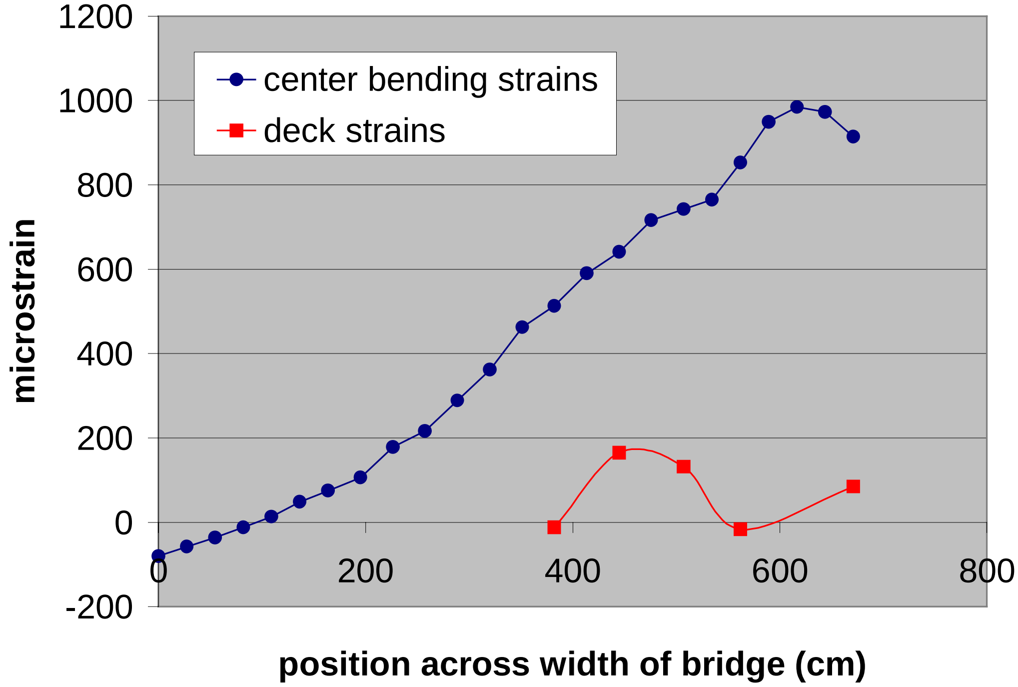

Figure 3-15. Center bending and deck strains under HS20-44 side loading (single connections). Note that positive strains are tensile, and the center bending strains were measured on the bottom flanges, while deck strains were measured on the top deck surface.

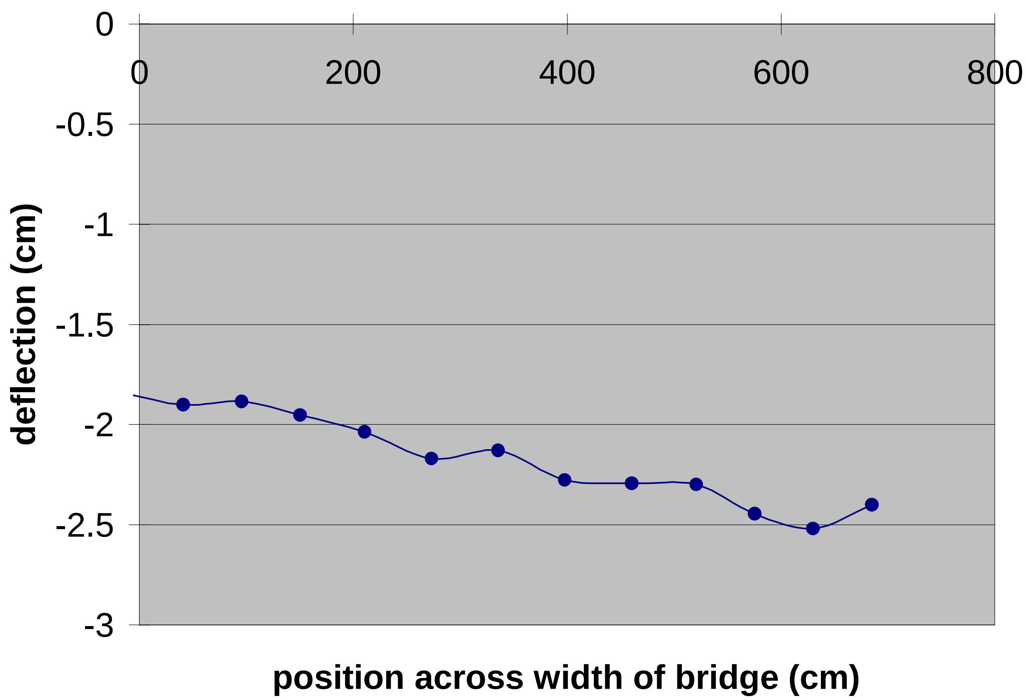

Figure 3-16. Deck panel deflections under tandem HS20 loads (single connections).

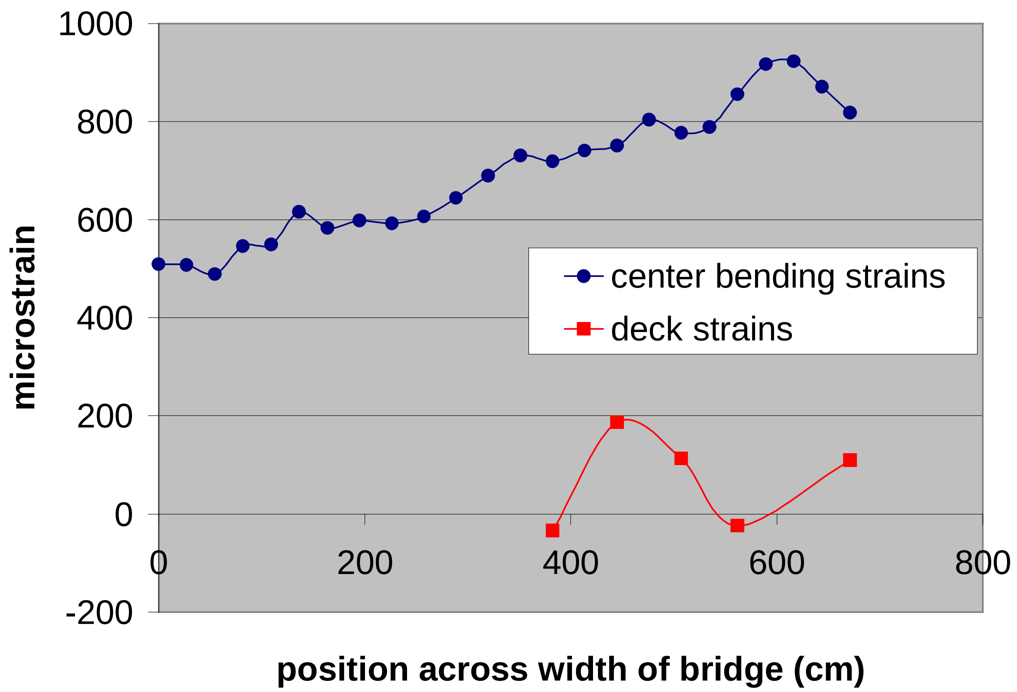

Figure 3-17. Center bending and deck strains under tandem HS20 loads (single connections).

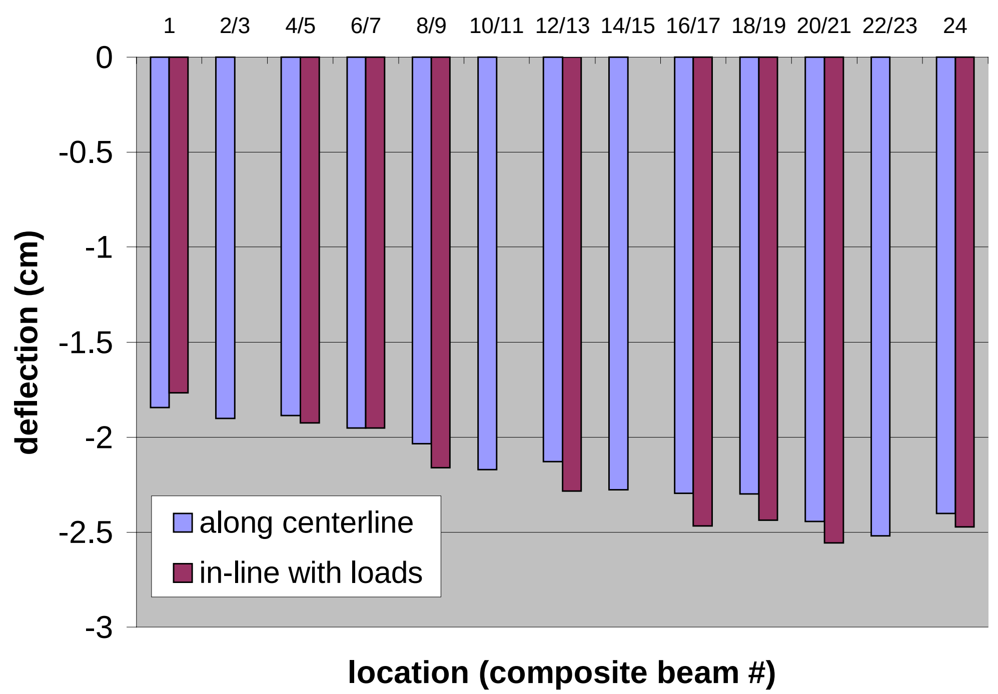

Figure 3-18. Deflections under tandem HS20 loads (single connections).

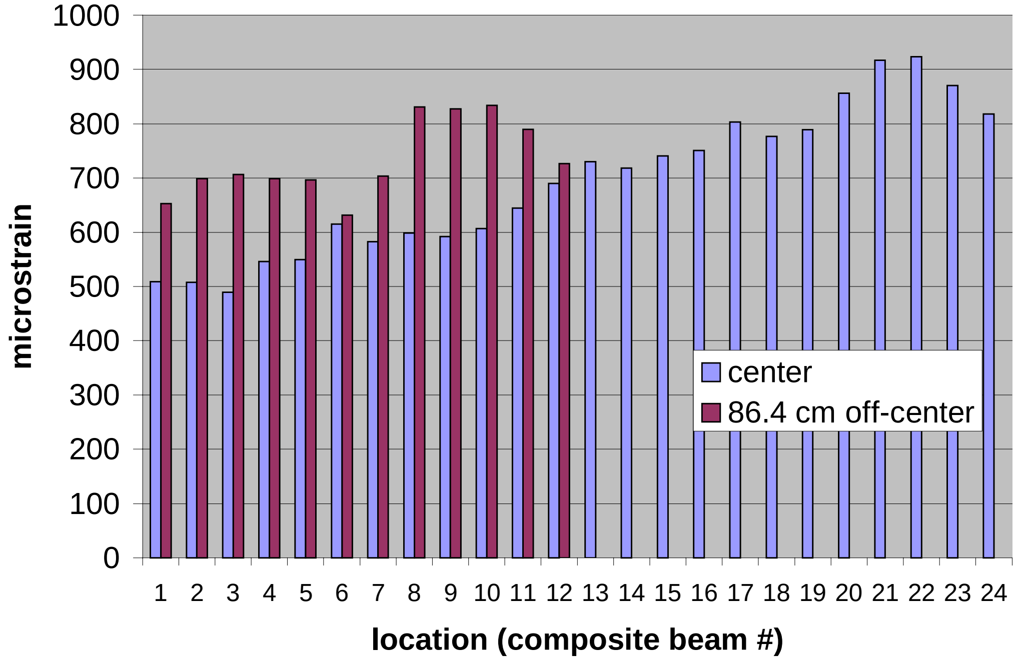

Figure 3-19. Center bending strains and off-center bending strains under tandem HS20 loads (single connections).

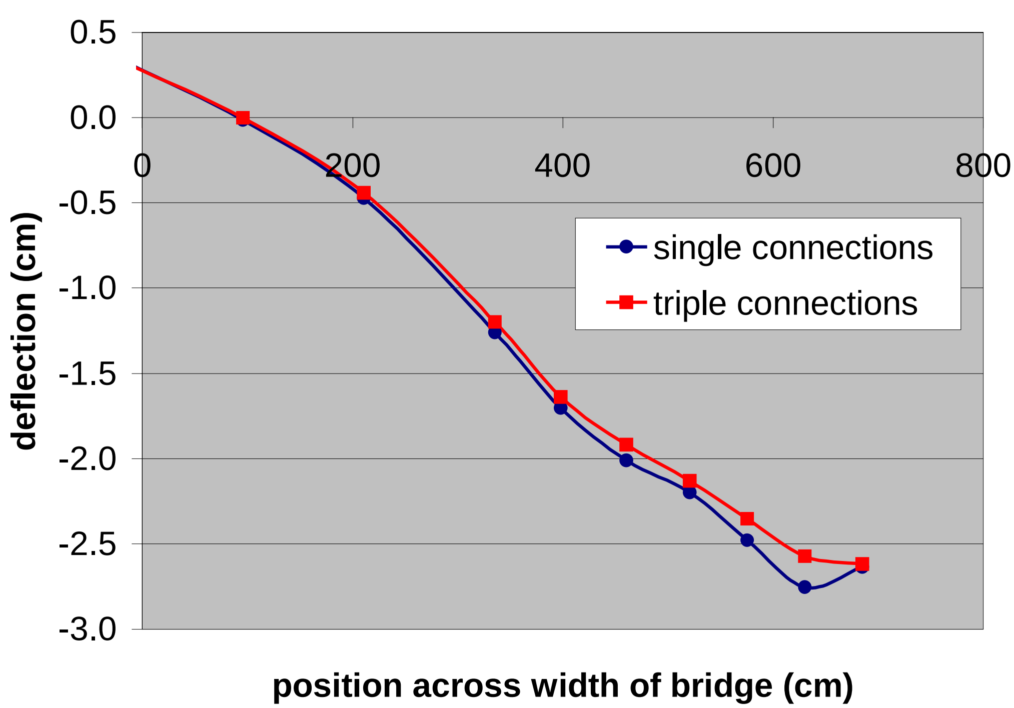

Figure 3-20. Deck panel deflections under HS20 side loading with two different connection sets.

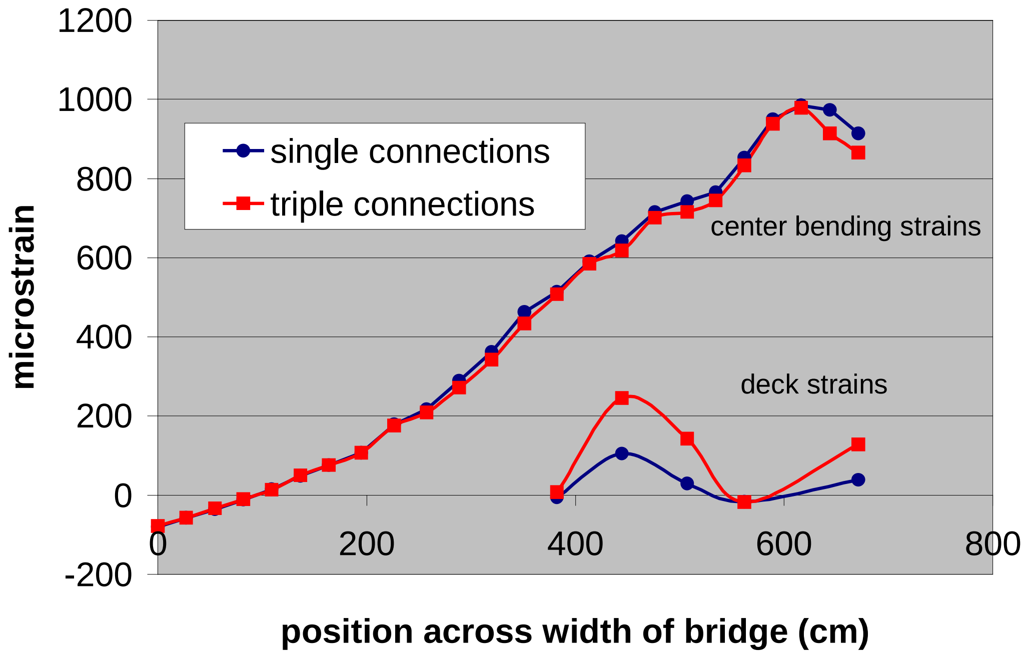

Figure 3-21. Center bending and deck strains under HS20 side loading with two different connection sets.

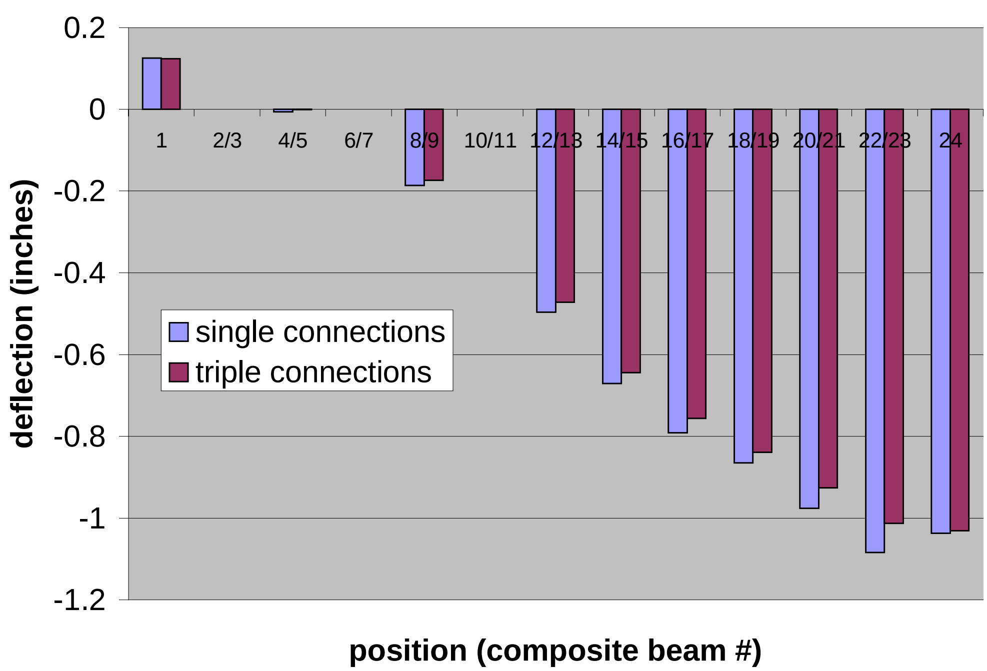

Figure 3-22. Deck panel deflections under HS20 side loading for two different connection sets.

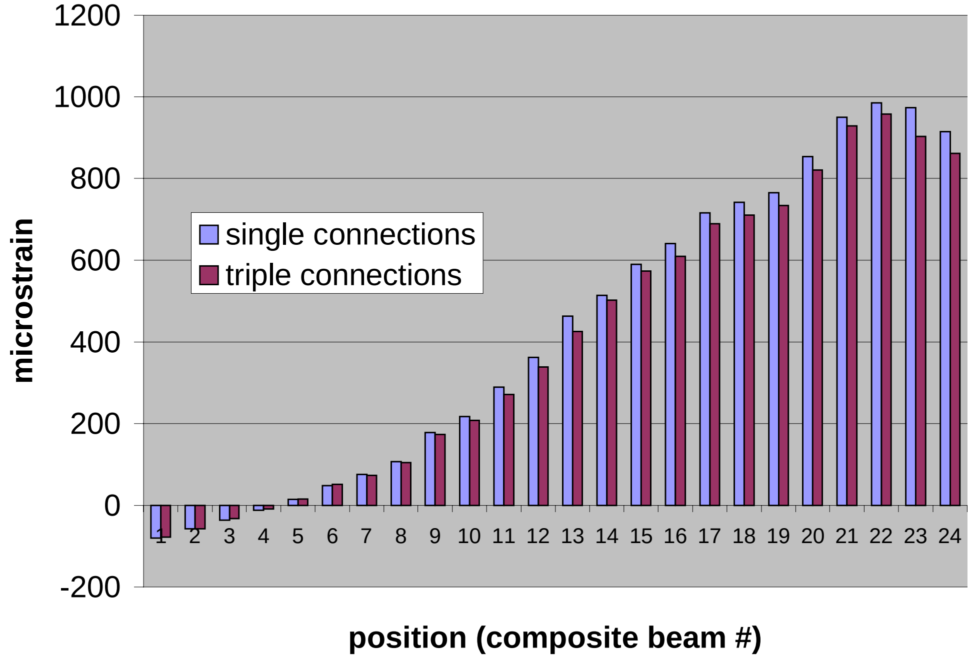

Figure 3-23. Center bending strains under HS20 side loading for two different connection sets.

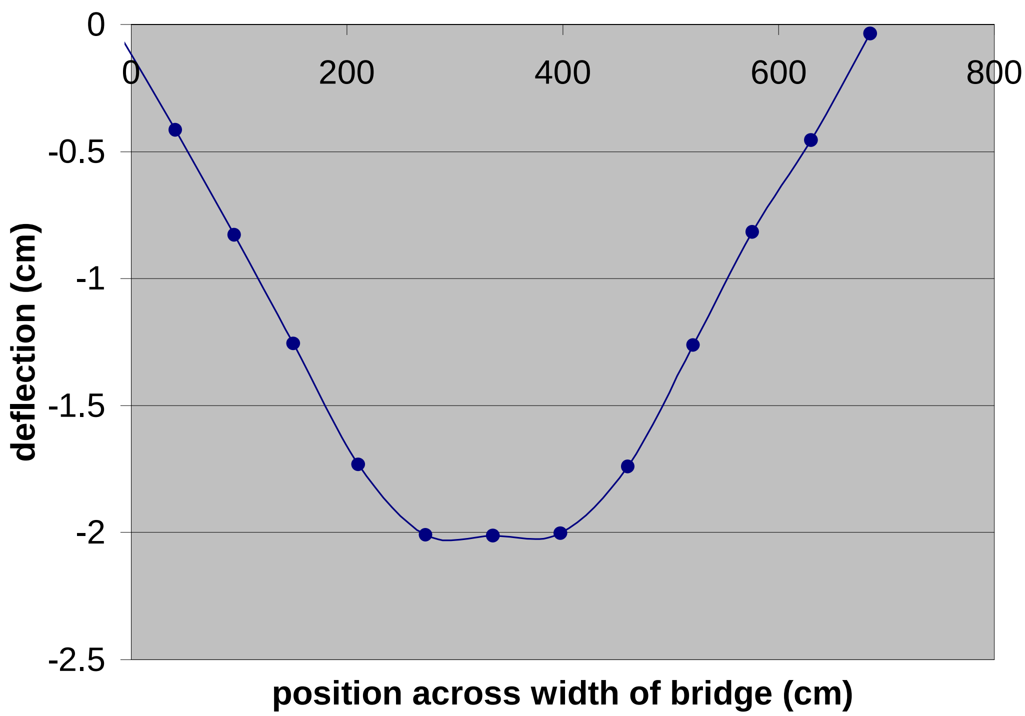

Figure 3-24. Deck panel deflections under HS20 center loading (triple connections).

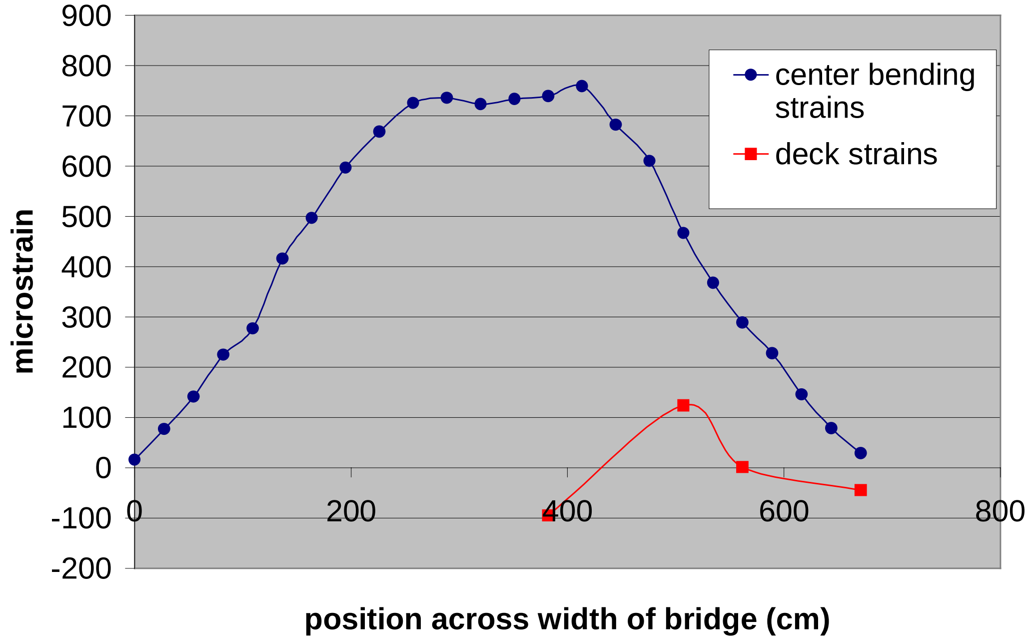

Figure 3-25. Center bending and deck strains under HS20 center loading (triple connections).

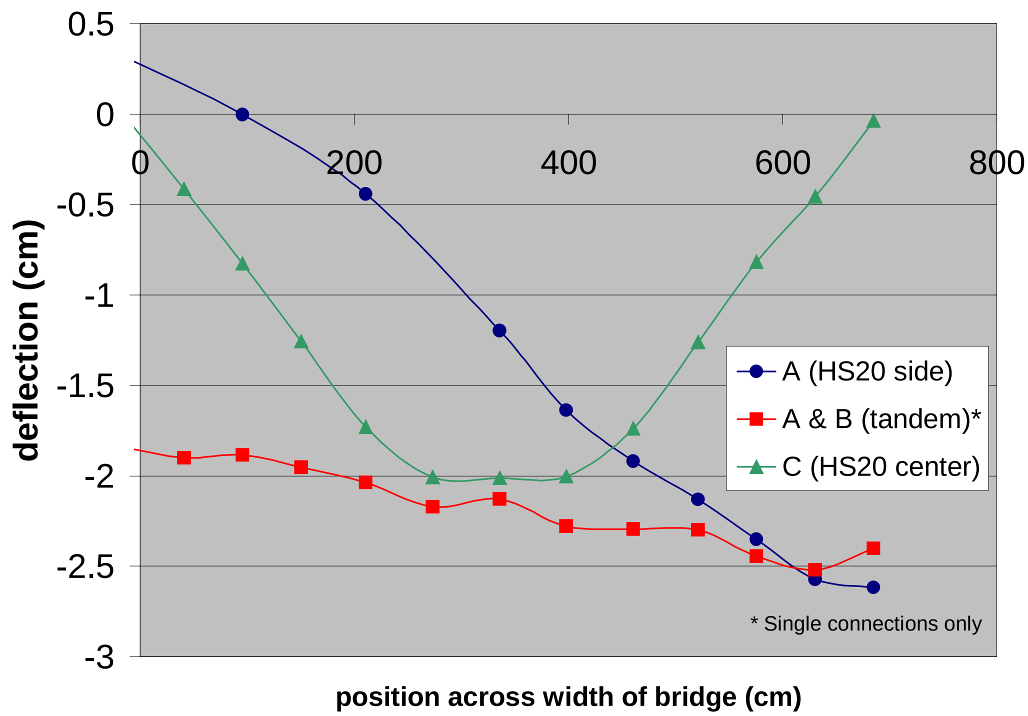

Figure 3-26. Comparison of deck panel deflections for three HS20 loading cases. Cases A and C are for triple connections, while the tandem loading results are for single connections only.

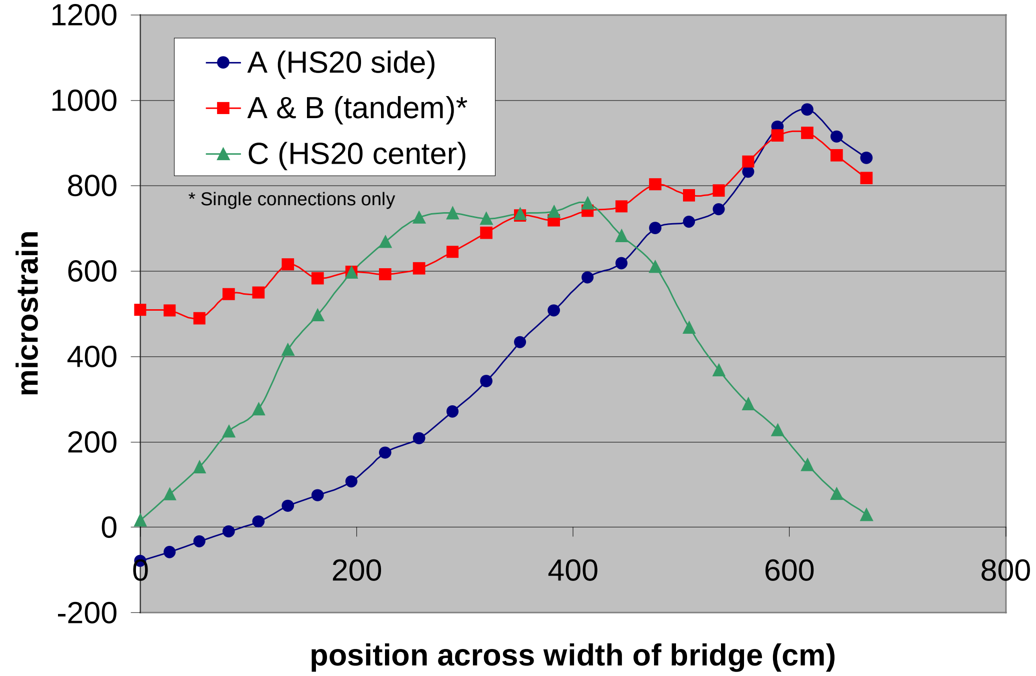

Figure 3-27. Comparison of center bending strains under different HS20 loading cases.

Chapter 4: Analytical Bridge Model

In order to assist in the future design of similar single-span bridges, an analytical model is developed using a mechanics of materials approach. This model provides an estimate of deflections and strains along the length of each composite beam under any given static loading. Timoshenko beam theory is utilized to derive deflection equations for a shear-deformable beam for use in the model, and shear correction terms are approximated using the experimental results from the proof testing, as well as a method developed by Cowper [68] and modified for thin-walled composite beams by Bank [40]. An estimate for the torsional stiffness of the composite beam is also calculated. The necessary equations for solving the beam deflection problem are presented and generalized for the construction of the model. Finally, predictions made utilizing the model are compared with a basic elasticity solution and data from the laboratory testing.

4.1 Development of the Model

In order to confirm the feasibility of the two-for-one beam replacement in the initial design for the Tom's Creek Bridge composite structure, a predictive model was needed that could estimate the response of the bridge under HS20-44 loading. A simplified version of the model detailed herein was first developed by Lesko and Moser [62]. This model provided a rough prediction but was limited by a difficult user interface, no consideration of shear deformation or torsional stiffness, and restricted output capabilities. Furthermore, the original code was written in *Mathematica*© and was not suited for interfacing with other routines. For these reasons, the model was rewritten using FORTRAN code and modular subroutines.

4.1.1. Model Formulation

For the purposes of this analysis, the bridge is modeled as a series of (deck) beams on an elastic foundation (superstructure). In the case of the repaired Tom's Creek

Bridge, the deck consists of seven wood glue-lam deck beams, which are supported by 24 composite girders (Figure 4-1). Hence, the elastic foundation is really comprised of N discrete elastic supports (Figure 4-2). The deck serves only to distribute the load to the girders and does not significantly contribute to the structure's stiffness; it is assumed that there is composite action between the deck and girders. The girders are also assumed to be of the same length, L, but the spacing between the centerlines of each girder can be varied. The bridge may be skewed so that the centerline of the girders is oriented at an angle, θ_s, to the transverse direction of the girders (see Figure 4-3). Finally, the deck beams are assumed to run parallel to the centerline of the girders (at the skew angle).

The analysis is performed for a concentrated (single point) load, and the results for combined loading (e.g. dual loads caused by a truck axle or a distributed load) are obtained using the principle of superposition. In order to simplify the analysis, only the deck beam directly under the applied load is considered. (A complete model would require a two dimensional mesh of nodes to model the connections between the girders and the other deck beams). The objective is to determine the deflections along the length of this single deck beam and to consequently determine the loads and resulting strains on each girder. This problem is statically indeterminate to the N-2 degree, and equilibrium alone cannot provide a solution. Deformation of the deck beam must be considered to generate the additional equations. The necessary equations are derived here by considering global equilibrium, continuity of deflection and slope between nodes, and equilibrium of moments and forces at each node. A variational approach could also be utilized to derive the equations.

The connections between the deck beam and the girder beams are represented by nodes 1 through N, which are centered at each girder (Figure 4-4). For each girder, a fourth order governing differential must be satisfied:

$$\frac{d^4 w_i(x)}{dx^4} = 0 \tag{4.1}$$

A simple polynomial solution is used, and the equations of deflection are constructed between each node, where the nodes are numbered i = 1 through N:

$$w_i(x) = a_i x^3 + b_i x^2 + c_i x + d_i \tag{4.2}$$

$w_i(x)$ is the deflection of the deck beam across its width measured from $x = 0$, and the coefficients a_i, b_i, c_i, and d_i are to be determined. For the case when the load is applied directly at a node, the number of nodes is N, and the number of deflection equations is N-1. This is referred to here as *at-node* loading. However, when the loading is applied between two girders, that reaction point must be modeled by another node. Then the number of nodes increases to N+1, and the structure becomes indeterminate to the N-1 degree. This is called *off-node* loading, and the node at the location of the external load is referred to as the *P-node*. The number of unknown coefficients then is 4N - 4 or 4N (4 per deflection equation) for the at-node and off-node cases, respectively. There are an additional N unknowns due to the undetermined reaction forces in each beam, F_i. The total number of unknowns and required equations then is 5N - 4 or 5N (at-node or off-node). To simplify the code necessary to solve these equations, an at-node load (P) is modeled as two off-node loads (P/2) which are located a distance δx on either side of the beam node. The remainder of this formulation assumes off-node loading.

To begin the derivation, the P-node is temporarily neglected and each beam is assigned a node i = 1, N. Equilibrium of external forces and moments acting on the deck beam (Figure 4-5) generates two equations:

$$\begin{aligned} &\sum_{i=1}^{N} F_i - P = 0 \\ &\sum_{i=1}^{N} \left(F_i x_i + T_i\right) - P x_p = 0 \end{aligned} \tag{4.3}$$

where F_i is the reaction force in each girder, P is the external load, x_i is the location of the ith girder/node, x_p is the location of the external load, and T_i is the reaction moment in each girder. The F_i and T_i terms are due to the bending and torsional stiffnesses of each girder and are calculated by:

$$F_i = k_i w_i$$
$$T_i = k_{\theta,i}\theta_i \tag{4.4}$$

where k_i and $k_{\theta,i}$ are effective spring constants for the cases of bending and torsion, respectively. Calculation of these parameters is considered further in Sections 4.1.2 and 4.1.4. The T_i term is considered optional in the model code, so that the connection between the deck and girders can be modeled as simple, with or without the capacity to carry a moment. The importance of including torsional rigidity in the model is examined in Section 4.2.2. Also, because the external force reactions are considered unknowns, matching the vertical displacements of the deck and the springs at each node is necessary and generates the following N equations:

$$\frac{F_i}{k_i} = w_i(x_i) \text{ for i = 1, } N \tag{4.5}$$

where F_i is the reaction force in each girder and k_i is the equivalent spring constant of each beam.

Now, the P-node is included so that the total number of nodes is N+1, and all remaining calculations include the P-node. The slope, moment, and shear in the deck beam along its length are computed using the first, second, and third derivatives of the displacement, respectively:

$$\begin{aligned} \theta_i(x_i) &= EI_{deck} w_i'(x_i) = EI_{deck}(3a_i x^2 + 2b_i x + c_i) \\ M_i(x_i) &= EI_{deck} w_i''(x_i) = EI_{deck}(6a_i x + 2b_i) \\ V_i(x_i) &= EI_{deck} w_i'''(x_i) = EI_{deck}(6a_i) \end{aligned} \tag{4.6}$$

where EI_{deck} is the bending stiffness of the deck beam. Continuity of displacement and slope across each interior node including the P-node (kinematic conditions) results in the following 2N - 2 equations:

$$
\begin{aligned}
&\mathrm{w_i}(x_i) = w_{i+1}(x_i) \;\; \text{and} \\
&3a_i x_i^{\,2} + 2b_i x_i + c_i - (3a_{i+1} x_i^{\,2} + 2b_{i+1} x_i + c_{i+1}) = 0 \quad \text{for i = 2, N}
\end{aligned}
\tag{4.7}
$$

Continuity of moment and shear across each interior node requires consideration of externally applied moments or forces in addition to those internal to the deck beam (see Figure 4-6). For instance, the reaction forces in each girder as well as the external load at the P-node constitute external shearing forces. In addition, the (optional) reaction moments in each girder constitute external moments. The moment and shear continuity equations (*N*-1 each) are:

$$
\begin{aligned}
&EI_{deck}\left(6a_i x_i + 2b_i\right) - EI_{deck}\left(6a_{i+1} x_i + 2b_{i+1}\right) + T_i = 0 \\
&\\
&EI_{deck}\left(6a_i\right) - EI_{deck}\left(6a_{i+1}\right) + F_i = 0 \text{ at the spring nodes, and} \\
&EI_{deck}\left(6a_i\right) - EI_{deck}\left(6a_{i+1}\right) - P_i = 0 \text{ at the P-node.}
\end{aligned}
\tag{4.8}
$$

Finally, at the first and last nodes, the net moment is set to zero (boundary conditions):

$$
\begin{aligned}
M_{net,1} &= -EI_{deck}(6a_1 x_1 + 2b_1) + T_1 = 0 \\
M_{net,N+1} &= EI_{deck}(6a_N x_{N+1} + 2b_N) + T_1 = 0
\end{aligned}
\tag{4.9}
$$

Thus, the net moments at each end consists of the internal moment in the deck beam and the torque caused by the reaction of the beam at that node. The total number of equations now is 5*N* for the off-node loading case, and the problem can be solved.

The deflections across the width of the deck panel (*x*-direction) are then calculated from Equation (4.1). Furthermore, since F_i are known, the deflections along the length of each composite girder can also be calculated using beam deflection theory. Thus, the deflections across the entire bridge can be determined. Sample plots showing predictions for deflections and strains are shown in Figure 4-7 and Figure 4-8, respectively. A sample surface plot showing the deflection response across the entire bridge is shown in Figure 4-9 and Figure 4-10 for right side loading and center loading, respectively.

4.1.2. Calculation of Effective Bending Spring Constant: Euler or Timoshenko Beams

Solution of the above equations requires that effective spring constants be inputted for the cases of bending and torsion. These constants are dependent both on the material properties of the girder and the geometry of the loading. For instance, the bridge geometry might be set so that the deck beam intersects the girders at different locations along their lengths. As the load on a girder is moved towards one end of the girder, the apparent or effective stiffness of the girder will increase. The same holds for the effective torsional stiffness, as the angle of twist (and therefore the effective stiffness) depends upon the length of the beam between applied torques.

The effective spring constant for the case of bending, k_i, can be found from straight forward use of the generalized Euler beam deflection equation for three-point bending with the preferred boundary conditions. For this analysis, the girders are assumed to be simply supported -- that is, the supports are "pinned-roller". This assumption should provide a conservative estimate of bridge response (over prediction of deflections) as compared to the clamped boundary conditions. The deflection at a distance x under a single load P applied at $x = a$ for a beam of length L (see Figure 4-11) can be determined using [65,66]:

$$\delta(x,a) = \begin{cases} \dfrac{Pb}{6LEI}\left[\dfrac{L}{b}(x-a)^3 - x^3 + (L^2-b^2)x\right] & \text{for x > a} \\ \dfrac{Pb}{6LEI}\left[-x^3 + (L^2-b^2)x\right] & \text{for x} \le \text{a} \end{cases} \tag{4.10}$$

The effective stiffness is then defined as the ratio of the applied force to the resulting deflection at the loading point:

$$k_{i,eff} = \frac{F_i}{\delta_i} \tag{4.11}$$

The Euler theory assumes no shear deformation (i.e. planes originally normal to the centerline remain plane and normal to the centerline during bending), but it has been demonstrated that shear deformation may be significant in fiberglass beams where the shear modulus of the web is significantly lower than the bending modulus. Derivation of a new beam deflection equation for the case of general three-point bending follows Timoshenko's shear deformable theory [67]. The basic derivation is presented here.

First, the slope of the beam centerline resulting from both bending and shear deformation is defined as

$$\frac{dw}{dx} = \psi(x) + \beta(x) \tag{4.12}$$

where $\psi(x)$ is the rotation due to bending alone and $\beta(x)$ is the rotation due to shear alone. The contribution of each rotation is demonstrated schematically in Figure 4-12. To facilitate the derivation, the shear strain is temporarily assumed to be the same over the entire beam cross-section. The displacement in the *x*-direction (parallel to the beam) is due only to bending and is defined so that it varies with position both in the *z*-direction (parallel to loading) and the *x*-direction:

$$\begin{aligned} u(x,z) &= -z\psi(x) = -z\left[\frac{dw}{dx} - \beta(x)\right] \\ w &= w(x) \end{aligned} \tag{4.13}$$

The resulting axial and shear strains are

$$\varepsilon_{xx} = -z\frac{d\psi(x)}{dx}, \quad \varepsilon_{xz} = \frac{1}{2}\beta(x) \tag{4.14}$$

A rectangular cross section is assumed, and using the approximation that $\tau_{xx} = E\varepsilon_{xx}$, the resultant moment and shear are then

$$\begin{aligned} M &= \int \tau_{xx} zbdz = -EI\frac{d\psi}{dx} \\ V &= \int \tau_{xz} bdz = \tau_{xz}\int bdz = \tau_{xz}A = GA\beta \end{aligned} \tag{4.15}$$

where b is the width of the cross-section, GA is the shear stiffness, and the integrals are taken over the height of the section. Now, the (invalid) assumption of a uniform shear strain distribution over the cross-section yields the following shear stress:

$$\gamma_{xz} = \frac{V}{A} = G\beta(x) \tag{4.16}$$

In order to account for the non-uniform shear stress distribution, a correction factor, K, is introduced:

$$V(x) = KGA\beta(x) \tag{4.17}$$

The constant K depends on geometry/shape, material properties, and also the frequency of vibration in dynamic problems [40,67,68].

Following the method of minimum total potential energy, the total potential energy of the beam is defined in terms of bending strains, shearing strains, and the external load. These terms are integrated over the length of the beam, and separate integrals must be written for the sections of the beam on either side of the load. The first variation of the total potential energy is taken and set equal to zero; this requires using integration by parts. What results are the Euler-Lagrange equations:

$$\begin{aligned} &\frac{d}{dx}\left(EI\frac{d\psi}{dx}\right) + KGA\left(\frac{dw}{dx} - \psi\right) = 0 \\ &\frac{d}{dx}\left[KGA\left(\frac{dw}{dx} - \psi\right)\right] = 0 \end{aligned} \tag{4.18}$$

Again, both equations must be constructed separately on either side of the loading point. The boundary conditions that apply for a pinned-pinned beam are as follows:

$$\begin{aligned}
& w_1(0) = 0,\ \ \mathrm{EI}\left.\frac{d\Psi_1}{dx}\right|_{x=0} = 0 \\
& w_2(\mathrm{L}) = 0,\ \ \mathrm{EI}\left.\frac{d\Psi_2}{dx}\right|_{x=L} = 0 \\
& \left.\frac{d\Psi_1}{dx}\right|_{x=a} = \left.\frac{d\Psi_2}{dx}\right|_{x=a} \\
& \mathrm{GA}\left.\left(\frac{\mathrm{dw}_1}{\mathrm{dx}} - \Psi_1\right)\right|_{x=a} - \mathrm{GA}\left.\left(\frac{\mathrm{dw}_2}{\mathrm{dx}} - \Psi_2\right)\right|_{x=a} = P \\
& w_1(a) = w_2(a),\ \ \Psi_1(a) = \Psi_2(a)
\end{aligned} \tag{4.19}$$

Solution of equations (4.17) and (4.18) yields the following solution for a single load P applied at $x = a$:

$$\begin{aligned}
w_1(x,a) &= \frac{Px(a-L)\left(-6EI + a^2KGA - 2KGALa + KGAx^2\right)}{6EIKGAL} \quad \text{for x < a} \\
w_2(x,a) &= \frac{aP(x-L)\left(-6EI + a^2KGA - 2KGALx + KGAx^2\right)}{6EIKGAL} \quad \text{for x} \geq \text{a}
\end{aligned} \tag{4.20}$$

If all of the material constants are known, Equation (4.19) can then be utilized to solve for the effective bending spring constant for each girder.

4.1.3. Calculation of the Shear Stiffness

Analytical Techniques

Computation of the shear stiffness KGA is difficult since G is difficult to obtain experimentally and cannot easily be estimated for a composite section. Furthermore, K is difficult to determine for a composite section. *KGA* must either be obtained experimentally using a method such as the one described in Section 1.3.8, or by estimating the shear modulus of the beam and calculating *K*. One method of calculating the shear correction factor is that of Cowper [68], which is based upon derivation of Timoshenko beam theory from three-dimensional elasticity. This approach and its application to thin-walled composite beams is discussed in Bank 1987 [40]. The approach is briefly summarized here.

In Cowper's approach, the mean deflection of the cross-section, *W*, the mean rotation, Φ, and the mean axial displacement, *U*, are defined as

$$
\begin{aligned}
W &= \frac{1}{A}\int\int u_y \, dydz \\
\Phi &= \frac{1}{I}\int\int y u_x \, dydz \\
U &= \frac{1}{A}\int\int u_x \, dydz
\end{aligned}
\tag{4.21}
$$

Residual displacements are then introduced into the definition of the mean variables to account for the warping of the cross-section that accompanies shear deformation. The residual displacement in the *x*-direction is solved for by equating the shear stress distribution in the cross-section obtained from equilibrium (assuming that the shear flow follows the cross section and is uniform throughout the thickness of the section) and the distribution found using a known, exact solution for a special case of beam flexure. The Cowper derivation yields the following form for the second Timoshenko equation:

$$
\frac{dW}{dx} + \Phi = \frac{Q}{K^* A E_x}
\tag{4.22}
$$

where E_x is the in-plane elastic modulus of the beam walls, *Q* is the resultant shear force, and *A* is the area of the cross-section.

K^* is a "modified shear coefficient" that allows the different in-plane moduli of the laminated walls to be accounted for. K^* can be found from the shear stress distribution by a closed integration around the contour of the section:

$$K^* = \frac{1}{\frac{1}{2}\oint \pm \nu_{sx} s^2 t ds + \frac{A}{I}\oint y \psi t ds} \tag{4.23}$$

where the contour integral is taken around the path *s*, and the ± sign depends upon whether integration is in the transverse or *z*-direction (positive sign) or the vertical or *y*-direction (negative sign). ν_{sx} is Poisson's ratio of the panels, *t* is the panel thickness, and *A* and *I* are the area and moment of inertia of the cross-section about the centerline, respectively. If the beam contains panels having different properties, a transformed moment of inertia must be calculated before using Equation (4.23). ψ is a "modified flexure function" which is used to relate shear stresses and axial displacement in the beam.

Bank's approach differs slightly from Cowper's method for isotropic materials by assuming that the Poisson's ratio through the thickness of the walls is zero, in order to simplify the integration. Furthermore, the cross-section is assumed to be composed of only vertical and horizontal elements. This uncouples the material constants in each wall and allows the individual laminate properties to be utilized. If a beam is constructed of walls having the same properties (i.e. all walls are made of identical laminated panels), then the standard shear correction factor *K* can be calculated using

$$K = K^* \frac{E_x}{G_{sx}} \tag{4.24}$$

where G_{sx} is the in-plane shear modulus of the beam walls. For a beam made of panels having different properties, however, a transformed section must be constructed before using Equation (4.23). This applies to most FRP composite beams.

Bank has derived the modified shear correction factor for several geometries using transformed sections, and his results are shown here. For a rectangular box beam with width *b* and height *h*,

$$K^* = 20(\alpha + 3m)^2 / [\frac{E_1}{G_1}\left(60m^2n^2 + 60\alpha mn^2\right) + \frac{E_1}{G_2}\left(180m^3 + 300\alpha m^2 + 144\alpha^2 m + 24\alpha^3\right) + \upsilon_1\left(-30m^2n^2 - 50\alpha mn^2\right) + \upsilon_2\left(30m^2 + 6\alpha m - 4\alpha^2\right)] \qquad (4.25)$$

where $n = b/h$, $m = t_1b/t_2h$, $\alpha = E_2/E_1$, and the subscripts 1 and 2 identify properties of the horizontal and vertical wall elements, respectively. An estimate for *K* for each beam using the box section solution is summarized in Table 4-1, using the measured E_x for each beam and an estimated G_{sx} of 6.89 GPa (1 Msi). In order to use the solution, the flange "wing" sections of the box I-beam are neglected in the calculation.

Experimental Techniques

While the analytical tools presented in the previous section may prove useful for design purposes, the primary objective here is to verify the bridge model with the lab testing data in this study, so that the properties (including shear stiffness) for every beam should preferably be known. In Section 1.3.8, a test method was introduced in which a beam is tested at various span lengths in either three- or four-point bending. Using this technique, the shear product term *KGA* can then be extrapolated from the data. While conducting tests at various span lengths increases the number of data points on this curve and therefore minimizes the error in the calculations, this method is time-consuming and impractical for proof testing a large number of beams. The following method employing data from a single four-point bending test at one span length should also yield an adequate estimate of *KGA*.

Bending strains measured within the shear-free region between the loading points of a four-point bending test are due only to bending deformation. Thus, an effective modulus (such as those obtained in the proof testing in Section 3.2) calculated using these strains will not reflect shear deformation, and *EI* will represent the actual bending stiffness of the beam. On the other hand, the mid-span deflection is a result of the total beam response, including shear deformation in the other regions of the beam. If the Timoshenko beam Equations (4.19) are utilized with the *E* calculated using strain data, then the shear product *KGA* can be solved for directly. This method was employed in this study to obtain *KGA* for each beam that was proof tested (Table 4-1). The average measured value for *KGA* was 3.5 Msi-in^2. For the four-point bending geometry used in this study, the low shear stiffness results in shear deformation that accounts for about 5% of the total deflection (assuming a bending modulus of 44.8 GPa or 6.5 Msi).

4.1.4. Calculation of Effective Torsional Spring Constant

The effective torsional spring constant of a beam also depends on both the torsional stiffness and the geometry (i.e. the location of the applied torque relative to the end constraints). For a beam of length L constrained by a moment at each end (T_1 and T_2) and acted upon by an external torque T_{ext} at $x = a$, the rotation at $x = a$ is

$$\phi = \frac{a(L-a)T_{ext}}{LGJ_{eff}} \qquad (4.26)$$

where GJ_{eff} is the effective torsional stiffness (e.g. $GJ_{eff} = GJ$ for a circular shaft). The effective torsional spring constant then is

$$k_{\theta,i} = \frac{LGJ_{eff}}{a(L-a)} \qquad (4.27)$$

However, without performing a torsion test on a structural member, the torsional stiffness GJ_{eff} is difficult to obtain. For members with non-circular cross-sections, linear distributions of stress and strain across the section cannot be assumed; the lack of axisymmetry of a non-circular section will cause the section to warp out of plane.

However, a fairly simple solution can be obtained for a linear elastic, isotropic thin-walled hollow member using the Prandt Elastic-Membrane Analogy [68] or an energy approach [67]. The solution yields the following expression relating the angle of rotation of the torsion member, ϕ, to the applied torque, T:

$$\varphi = \frac{TL}{4A^{*2}G}\oint\frac{ds}{t} \tag{4.28}$$

where t is the wall thickness and the integral is taken around the mean perimeter of the cross-section, s. A^* is the area enclosed by the mean perimeter, and G is the shear modulus of the wall material (assumed to be constant for all walls). This solution assumes that, while the wall thickness may vary, it is very small compared to the other dimensions of the member. This condition insures that the shear stress is constant through the thickness. Once the relationship between ϕ and T is known, an effective torsional stiffness can be obtained using

$$GJ_{eff} = \frac{T}{\phi} \tag{4.29}$$

where GJ_{eff} is analogous to the GJ term in the solution for a circular member.

Equations (4.28) and (4.29) may be utilized to obtain a rough estimate of the torsional stiffness of the composite box I-beam utilized in this project, if several assumptions are made. First of all, only the box section of the beam is considered -- that is, the 3.81 cm (1.5 in) flange sections off either side of the large interior box are neglected. Secondly, a constant shear modulus, G, must be assumed for both the side walls (web sections) and the top and bottom walls (flange sections). In this analysis, the shear modulus G_{12} of the web sections is assigned to all walls. This is probably a good assumption considering the similarity of the layup between the web and an interior section of the flanges[6]. The outer layer of the flange has a lower shear modulus G_{12}, so

[6] Although the layup of Strongwell's hybrid box I-beam is proprietary, it is appropriate to note that the flange can be modeled as a sandwich of two different laminates, the inner layer of which is similar to the web.

an "apparent thickness" for that part of the flange is assumed and the web shear modulus is then assigned to all walls.

Based on these assumptions, the following box geometry is utilized: the mean perimeter is 50.8 cm (20.0 in) and the enclosed area is 125 cm (19.3 in^2). Using Classical Laminate Theory (CLT) analysis, a shear modulus of approximately 1.1 Msi is obtained for the web laminate. Using Equations (4.28) and (4.29), the effective torsional stiffness is estimated to be 9150 GPa-cm^4 (31.9 Msi-in^4). This value can then be entered into Equation (4.27) to obtain an effective torsional spring constant for each girder based upon its location relative to the loaded deck beam. It is assumed that the composite beams are prevented from rotating at their ends -- that is, they are fixed and capable of supporting a moment.

4.2 Model Predictions and Comparison with Laboratory Test Data

4.2.1 Comparison with Elasticity Solution for Semi-Infinite Beam on an Elastic Foundation

In order to verify the model solution, an elasticity approximation is computed. The elasticity problem is solved for N number of elastic springs (all having the same spring constant) and equal spring spacing, and then the results are compared with the bridge model using identical inputs. For this analysis, the deck beam is considered to be semi-infinite, so that the deflection at the ends of the beam go to zero. Furthermore, the torsional stiffness of the girders is neglected. If the deflections are relatively small, then the Winkler foundation solution can be utilized. This solution assumes that the restoring force of the foundation acts in a linear elastic manner upon the beam. This solution is taken from in Boresi et al. [69].

To model equally-spaced, discrete elastic supports, an effective spring constant for the foundation, k, is calculated by dividing the spring constant of each girder, K, by the spacing between girders, l:

$$k = \frac{K}{l} \tag{4.30}$$

Since the foundation is modeled as elements of width l centered about each spring, the width of the deck beam is extended to

$$L'' = Nl \tag{4.31}$$

The deflection under a concentrated (single-point) load, P, then can be computed from

$$y(z) = \frac{P\beta}{2k} e^{-\beta z}(\sin \beta z + \cos \beta z),\ \mathrm{z} \geq 0 \tag{4.32}$$

where z is measured along the length of the deck beam, and β is defined as

$$\beta = \sqrt[4]{\frac{k}{4EI_{deck}}} \tag{4.33}$$

The approximation improves as the spacing decreases, and it has been shown that the error in the solution is small if

$$l \leq \frac{\pi}{4\beta} \tag{4.34}$$

and

$$L'' \geq \frac{3\pi}{2\beta} \tag{4.35}$$

Comparisons of the elasticity and the bridge model predictions are shown in Figure 4-13. These predictions utilize E_{deck} = 11.0 GPa (1.6 Msi), I_{deck} = 15.6 x 10^3 cm^4 (374 in^4), and a fixed bridge width of 673 cm (265 in). The spring constant K is calculated to be 7580 N/cm (4330 lb/in) using composite beam properties of E_{comp} = 44.8

GPa (6.5 Msi), I_{comp} = 5.35 x 10^3 cm^4 (128.55 in^4), and L_{comp} = 533 cm (210 in), and assuming no shear deformation. These parameters roughly approximate the actual composite beam properties and geometry of the Tom's Creek Bridge, although the skew angle is assumed to be zero. The number of girders is varied between 12 and 48 in order to explore the effect of increasing girder density (i.e. number of springs per length of deck beam).

The results indicate that as the number of girders increases, the two model predictions converge. Even for a relatively less number of girders, the maximum predicted deflections are still very close; however, the discrepancy in values at the ends of the deck beam begins to become significant at 12 girders (0.426 cm or 0.168 in). For 24 girders, the discrepancy between the two models is less significant (0.248 cm or 0.0976 in), but the response predicted by the bridge model at the sides of the bridge is slightly different than the elasticity solution. The difference can, of course, be attributed to the difference in boundary conditions at x = 0 and 626 cm (247 in) for the two models.

4.2.2 Bridge Model Predictions: Comparison with Lab Testing Data

In order to verify data from the laboratory testing of the bridge mock-up, several model simulations were run:

I. Shear deformation and torsional resistance not permitted (single-point loads).

II. Shear-deformable theory utilized with *KGA* values obtained experimentally (single-point loads).

III. Shear deformation and torsional resistance permitted (single-point loads).

For each case, the appropriate skew angles, beam material properties, and geometry were held constant. Each simulation was run for four loading cases:

a. Single point loading in the middle of the bridge,
b. Single point loading at one side of the bridge,

c. Single axle loading (2 loads spaced 1.83 m or 6 ft apart) in the middle of the bridge, and
d. Single axle loading at one side of the bridge (design case: HS20-44)

The results of the model predictions are summarized in Figure 4-14 through Figure 4-17. The three different predictions (I-III) for loading case (a) are compared with the lab test data in Figure 4-14. For the single-patch tests, only center bending strains were monitored, so strains are predicted using Equation (3.1). This equation is applicable to both the Euler and Timoshenko predictions. The first prediction (utilizing Euler beam theory and neglecting the torsional stiffness of the girders) predicts the maximum bending strain very closely (within 3% at the maximum data point), but the predicted load distribution is broader. All of the models, in fact, predict a wider distribution of load. The experimental data, on the other hand, indicates that the load is highly concentrated near the load patch. The predicted response near the ends of the deck beams is in error by 100 microstrain (compared to the maximum strain of 657 microstrain). The effect of shear deformation in the first loading case is insignificant, as it lowers the maximum strain only slightly and has little effect on the response far away from the load. Inclusion of both shear deformation and torsional stiffness for the composite girders improved the prediction near the sides of the bridge, but under-predict the maximum strain.

In loading case (b) (single load patch at side), the model prediction is improved by the inclusion of shear deformation (Figure 4-15). Notice the feature in the data just to the left of the 600 cm (236 in) location indicating a localized increase in strain. This feature cannot be predicted using the simple model (I), but by including shear deformation, this feature becomes apparent in the model as well. A review of the measured *KGA* values (Table 4-1) reveals that beam 20 had a relatively low value for the shear product (65.3 GPa-cm^2). Evidently, this beam's low shear modulus is significant enough to affect, at least locally, the response of the deck panel. Inclusion of both shear deformation and torsional stiffness improves the model prediction away from the load but again tends to under-predict the strain at the loading point.

The model predictions for deflections under HS20 loading (c) in the center location are compared with the laboratory test data in Figure 4-16. In this case, the inclusion of shear deformation over-predicts the maximum deflections by about 12%. The addition of torsional stiffness again tightens the response near the loading point, and slightly improves the prediction near the ends of the deck beams. The error at maximum strain is then reduced to 6-7%. However, the error remains large at the sides: nearly a 0.5 cm (25%) difference.

Finally, the predictions for loading case (d) are compared with the laboratory data in Figure 4-17. The data from the field testing is also shown here. Compared to the lab data, the models under-predict the actual deflections at the location of the load by about 0.5 cm (50%); the maximum measured deflection was 2.62 cm. The prediction matches the lab data well near the left load patch and also near the left end of the deck panel. A combination of both shear deformation and torsional stiffness appears to be most adequate for the HS20 side loading case. It is also interesting to note that the model over predicts deflections in the center loading case while under predicting deflections for the side loading case. In general, the models more accurately predict the response of the lab structure, while the deflections of the field structure are over-estimated.

4.3 Summary

An analytical, finite-difference model has been constructed to predict bridge deflections for a single, short-span bridge. The model represents the girders by linear and torsional springs, which act in a linear fashion on the deck. The deck is modeled by a single deck panel, which acts primarily to distribute load to the supporting girders. The deformation of the deck panel along its length is considered to solve this indeterminate statics problem. Euler or Timoshenko beam theory is utilized to construct beam deflection equations for the composite beams. The Timoshenko shear correction coefficient is estimated using Bank's adaptation of Cowper's method to beams composed of orthotropic plates. The total shear product *KGA* is determined experimentally for input into the model. An estimate of the torsional stiffness of the composite beams is made using a model for an isotropic box section.

The effects of shear deformation and torsional stiffness have been explored by comparing the model predictions with the experimental data for the bridge mock-up tests. The predictions demonstrate reasonable agreement with the lab data, but the model appears to be deficient in predicting deflection and strain response at the sides of the bridge. This may be due to the fact that the assumed boundary conditions for the composite girders are inappropriate. The beam deflection equations (both Euler and Timoshenko) were derived for a simple beam; the boundary conditions are 1) net the moment is zero and 2) the vertical displacement is prescribed. In fact, the second condition prevents any vertical displacement at the ends of the deck beam.

However, if the net load on a girder is negative, the girder will deflect up (i.e. in the positive y direction). In the case of the lab test set up, the composite beams were simply laid on the foundation beams and were not constrained so as to prevent upward displacement. Thus, the boundary conditions on the girders in the laboratory were not actually “simple”. Furthermore, the field structure utilizes girder-to-abutment connections, which may tend to provide some clamping action, further stiffening in the structure. Finally, the inclusion of shear deformation and torsional stiffness in the composite beams tends to improve the model predictions, although only slightly.

4.4 Figures and Tables

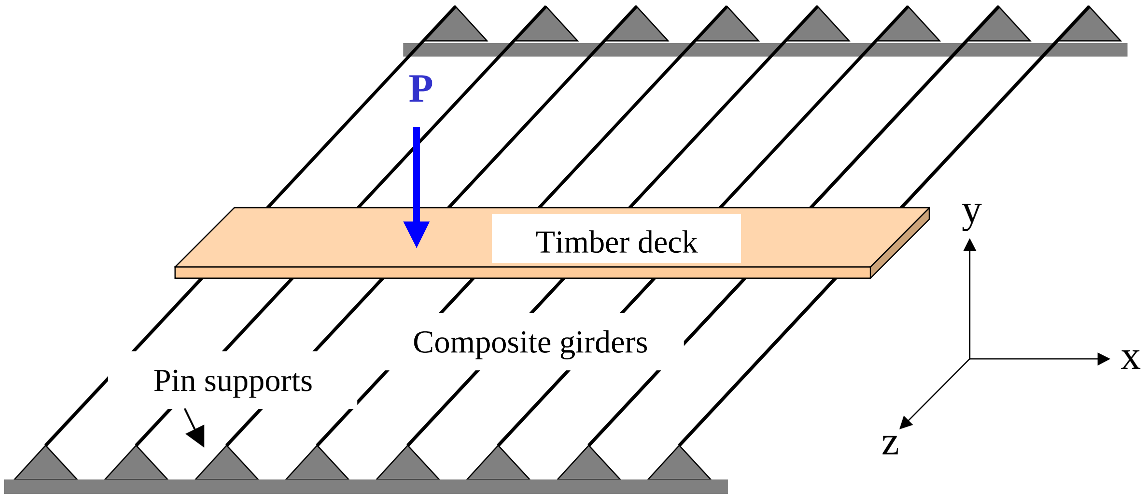

Figure 4-1. Model of bridge as single deck beam on underlying girders (only eight girders are shown).

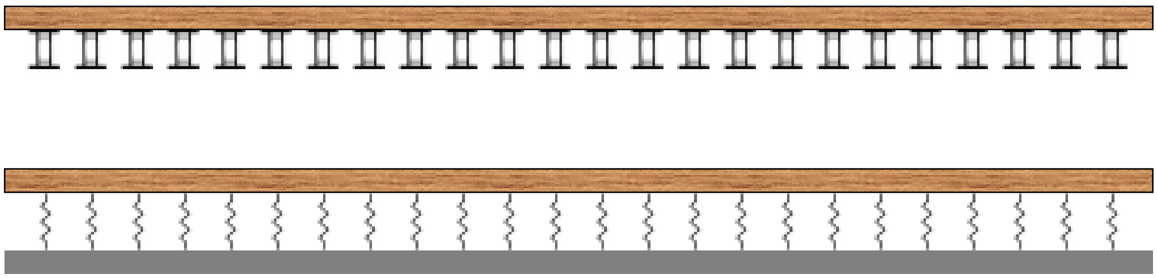

Figure 4-2. Representation of composite girders (top) as linear and torsional springs (bottom). (Torsional springs not shown).

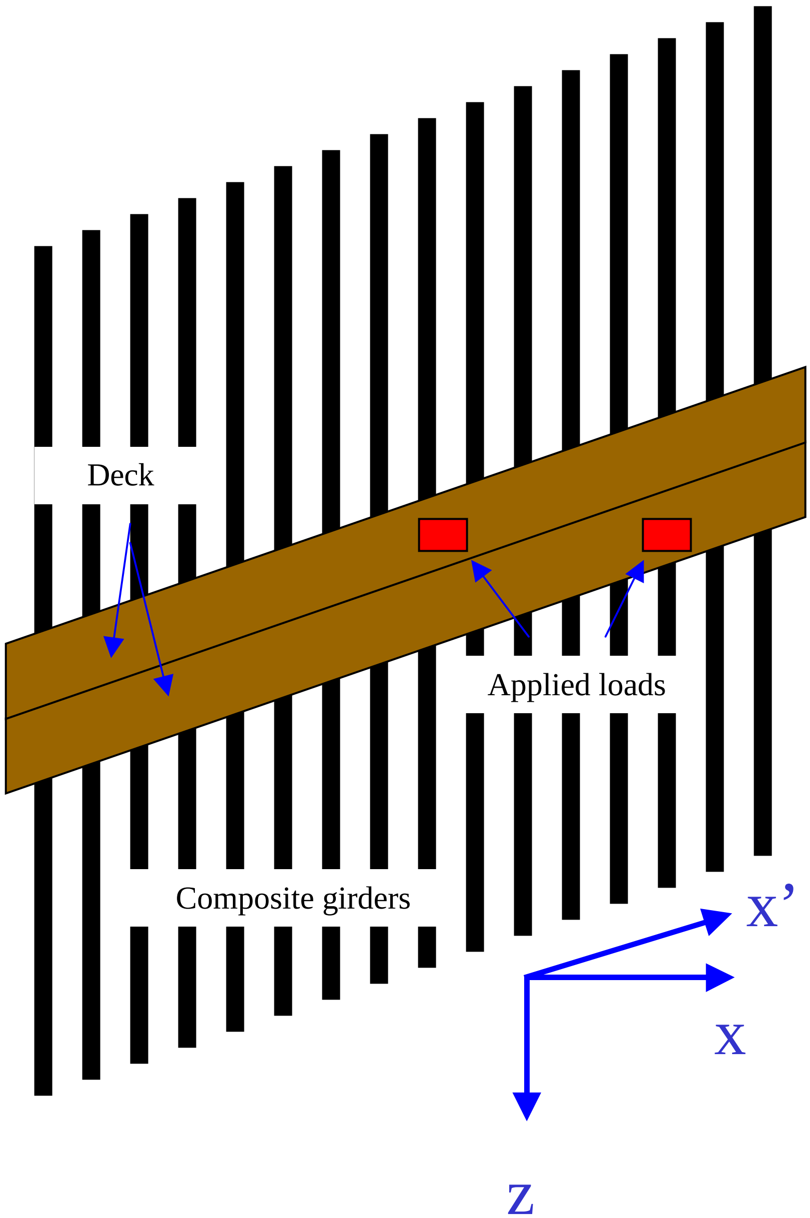

Figure 4-3. Top view schematic of bridge showing superposition of multiple loads. The x′ scale runs parallel to the deck panels. Deflections are computed along the length of this axis.

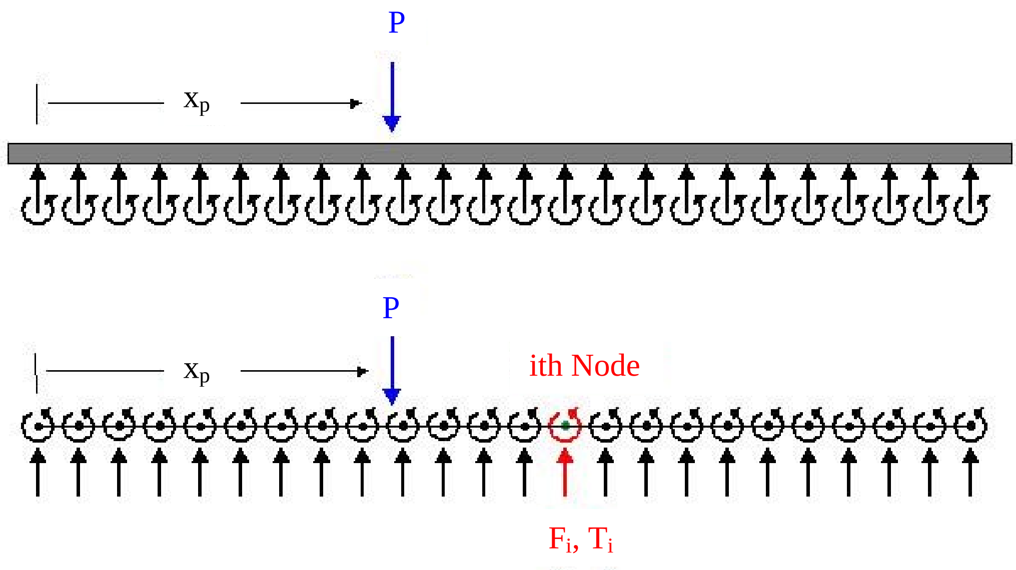

Figure 4-4. Free body diagram of deck beam (top). The girders provide both a reaction force F_i and a reaction moment T_i at the *i*th node (bottom).

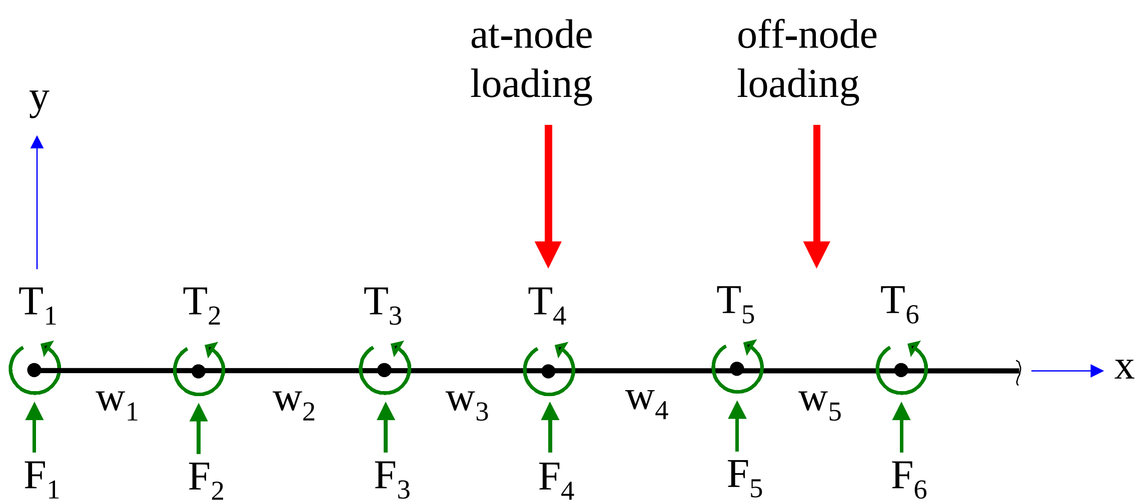

Figure 4-5. Representation of deck beam as 1-D array of nodes with external loads and reaction forces and moments shown.

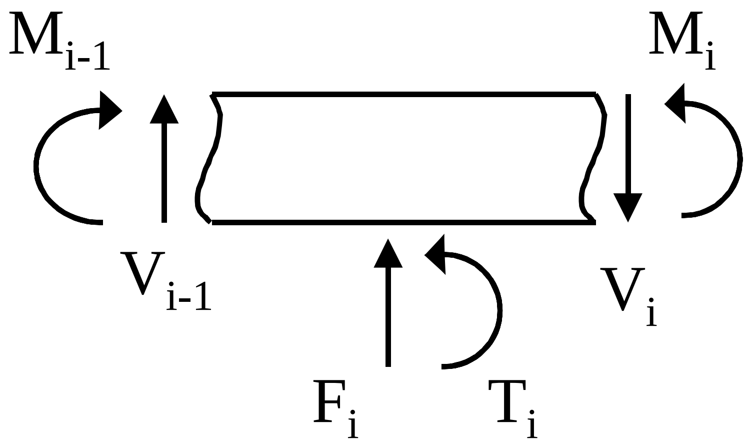

Figure 4-6. Free body diagram of segment of beam centered about the *i*th node.

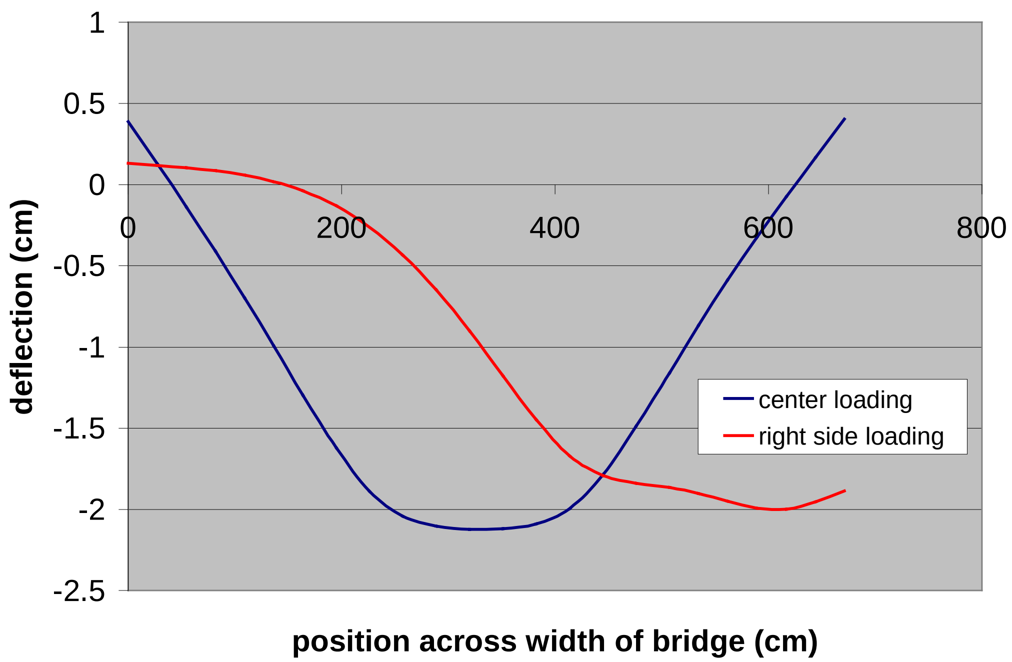

Figure 4-7. Sample model predictions for center and right side loading: deflections across width of bridge, measured along skewed centerline.

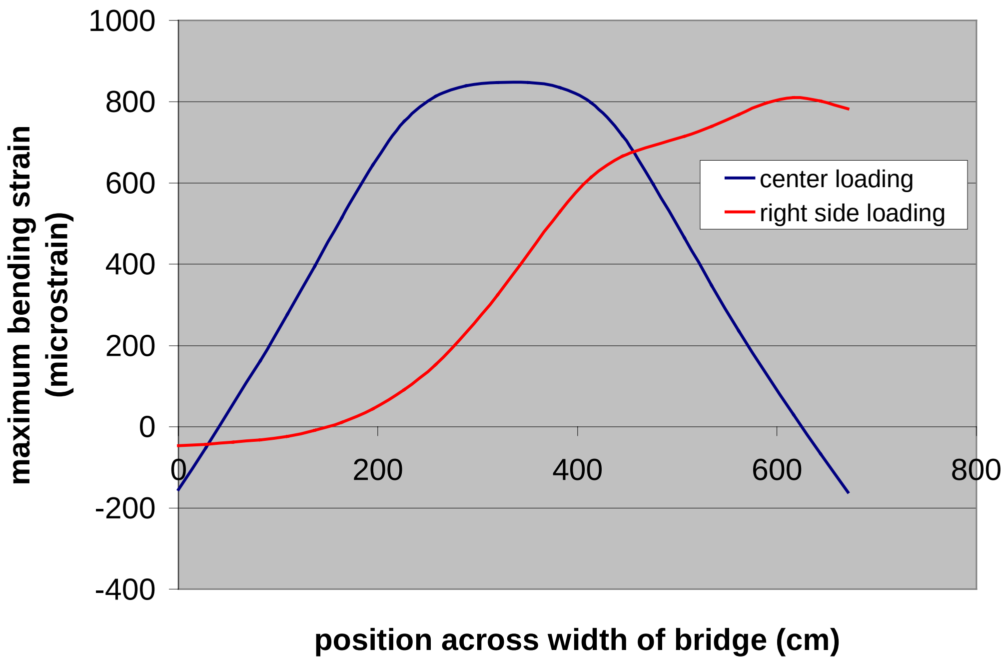

Figure 4-8. Sample model predictions for center and right side loading: maximum bending strains across width of bridge, measured along skewed centerline.

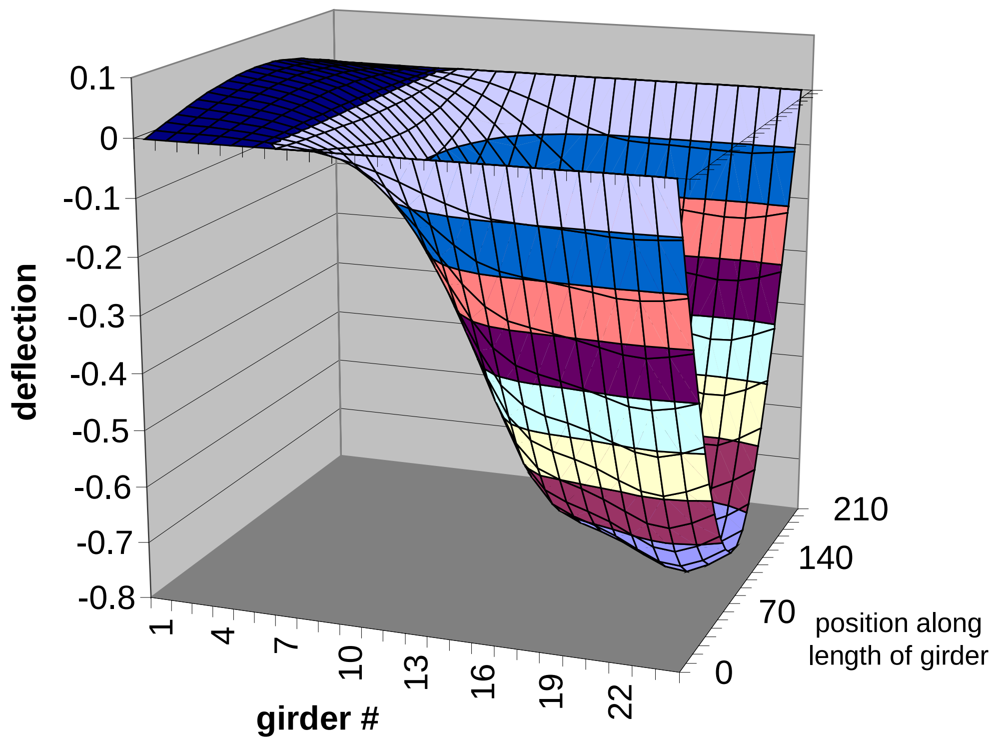

Figure 4-9. Sample model prediction for right side loading: deflections across entire bridge.

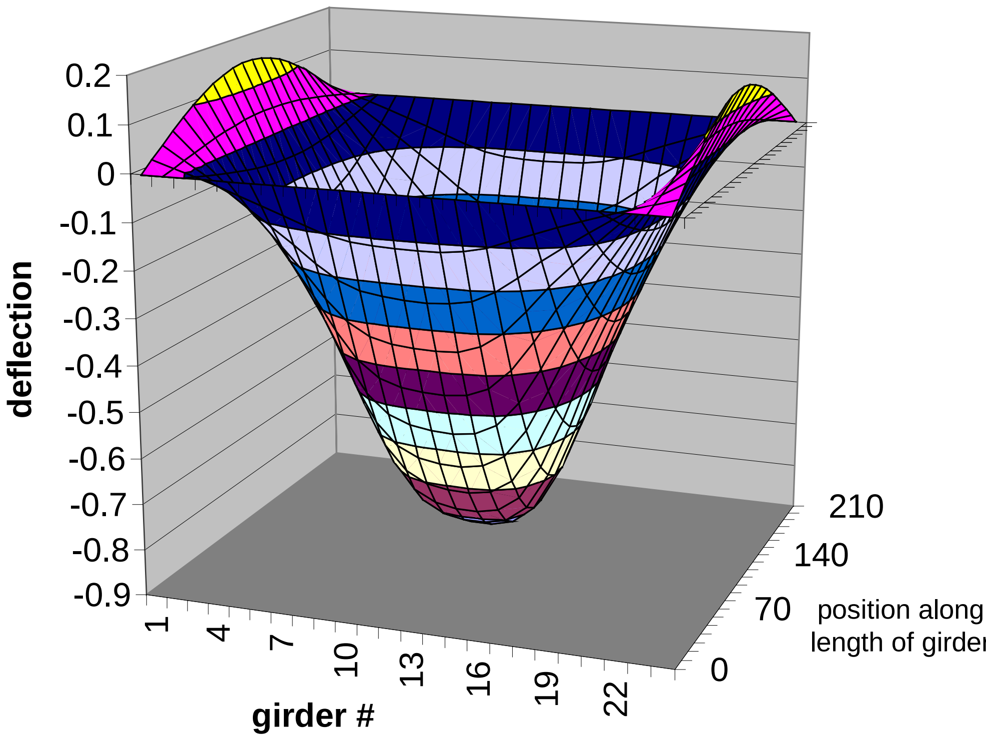

Figure 4-10. Sample model prediction for center loading: deflections across entire bridge.

Table 4-1. Calculated K values utilizing an estimated G_{sx} of 6.89 GPa (1 Msi) and KGA values which were obtained experimentally.

beam #	E GPa	E Msi	K (box)	KGA 10^6 GPa-cm^2	KGA 10^6 Msi-in^2
1	49.4	7.17	1.106	156	3.50
2	47.6	6.90	1.064	191	4.29
3	48.6	7.05	1.087	153	3.44
4	48.2	6.99	1.078	152	3.41
5	47.0	6.81	1.050	181	4.07
6	46.2	6.70	1.033	146	3.27
7	45.6	6.62	1.021	128	2.89
8	45.1	6.54	1.008	136	3.05
9	44.3	6.43	0.991	175	3.94
10	44.3	6.43	0.991	137	3.08
11	43.6	6.33	0.976	130	2.92
12	42.9	6.22	0.959	154	3.47
13	42.7	6.20	0.956	125	2.80
14	44.0	6.38	0.984	136	3.06
15	44.0	6.38	0.984	164	3.69
16	44.2	6.41	0.988	289	6.49
17	44.5	6.45	0.995	185	4.15
18	44.7	6.48	0.999	138	3.11
19	46.1	6.69	1.032	121	2.72
20	46.7	6.77	1.044	65	1.47
21	47.5	6.89	1.062	149	3.36
22	48.1	6.97	1.075	161	3.62
23	48.7	7.06	1.089	153	3.45
24	49.4	7.16	1.104	209	4.71

* These values are based on average K* for all other beams; the test data for these beams was insufficient to estimate KGA.

Table 4-2. Input parameters for model and elasticity solution comparisons with the bridge width held constant at 6.72 m (265 in).

E_{deck}	I_{deck}	$E_{comp.}$	$I_{comp.}$	Skew angle	# of beams	spacing
13.8 GPa (2.0 Msi)	1780 cm^4 (42.7 in^4)	89.6 GPa (13.0 Msi)	5350 cm^4 (128.6 in^4)	0°	12	61.1 cm (24.0 in)
					24	29.2 cm (11.5 in)
					48	14.3 cm (5.63 in)

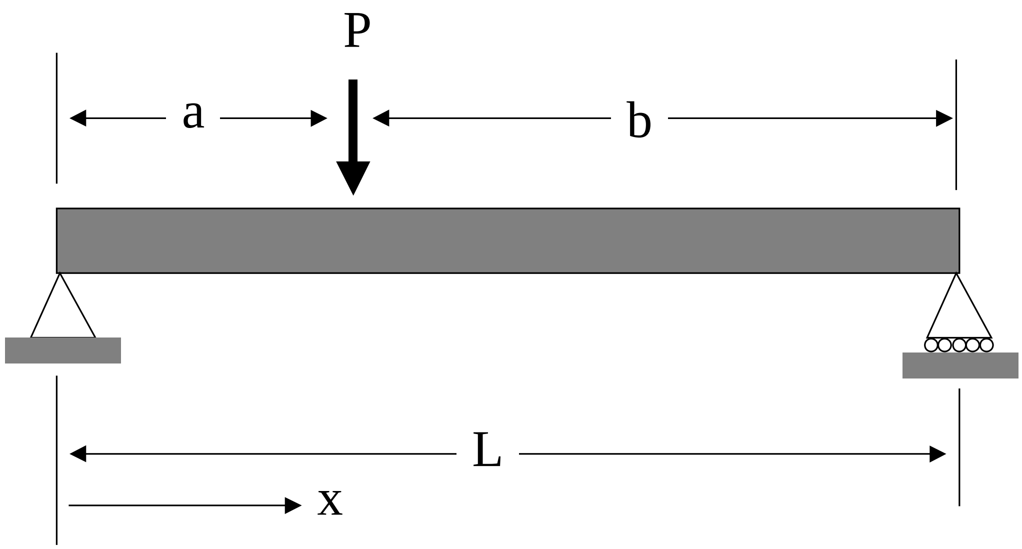

Figure 4-11. Three-point bending geometry.

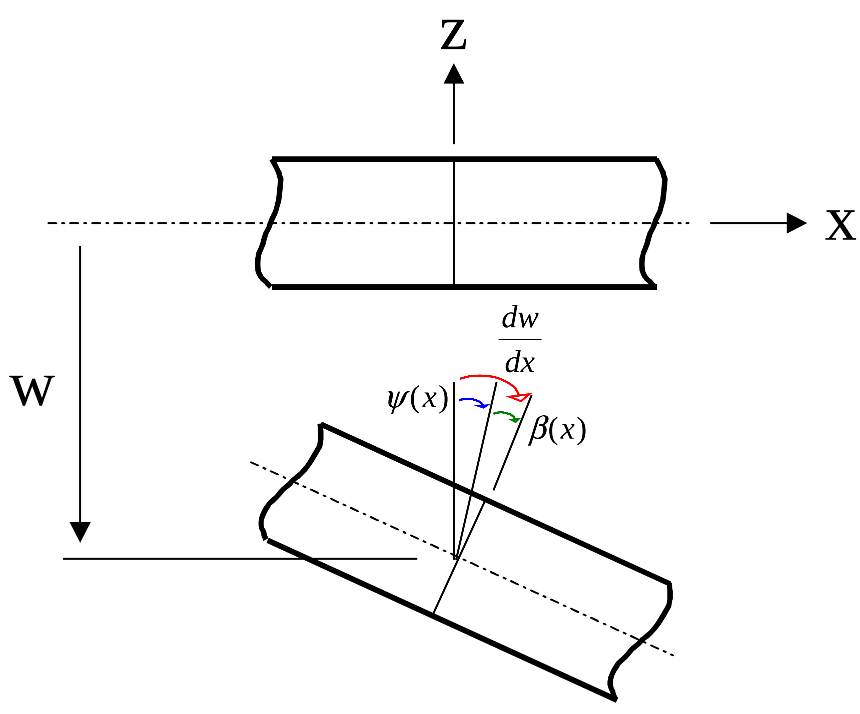

Figure 4-12. Shear-deformable beam: schematic showing rotation of a beam segment due to both bending and shear deformation.

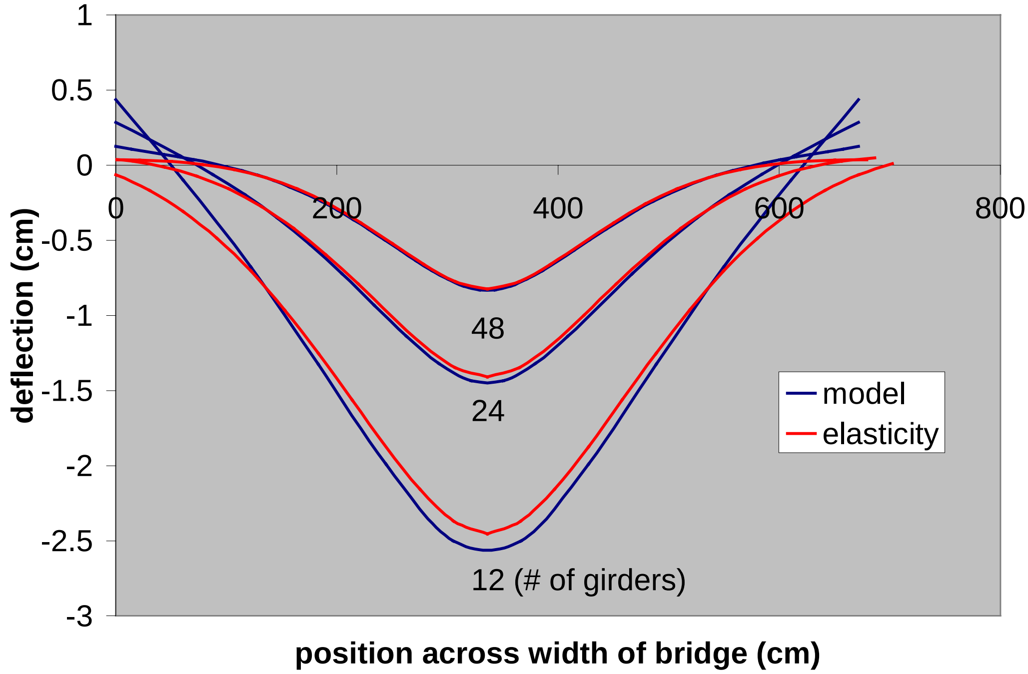

Figure 4-13. Comparison of model prediction and elasticity solution for different number of composite beams and fixed bridge width.

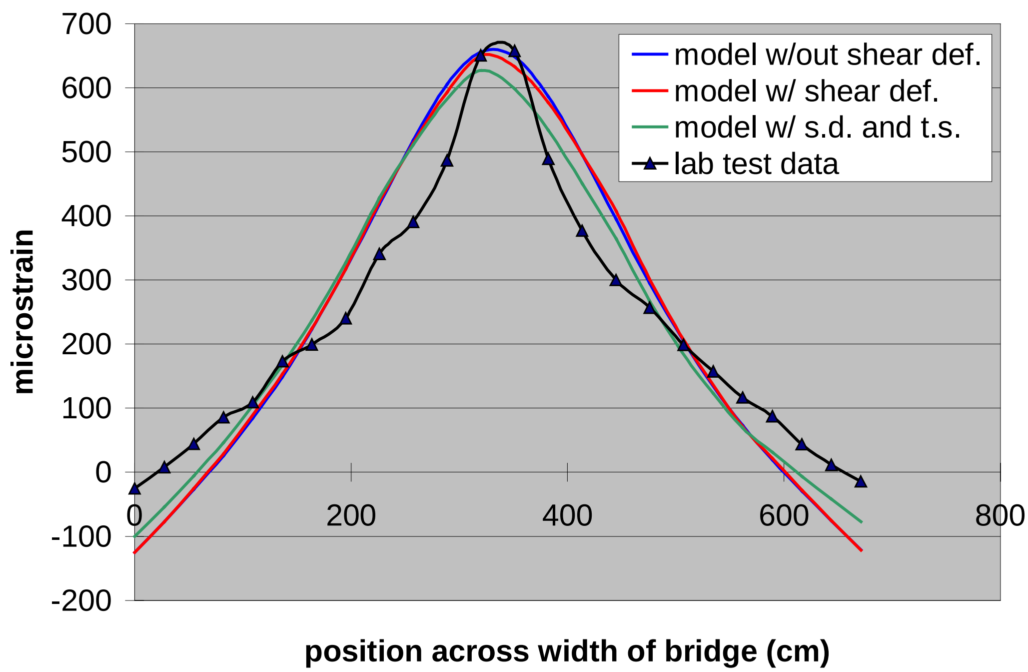

Figure 4-14. Comparison of model predictions and lab test data for single patch load at center of bridge (strains).

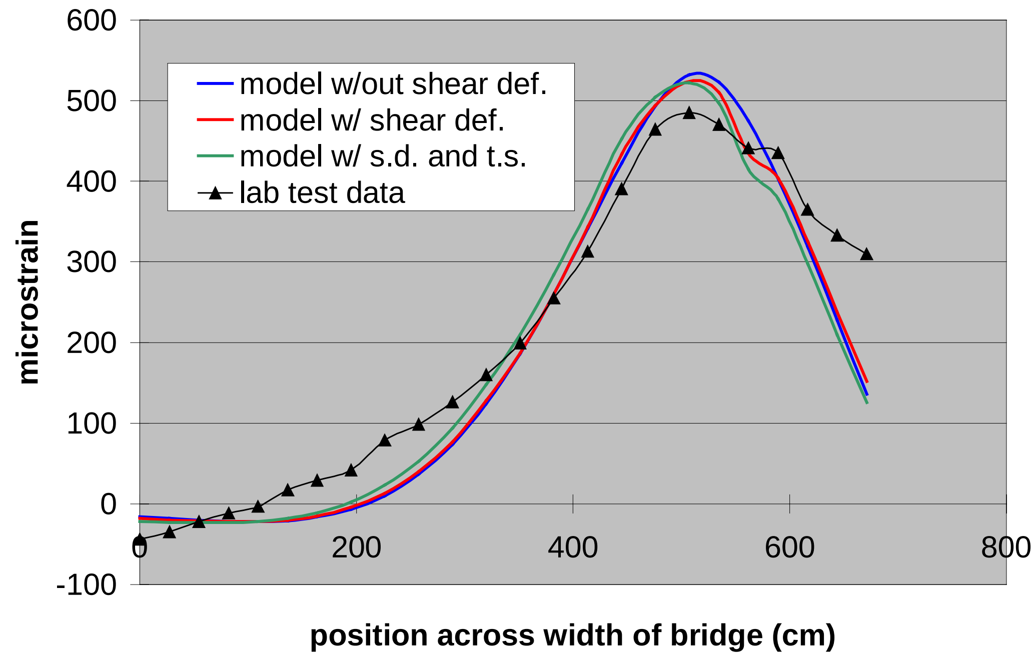

Figure 4-15. Comparison of model predictions and lab test data for single patch load on side of bridge (strains).

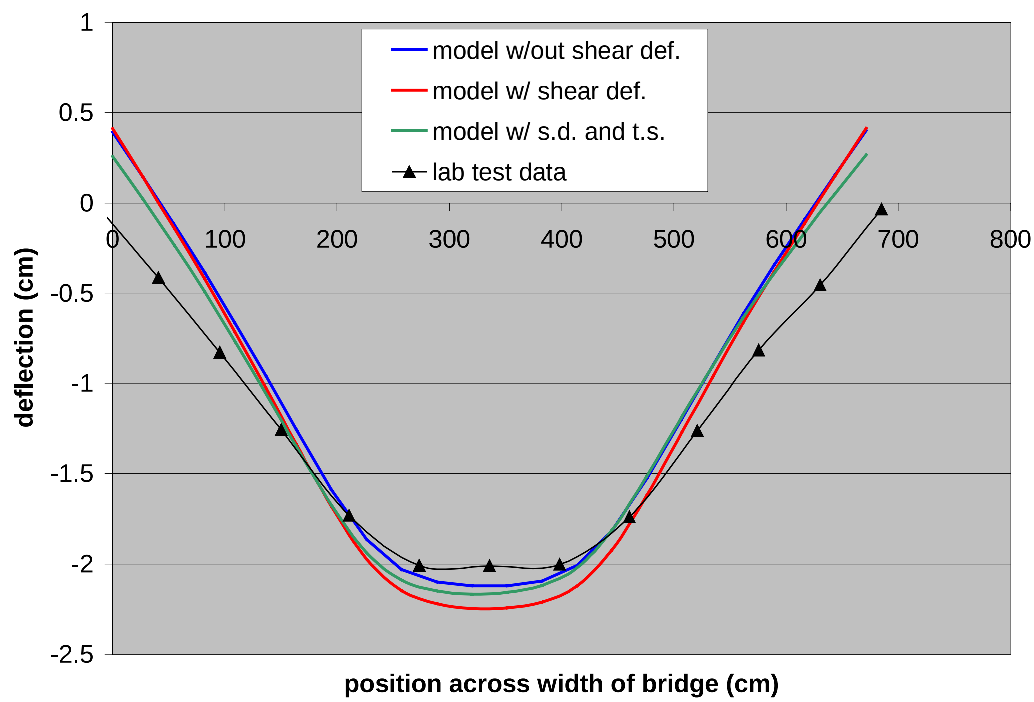

Figure 4-16. Comparison of model predictions and lab test data for single axle loading in center of bridge (deflections).

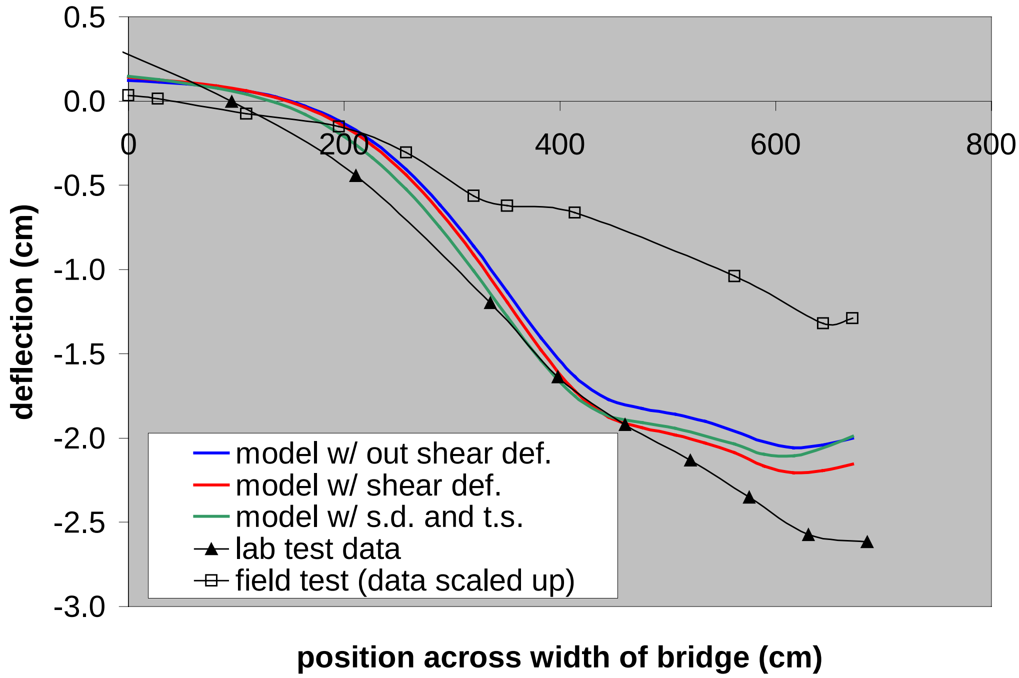

Figure 4-17. Comparison of model predictions and lab test data for single axle loading at side of bridge (deflections).

Chapter 5: Parametric Investigations

In order to evaluate the sensitivity of the model developed in Chapter 4 to the various input parameters (beam properties, bridge geometry, etc.), several basic parametric investigations have been conducted. The influence of changes in a few particular parameters are discussed and recommended input for suitable predictions are suggested. Next, a mechanics of laminated beam (MLB) model is constructed for the 20.3 cm (8 in) deep composite beam. Recommendations for modifying the beam design are made by first determining the beam bending stiffness required to meet various serviceability deflection criteria using the bridge model and then using MLB to determine a geometric scaling factor for the beam cross section that would be necessary to meet the stiffness requirements.

5.1 Influence of Material Properties

The influence of the various material parameters on the global bridge response is investigated. These parameters include the bending stiffnesses of the deck beams and the composite girders, as well as the shear deformation product, *KGA*. For these model predictions, the moment of inertia of the deck beam, I_w, is assumed to be a constant 15.6 x 10^3 cm^4 (374 in^4). The unsupported length of the girders is set at 533 cm (210 in), and the bridge is oriented with no skew angle (0°). All girders are assigned the same bending and shear stiffnesses. The girders are not allowed any torsional stiffness, and shear deformation is permitted only in specific cases.

5.1.1 Deck Beam Stiffness

The composite girders were assigned a modulus of 44.8 GPa (6.5 Msi) and a moment of inertia of 5370 cm^4 (129 in^4). The actual girder spacing of the Tom's Creek Bridge was also utilized. Shear deformation of the composite girders was not permitted. The deck beam modulus was varied between 6.89 and 13.8 GPa (1 and 2 Msi), where

11.0 GPa (1.6 Msi) was the value utilized for the model verification in Chapter 4. The results of these predictions for HS20 center loading are shown in Figure 5-1. As assumed in the development of the model, the deck beam stiffness has little effect on the total bridge response for this (relatively low) modulus of wood. The maximum deflection varies less than 3% for a variation in the modulus of 6.89-13.8 GPa.

5.1.2 Girder Bending Stiffness

The influence of the girder bending stiffness and shear stiffness on the global bridge response is of utmost interest, since some reduction in these properties with time is likely due to environmental degradation. The same parameters of Section 5.1.1 were utilized here again, with the exception that the modulus of the deck beam was assigned a value of 11.0 GPa (1.6 Msi), and the girder modulus was varied between 37.9 and 44.8 GPa (5.5 and 6.5 Msi). In addition, shear deformation was permitted with the *KGA* product equal to 1000 GPa-cm^4 (3.5 Msi-in^4) and was held constant for all values of *EI*. The results of these model runs are shown in Figure 5-2. The maximum deflection scales nearly linearly with changes in girder modulus. For an almost 8% drop in girder modulus (from 44.8 to 41.3 GPa), the maximum deflection increases almost 8%. For a 15% drop in the modulus, the maximum deflection increases by 16%.

5.1.3 Girder Shear Stiffness

In order to determine the influence of shear deformation in the composite girders on the global bridge response, predictions were made with the bridge model using Timoshenko beam theory for the composite girders. Using the input parameters of Section 5.1.1 with a modulus of 44.8 GPa (6.5 Msi) for the composite girders and a shear stiffness term *KGA* of 1000 GPa-cm^2 (3.5 Msi-in^2), the total deflection under HS20 side loading increases by 7% according to the model predictions. Next, the shear stiffness was varied to investigate the influence of a reduction in the shear stiffness that might accompany environmental and mechanical degradation. *KGA* was varied between 1000 and 714 GPa-cm^2 (3.5 and 2.5 Msi-in^2), where the values measured in the beam testing ranged from 65.0 to 289 GPa-cm^2 (1.47 to 6.49 Msi-in^2). The higher value is the average value measured experimentally during the beam proof tests (see Section 4.1.3). The results of these predictions for HS20 center loading are shown in Figure 5-3. For a 14% reduction in *KGA*, the maximum deflection increases by less than 1%. A 29% reduction in *KGA* only causes about a 2% increase in deflection. Within this range of shear stiffness values, the effect of shear deformation on global bridge response is minimal.

5.1.4 Determination of an Upper Bound for Degree of Composite Action

In order to determine an upper bound for the amount of composite action (an upward shift in the neutral axis caused by a contribution of the deck to the bending stiffness of the girders) in the Tom's Creek Bridge, model predictions were performed utilizing a composite area moment of inertia. The moment of inertia of the 13 cm (5.13 in) thick wood deck was lumped into the moment of inertia of the composite girders by first modeling the deck beam under each load as 24 discrete sections centered over each girder. The moment of inertia of each deck section was then transformed by decreasing the effective width of the deck by a ratio *n*, determined by:

$$n = \frac{E_{wood}}{E_{composite}} \qquad (5.1)$$

The composite moment of inertia was then calculated at the centroid of the girders and shifted to the centroid of the composite area using the parallel-axis theorem. The shift in the neutral axis by inclusion of the deck section was 8.33 cm (3.28 in). This approach assumes that there is no plate action of the deck beam assembly.

New girder stiffnesses, *EI*, were next determined for each composite girder using the experimentally measured modulus values, and a model prediction was performed. Neither shear deformation nor torsional stiffnesses were permitted. The resulting increase in the girder stiffnesses was around 250%, and this caused a decrease in the maximum deflection of 66%. The deflections across the width of the bridge for both cases are shown in Figure 5-4. The deflection-to-span ratio increased from L/237 to L/715 with the inclusion of the deck moment of inertia. These results indicate that the girth of the wood deck beams in the Tom's Creek Bridge could potentially provide significant additional stiffness to the bridge structure, if composite action could be achieved. The degree of composite action will, however, depend upon the efficiency of the connections to transmit stress from the girders to the deck.

5.1.5 Effect of the Wood Rub Rails Modeled as Stiff Girders

The rub rails as designed for the Tom's Creek Bridge consist of two 15.2 cm x 20.3 cm (6 in x 8 in) timber beams that are bolted to the wood deck (Figure 1-6). These beams were included in a model simulation by adding a much stiffer girder on each side of the bridge model for a total of 26 girders. These two girders were assigned a bending modulus of 11.0 GPa (1.6 Msi) for wood and a moment of inertia determined by transferring the value of the combined 30.5 cm (12.0 in) deep rails and 13.0 cm (5.13 in) deep deck at its centroid to the neutral axis of the composite girders. The resulting bending stiffness, *EI*, was 44 times larger than that of the composite girders. The composite beam properties and bridge geometry of the Tom's Creek Bridge was utilized, and again, shear deformation and torsional stiffness was not permitted for any of the girders.

The resulting deflection response under HS20 center loading is shown in Figure 5-5. This modification had little effect, decreasing the maximum deflection by less than 3%. There were, however, local reductions in uplift at the outer edges due to the presence of the rub rails. For HS20 side loading, the effect of the right outer beam is more pronounced. The shape of the response is considerably different as the deflections near the edge of the bridge are greatly reduced. The maximum deflection is reduced by 9%, and in the model prediction performed using stiffer outer beams, the maximum deflection occurs at the left wheel patch rather than the right patch, as in the case of the standard model prediction (Figure 5-6).

5.1.6 Effect of Wheel Loading Positions

The position of the wheel patch loads can be important in determining the shape of the deflection response, especially when a load is applied near the side of the bridge. In order to investigate the sensitivity of the model to the location of the loads, the model was run for the geometry and properties of the Tom's Creek Bridge without shear deformation or torsional stiffnesses included. HS20 side loading was simulated with both wheel patches moved laterally in 12.7 cm (5 in) increments to either side. The results indicate that for the side loading, small variations in loading position can have fairly significant effects on the maximum deflections observed. For instance, when the wheel loads are moved 25.4 cm (10 in) to either side, the maximum deflection varies by nearly 50% of the value obtained for the HS20 case where the right wheel patch is located 61.0 cm (24 in) from the right edge (see Figure 5-7). These results emphasize the importance of the loading position in the lab and field testing of the bridge.

5.2 Design considerations

The bridge model is utilized to determine the bending stiffnesses required in the composite girders to achieve various serviceability criteria for both 24 and 12 beam bridge designs. Recommendations for new beam designs are made by suggesting changes in geometry only. These recommendations are made using a mechanics of laminated beams model. The model is first verified by predicting the properties of the 20.3 cm (8 in) composite beam and comparing the results with the test data.

5.2.1 Mechanics of Laminated Beams

The design of a composite beam constructed from laminated panels is complicated due to the orthotropy of the material, and the constituent panels (i.e. web and flange) are generally composed of laminates with different lay-ups. The difficulty of controlling the manufacturing process to construct specific laminate geometries adds further constraints on beam design. In addition, the theory of laminated beams is not as well established as the mechanics of laminated plates. A summary of the progress in this area is given by Barbero et al. [42] of West Virginia University (WVU) and they present their own approach to the mechanics of laminated beams (MLB) [42,49]. That approach is summarized in the following.

The WVU group's approach considers a beam to be composed of laminated panels in either an open or closed section geometry (see Figure 5-8). The middle surface of the beam section is represented by a contour line that is referenced to the cross section's principal axes (s_i, along the contour, and z_i, along the axis of the beam) and the angle of orientation of each plate, ϕ_i. Transverse loads are assumed to be applied through the shear center within a plane normal to the principal axes, so that bending is decoupled from torsion. Following Timoshenko beam theory, the contour is assumed not to deform in its own plane. Furthermore, plane sections which were originally normal to the beam axis remain plane, but may skew relative to the beam axis. Residual displacements in the z-direction due to warping are not considered.

According to Classical Laminate Theory (CLT), the constitutive relations for each laminated plate are constructed:

$$\begin{Bmatrix} \{\overline{N}\} \\ \{\overline{M}\} \end{Bmatrix} = \begin{bmatrix} [A] & [B] \\ [B] & [D] \end{bmatrix} \begin{Bmatrix} \{\overline{\varepsilon}\} \\ \{\overline{\kappa}\} \end{Bmatrix} \tag{5.2}$$

where the laminate resultant forces and moments are

$$\{\overline{N}\} = \begin{Bmatrix} \overline{N}_z \\ \overline{N}_s \\ \overline{N}_{sz} \end{Bmatrix} \text{ and } \{\overline{\mathrm{M}}\} = \begin{Bmatrix} \overline{\mathrm{M}}_z \\ \overline{\mathrm{M}}_s \\ \overline{\mathrm{M}}_{sz} \end{Bmatrix} \tag{5.3}$$

and the laminate strains and curvatures are

$$\{\bar{\varepsilon}\} = \begin{Bmatrix} \bar{\varepsilon}_s \\ \bar{\varepsilon}_z \\ \bar{\varepsilon}_{sz} \end{Bmatrix} \quad \text{and} \quad \{\bar{\kappa}\} = \begin{Bmatrix} \bar{\kappa}_s \\ \bar{\kappa}_z \\ \bar{\kappa}_{sz} \end{Bmatrix} \tag{5.4}$$

If the [*ABD*] stiffness matrix of Equation (5.2) is inverted, then

$$\begin{Bmatrix} \{\bar{\varepsilon}\} \\ \{\bar{\kappa}\} \end{Bmatrix} = \begin{bmatrix} [\alpha] & [\beta] \\ [\beta]^T & [\delta] \end{bmatrix} \begin{Bmatrix} \{\bar{N}\} \\ \{\bar{M}\} \end{Bmatrix} \tag{5.5}$$

where the [$\alpha\beta\delta$] matrix is termed the compliance matrix.

Consistent with a plane stress assumption, the resultant forces and moments due to transverse normal stresses are then considered to be negligible so that

$$\bar{N}_s = \bar{M}_s = 0 \tag{5.6}$$

and for the case of bending without torsion,

$$\bar{M}_{sz} = 0 \tag{5.7}$$

Furthermore, in order to simplify the variational solution, the laminates composing the beam are all assumed to be balanced, symmetric so that

$$\alpha_{16} = \beta_{16} = 0 \tag{5.8}$$

These assumptions simplify Equation (5.5) to the following form:

$$\begin{Bmatrix} \bar{\varepsilon}_z \\ \bar{\kappa}_z \\ \bar{\gamma}_{sz} \end{Bmatrix} = \begin{bmatrix} \alpha_{11} & \beta_{11} & 0 \\ \beta_{11} & \delta_{11} & 0 \\ 0 & 0 & \alpha_{66} \end{bmatrix} \begin{Bmatrix} \bar{N}_z \\ \bar{M}_z \\ \bar{N}_{sz} \end{Bmatrix} \tag{5.9}$$

If Equation (5.9) is inverted back,

$$\begin{Bmatrix} \overline{N}_z \\ \overline{M}_z \\ \overline{N}_{sz} \end{Bmatrix} = \begin{bmatrix} \overline{A}_i & \overline{B}_i & 0 \\ \overline{B}_i & \overline{D}_i & 0 \\ 0 & 0 & \overline{F}_i \end{bmatrix} \begin{Bmatrix} \overline{\varepsilon}_z \\ \overline{\kappa}_z \\ \overline{\gamma}_{sz} \end{Bmatrix} \tag{5.10}$$

where the extensional stiffnesses for each *i*th laminate are:

$$\begin{aligned} \overline{A}_i &= \frac{\delta_{11}}{\alpha_{11}\delta_{11} - \beta_{11}^2}, \text{ extensional stiffness} \\ \overline{B}_i &= \frac{-\beta_{11}}{\alpha_{11}\delta_{11} - \beta_{11}^2}, \text{ bending-extension coupling stiffness} \\ \overline{D}_i &= \frac{\alpha_{11}}{\alpha_{11}\delta_{11} - \beta_{11}^2}, \text{ bending stiffness} \\ \overline{F}_i &= \frac{1}{\alpha_{66}}, \text{ shear stiffness} \end{aligned} \tag{5.11}$$

The total beam stiffnesses then are defined in terms of summations of the above laminate stiffnesses:

$$\begin{aligned} A_z &= \sum_{i=1}^{N} \overline{A}_i b_i \\ B_y &= \sum_{i=1}^{N} \left[\overline{A}_i (\overline{y}_i - y_n) + \overline{B}_i \cos(\phi_i) \right] b_i \\ D_y &= \sum_{i=1}^{N} \left[\overline{A}_i \left((\overline{y}_i - y_n)^2 + \frac{b_i^2}{12} \sin^2 \phi_i \right) + 2\overline{B}_i (\overline{y}_i - y_n) \cos(\phi_i) + \overline{D}_i \cos^2 \phi_i \right] b_i \\ F_y &= \sum_{i=1}^{N} \overline{F}_i b_i \sin^2 \phi_i \end{aligned} \tag{5.12}$$

where b_i are the lengths of each panel (in the *s*-direction), y_i are the locations of the centroids of each panel, and y_n is the location of the beam's neutral axis. D_y is the bending stiffness of the beam, normally denoted *EI*. F_y is the shear stiffness of the beam, usually represented by *GA*. A shear correction factor, K_y, can also be determined using this approach; the equations are not presented here but can be found in Reference [42].

5.2.2 MLB Predictions: Comparison with Test Data

In order to verify the accuracy of this MLB approach, the bending and shear stiffnesses of the 20.3 cm (8 in) deep composite box I-beam utilized in the Tom's Creek Bridge rehabilitation were calculated. The beam geometry was resolved into its constituent panels (Figure 5-9), and the lay up of each panel was determined from the thread-up information [70]. A FORTRAN code was utilized to determine the stiffness matrix of Equation (5.2) by CLT using typical properties for carbon (Hercules AS4) and E-glass fibers and vinyl ester resin. The properties of these materials utilized are summarized in Table 5-1. The calculations of Equations (5.11) and (5.12) were also performed using a FORTRAN subroutine. The following results were obtained:

$$D_y = EI = 247 \times 10^3 \text{ GPa-cm}^4 \text{ (891 Msi-in}^4\text{)}$$
$$F_y = GA = 281\text{x } 10^3 \text{ GPa-cm}^2 \text{ (6.31 Msi-in}^2\text{)}$$

Using the moment of inertia I_{zz} = 5350 cm^4 (129 in^4), the effective bending modulus E is 47.8 GPa (6.93 Msi). This correlates very well with the experimental data; the average measured modulus for the Batch 1 beams which utilized the higher-modulus Hercules AS4 carbon fiber was 48.1 GPa (6.98 Msi). If it is assumed that the flanges do not contribute to the shear stiffnesss (for a cross-sectional shear area of 13.6 cm^2 or 5.36 in^2), then the effective shear modulus G can be approximated as 7.38 GPa (1.07 Msi). Using Bank's calculations for the shear correction factor in Equation (4.25) with the E and G determined here, K is determined to be 1.07. The shear term KGA is then calculated to be 300 x 10^3 GPa-cm^2 (6.75 Msi-in^2); this value is almost twice the averaged measured value of 157 GPa-cm^2 (3.5 Msi-in^2). The discrepancy may possibly be attributed to errors in the calculation of K or the F_y value predicted using MLB.

Bridge Design Recommendations

The bridge model was utilized to determine the composite beam bending stiffness necessary for certain serviceability criteria, so that recommendations for different beam designs can be made. First, the bending stiffness values (*EI*) required to improve the stiffness of the 24-beam Tom's Creek Bridge design to L/300, L/600, and L/900 were determined. All composite girders were assigned the same bending and shear stiffness values (*EI* and *KGA*), and these values were incrementally increased until the desired deflection criterion was met. Model predictions were run for the cases of 1) no shear deformation or torsional stiffness, 2) shear deformation only, 3) torsional stiffness permitted, but not shear deformation, and 4) both shear deformation and torsional stiffnesses permitted. As a first approximation, the shear stiffness *KGA* was scaled linearly with *E* according to a ratio determined from the experimental beam data. The validity of this assumption is discussed further below.

The results of the model calculations for a 5.33 m (17.5 ft) span bridge utilizing 24 girders at a 29.2 cm (11.5 in) spacing (no skew) are presented in Figure 5-10. Here, the bending stiffness that is required for each different deflection criteria is determined for the four model types. The second model type utilizing only shear deformation is of course the most conservative of the four models as the predicted deflections are greatest, so results from this model would be most appropriate for design. However, the combined effect of shear deformation and torsional stiffness is fairly insignificant, at least for the current 20.3 cm (8 in) deep section. Still, the assumption that *EI/KGA* is a constant is not necessarily correct. For instance, if the geometry of the beam is scaled up without affecting the individual panel properties (as is assumed in the next section) so that *EI* can be increased by only increasing the moment of inertia, *I*, then the span-to-depth ratio will decrease. Shear deformation will then become more significant, and the ratio *EI/KGA* will increase. Given the uncertainty of how to scale up the shear stiffness, shear deformation (and torsional stiffness) is neglected in the following design recommendations. Thus, the bridge stiffness is a function of only the composite beam bending stiffness, *EI*.

The results for the model indicate that in order to improve the stiffness of a structure like the Tom's Creek Bridge from L/255[7] to L/300, the average *EI* of each beam would have to be increased to 310 x 10^3 GPa-cm^4 (1080 Msi-in^4), an increase of 29% (see Figure 5-11). It is noted, however, that the arrangement of the stiffer composite

---

[7] This is the serviceability rating for the Tom's Creek Bridge determined in the lab testing.

beams at the outer edges of the bridge and the variable spacing should stiffen the structure; these factors are neglected in these calculations. To improve the stiffness of the same bridge configuration to L/600 or L/900, the model predicts required stiffnesses of 626 x 10^3 and 959 x 10^3 GPa-cm^4 (2180 and 3340 Msi-in^4), respectively, for the composite beam. These are increases of 161 and 300%, respectively.

If the number of composite girders is reduced to 12 and a spacing of 61.0 cm (24 in) is utilized, as in the original Tom's Creek Bridge structure with steel I-beams, then the beam stiffness requirements essentially double (Figure 5-12). For instance, using the standard bridge model, the predicted *EI* necessary to achieve an L/300 deflection criterion is 588 x 10^3 GPa-cm^4 (2050 Msi-in^4). This is an increase of 145% over the bending stiffness of the current 20.3 cm (8 in) box I-beam.

Composite Beam Design Recommendations

As a first attempt at recommending a new beam design for the various deflection criteria, only the beam geometry is adjusted. As a further simplification, all beam cross-sectional dimensions are scaled linearly by the same factor. This assumption requires that the scaling of individual panels will not affect the lay up and fiber volume fractions, although in actuality, the number of laminae will increase. This increase in scale will increase the moment of inertia, but will also affect the plate stiffnesses and, therefore, beam stiffnesses as well.

Using the scale-up method, a scaling factor was determined for the three deflection-to-span ratios L/300, L/600, and L/900 for the 12 beams and 61.0 cm (24.0 in) spacing design previously examined. The scaling factor was iteratively increased in the MLB code until the desired bending stiffness was obtained. To simplify the calculations, shear deformation was not considered. The results of these calculations are shown in Table 5-2. For the L/300 criterion, a geometric scaling of 1.23 is required, while the L/600 and L/900 criteria require scaling factors of 1.48 and 1.65, respectively. The resulting properties and dimensions of the scaled beams are also shown in the table. Using the scaling assumptions mentioned above, the bending and shear moduli, *E* and *G*, remain constant. However, the ratio of *EI/KGA* increases with scaling, so that the effects of shear deformation will become more significant. The variation in this ratio with scaling factor is shown in Figure 5-13.

Because shear deformation becomes more significant with scaling, the bridge model code was rewritten to include the MLB calculations. Thus, as the scaling factor is increased, both *EI* and *KGA* can be determined for the new dimensions and both quantities can be included in the bridge model predictions. This approach will be more conservative as the inclusion of shear deformation will necessitate somewhat greater scaling factors to meet the same serviceability ratios. The results from this modified bridge/MLB model are summarized in Table 5-3 for the same 12-beam bridge model previously investigated. The results indicate that the increase in scaling factors necessary due to the inclusion of shear deformation in the model is less than 3%. Therefore, the simplified approach that neglects shear deformation provides a very good method for designing alternate beam sections *for the particular bridge design investigated here*. Changes in girder span, number of girders, and spacing may cause shear deformation to play a more important role.

Finally, it is noted that alternate approaches to modifying the beam design would be to alter the beam lay up, fiber volume fractions, percentage of carbon fiber in the flanges, etc. In fact, a combination of changes in both geometry and lay up may provide the most feasible designs, but would complicate design optimization. Such design changes are outside the scope of this study.

5.3 Figures and Tables

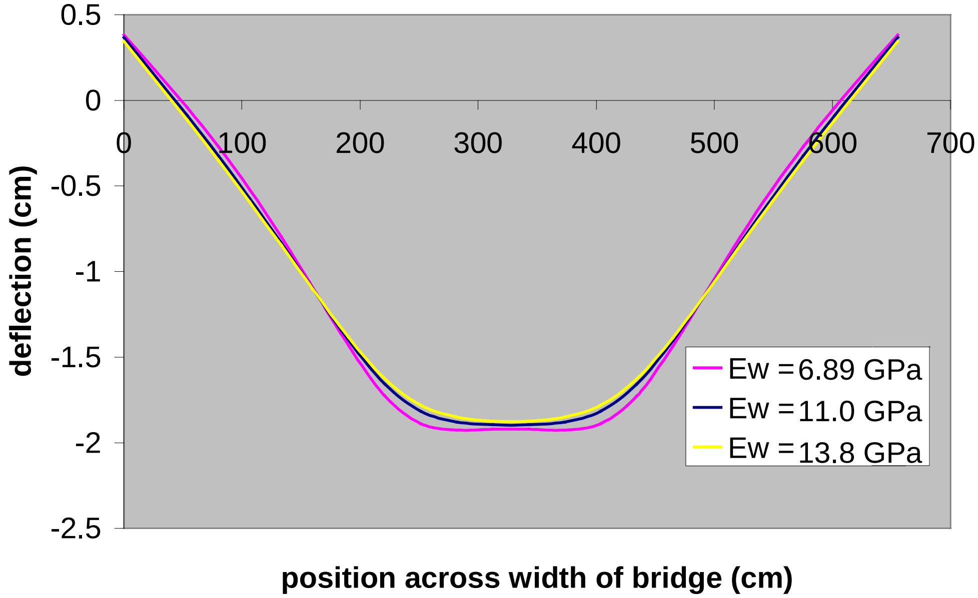

Figure 5-1. Influence of deck beam stiffness on bridge model response. (E_{comp} = 44.8 GPa, KGA = ∞)

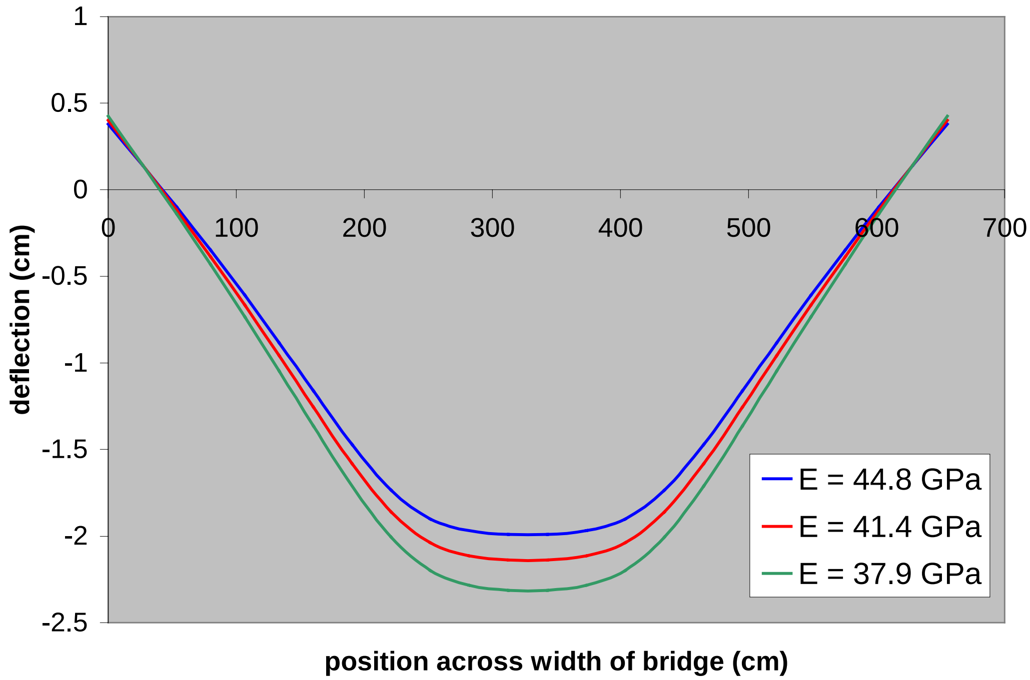

Figure 5-2. Effect of girder modulus on bridge response with shear deformation permitted. (E_w = 11.0 GPa, KGA = 157 GPa-cm^2)

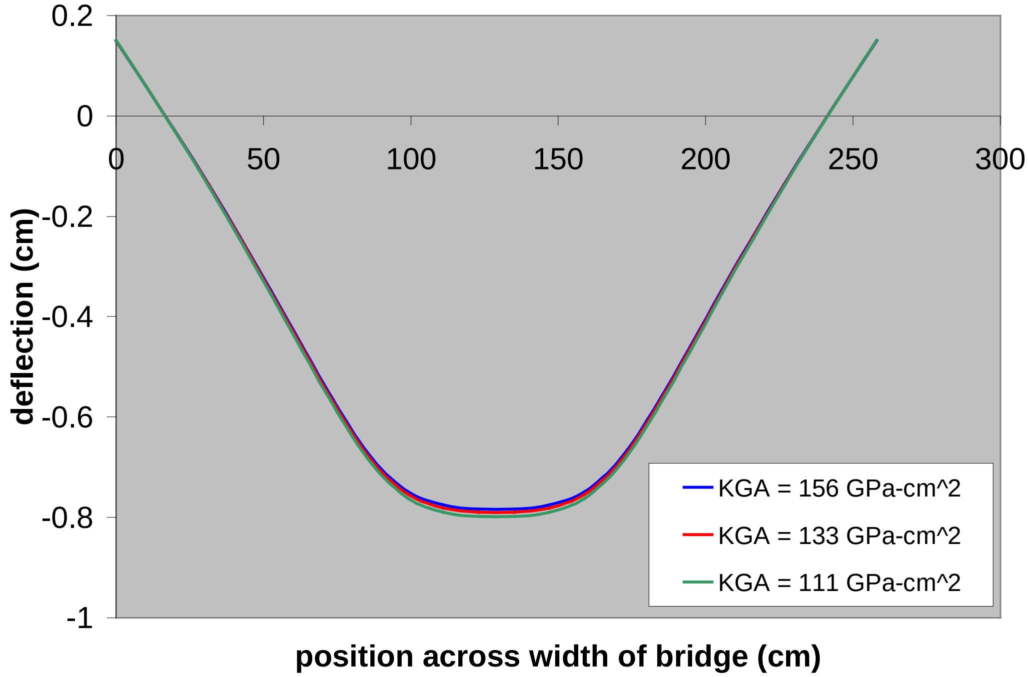

Figure 5-3. Effect of reductions in shear stiffness term, KGA, on total deflection response of bridge at HS20 center loading. (E_w = 11.0 GPa, E_{comp} = 44.8 GPa)

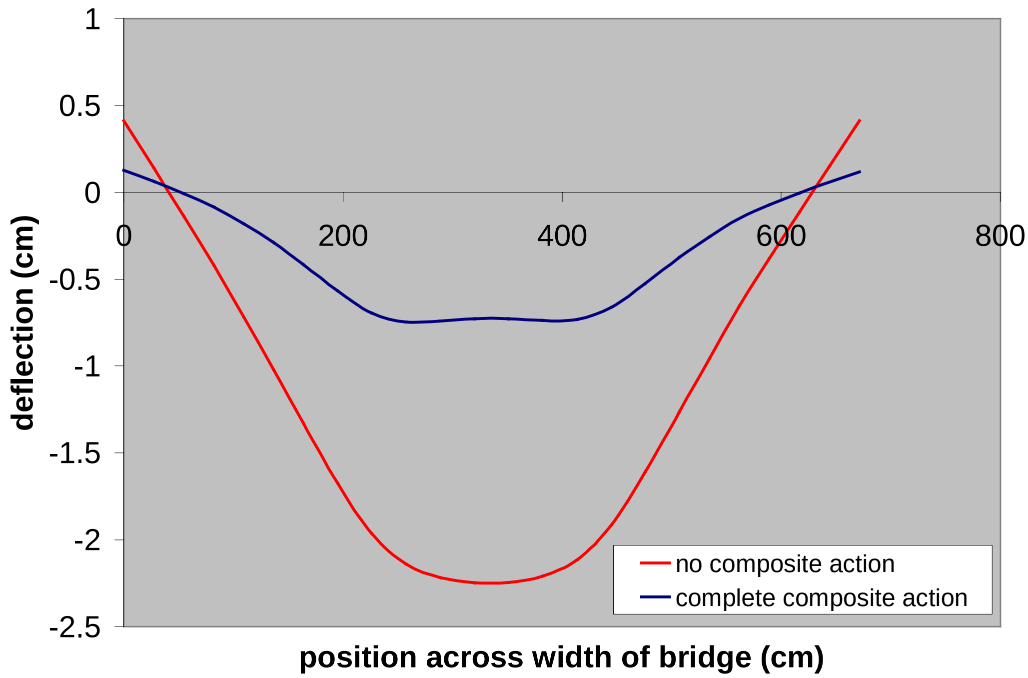

Figure 5-4. Effect of composite action caused by complete contribution of wood deck beam to girder stiffness by an increase in the moment of inertia.

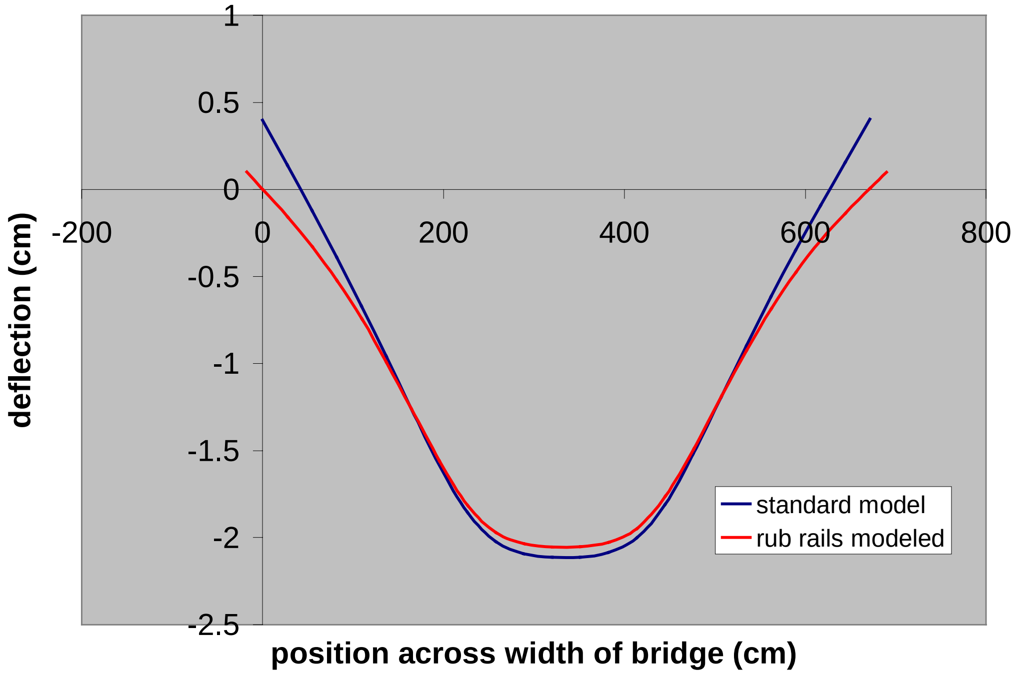

Figure 5-5. Effect of stiff exterior beams to simulate wood rub rails. (E_w = 11.0 GPa, E_{comp} = 44.8 GPa)

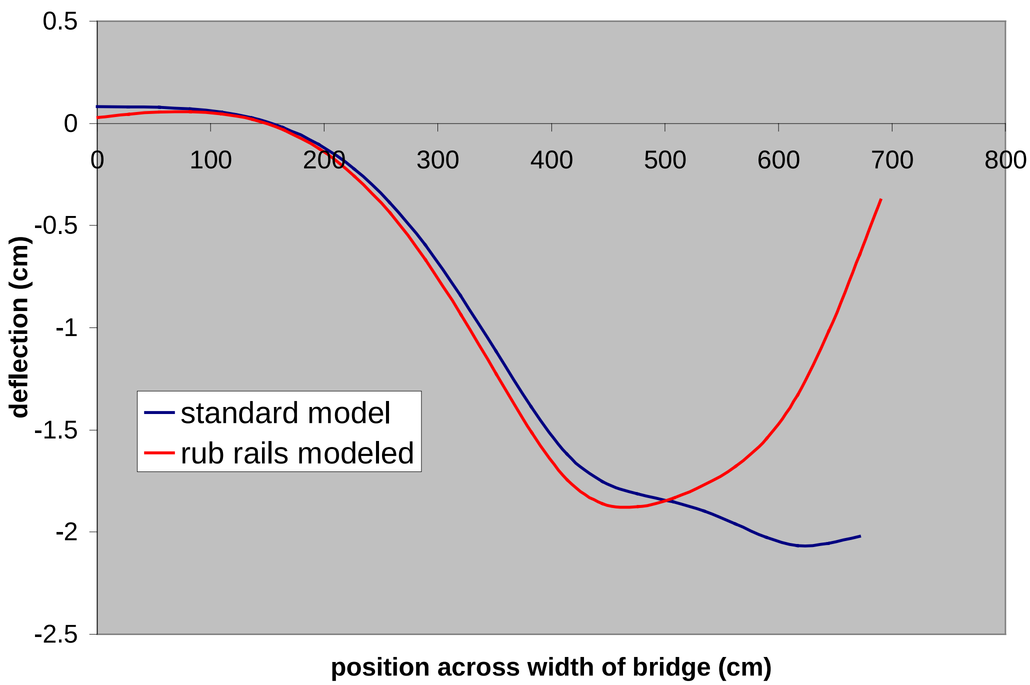

Figure 5-6. Effect of stiff exterior rub rails on deflections under HS20 side loading.

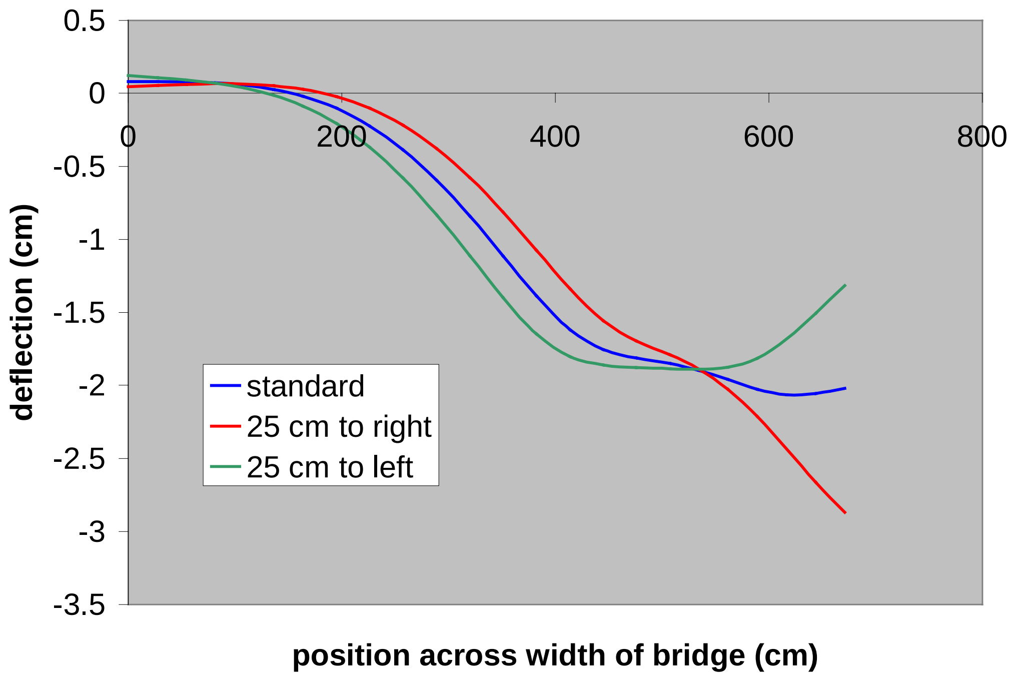

Figure 5-7. Effect of loading position on bridge response for HS20 side loading.

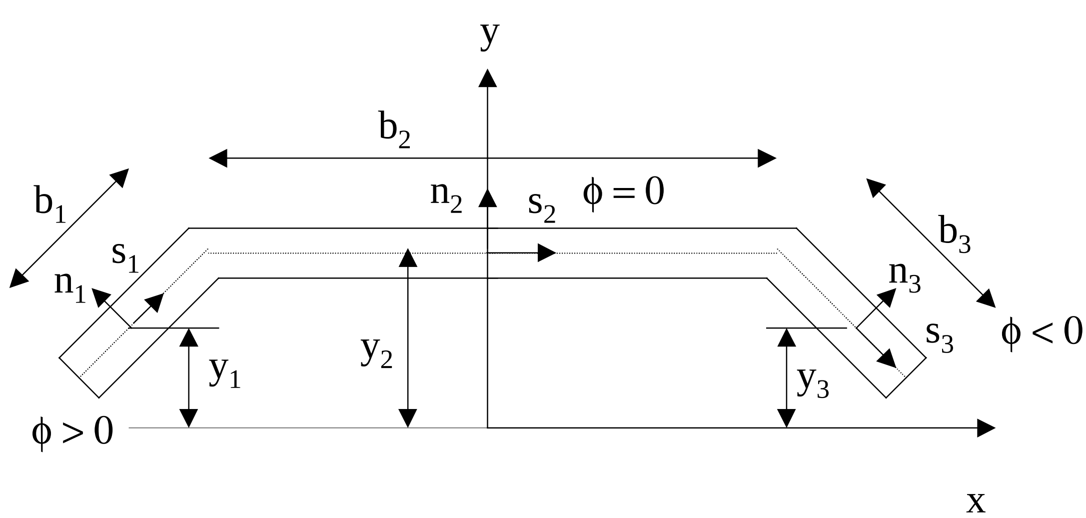

Figure 5-8. MLB beam model showing coordinate system and definition of contour. (After Davlos et al. [49]).

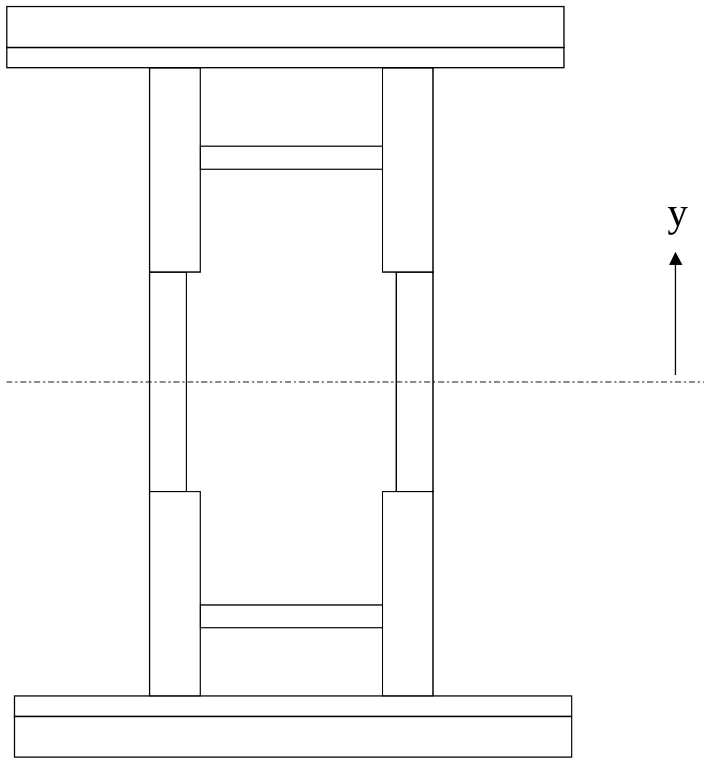

Figure 5-9. The 20.3 cm (8 in) deep composite beam modeled as a construction of laminated panels.

Table 5-1. Material Properties Utilized in CLT Analysis of Beam Laminates.

	Constituent Material		
Property	**E-glass fiber**	**AS4 carbon fiber**	**Vinyl ester resin**
E_{11}, GPa (Msi)	72.4 (10.5)	234 (34.0)	3.38 (0.490)
E_{22}, GPa (Msi)	72.4 (10.5)	22.4 (3.25)	3.38 (0.490)
G_{12}, GPa (Msi)	30.2 (4.38)	22.1 (3.20)	1.37 (0.198)
ν_{12}	0.200	0.300	0.240

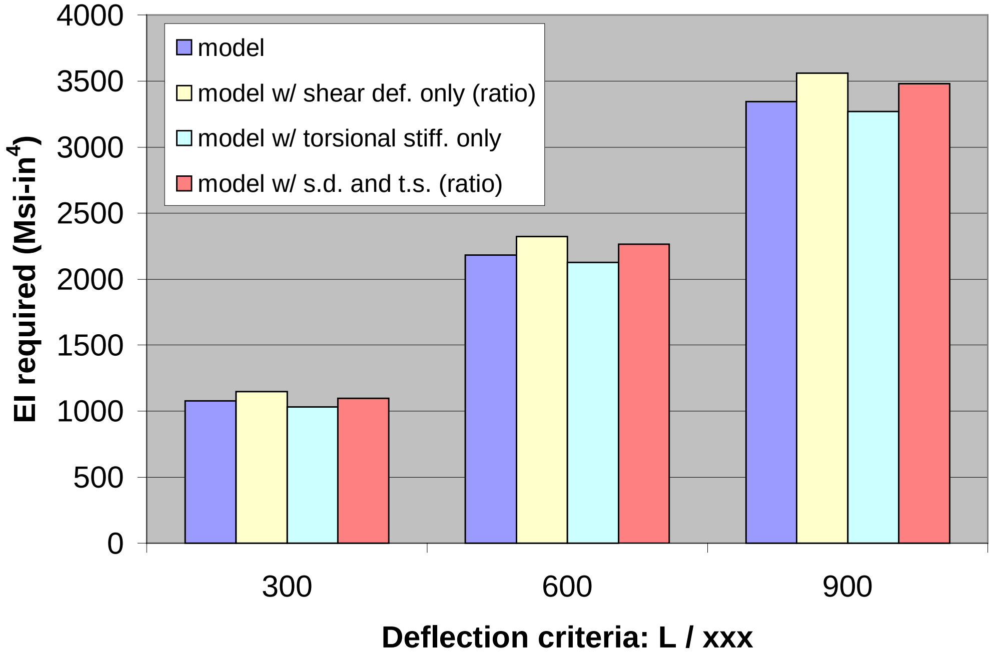

Figure 5-10. Calculated bending stiffnesss, EI, for three different deflection criteria and various model types for 24 beams, 29.2 cm spacing.

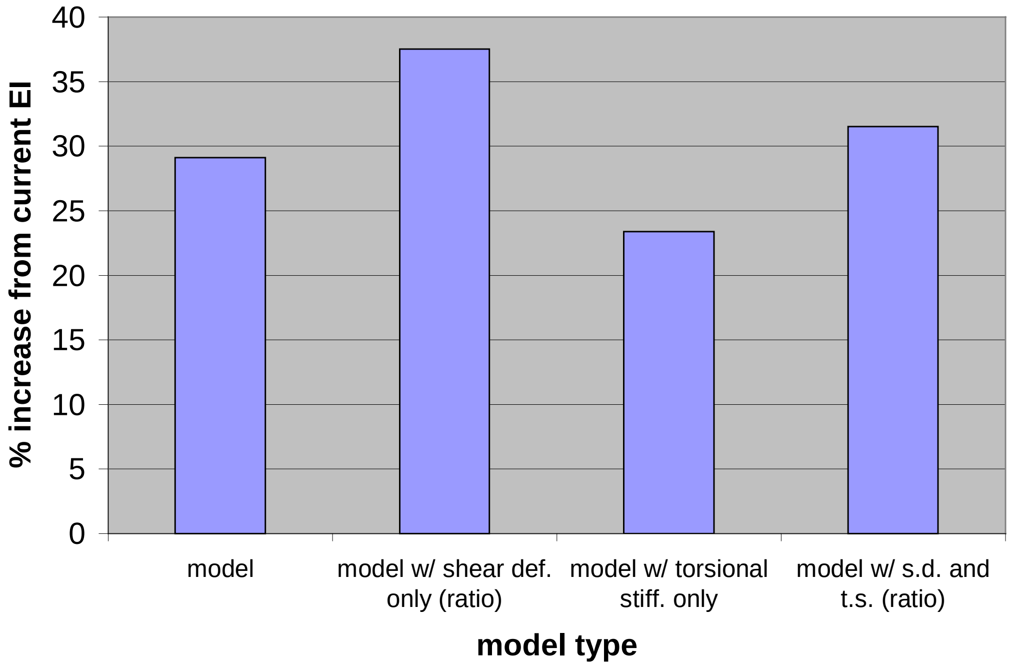

Figure 5-11. Percent increase in girder stiffness to achieve L/300 deflection, compared to current average beam stiffness for 24 beams, 29.2 cm spacing.

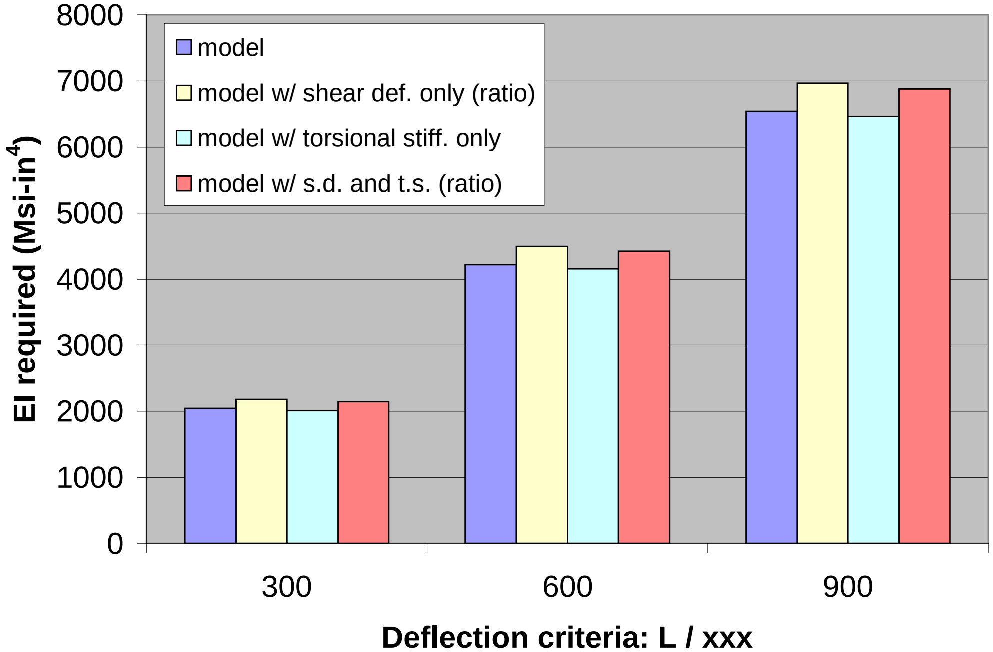

Figure 5-12. Required bending stiffnesses for 12 beams, 61.0 cm spacing.

Table 5-2. Geometric scaling factors required to meet the specified deflection-to-span criteria (shear deformation not considered).

	L/xxx		
	300	**600**	**900**
Required EI 10^3 GPa-cm^4 (Msi-in^4)	588 (2050)	1210 (4220)	1880 (6540)
Scaling factor	1.23	1.48	1.65
F_y = GA GPa-cm^2 (Msi-in^2)	426 (9.58)	609 (13.7)	761 (17.1)
EI / KGA cm^2 (in^2)	1380 (214)	1990 (308)	2460 (382)
I_{xx} 10^3 cm^4 (in^4)	12.3 (296)	25.3 (609)	39.3 (943)
Area cm^2 (in^2)	134 (20.8)	192 (29.8)	239 (37.1)
New beam depth cm (in)	25.0 (9.86)	30.1 (11.8)	33.4 (13.2)
New flange width cm (in)	18.8 (7.39)	22.5 (8.85)	25.1 (9.88)

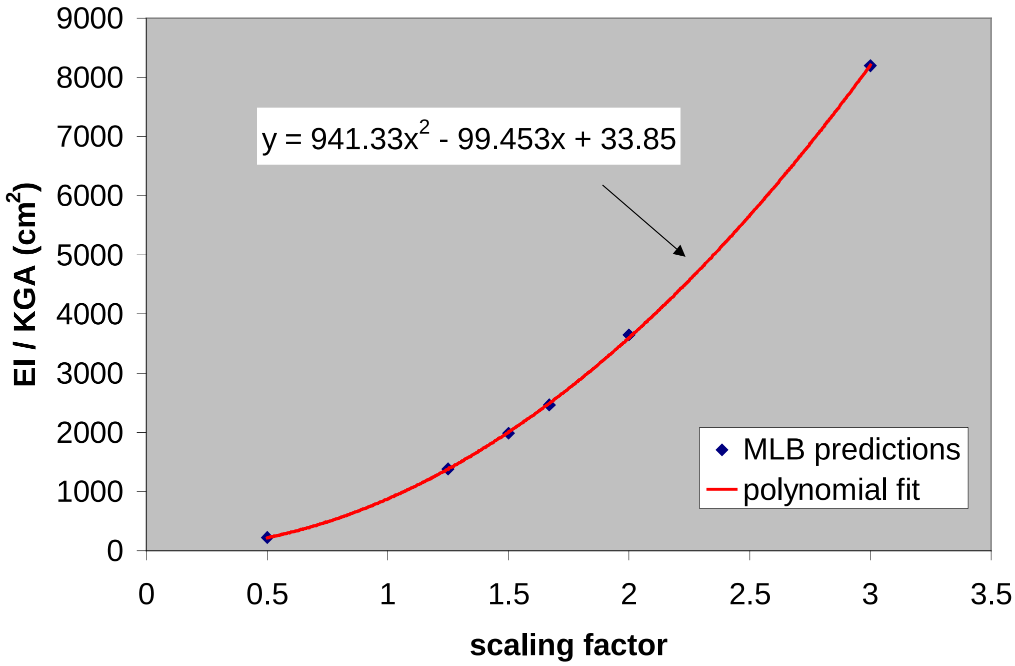

Figure 5-13. Variation in EI / KGA with geometric scaling.

Table 5-3. Geometric scaling factors required to meet the specified deflection-to-span criteria and resulting beam properties (shear deformation included).

	L/xxx 300	600	900
Scaling factor	1.25	1.50	1.69
D_y = EI 10^3 GPa-cm^4 (Msi-in^4)	620 (2160)	1310 (4560)	2070 (7200)
F_y = GA GPa-cm^2 (Msi-in^2)	437 (9.83)	635 (14.3)	796 (17.9)
EI / KGA cm^2 (in^2)	1420 (220)	2060 (319)	2590 (402)
I_{xx} 10^3 cm^4 (in^4)	13.0 (312)	27.4 (658)	43.3 (1040)
Area cm^2 (in^2)	138 (21.4)	200 (31.0)	252 (39.0)
New beam depth cm (in)	25.4 (9.98)	30.6 (12.0)	34.3 (13.5)
New flange width cm (in)	19.0 (7.49)	22.9 (9.02)	25.7 (10.1)

Chapter 6: Conclusions and Recommendations

Based on the investigations conducted within the scope of this thesis, the following conclusions and recommendations are made:

- The individual beam testing provided a measure of the manufacturing consistency, as well as specific beam properties for this particular bridge rehabilitation project. The proof testing revealed a noticeable difference in the flexural stiffness between two different batches of beams; the difference was attributed to the use of two different types of carbon fiber in the pultrusion process. The proof testing information also proved useful in assisting the Engineer of Record on the project in developing a more optimal design (given the constraints of beam properties and bridge geometry).

- The fatigue and creep tests serve as simple baseline indicators of the long-term durability of the composite beam. However, additional tests are required to determine creep deflections and stiffness reductions under fatigue for various stress levels and environmental factors before serious bridge design using these composite members can be conducted.

- The testing of the full-scale bridge mock-up in the laboratory provided valuable information to both the research group and the construction crew that was employed in the bridge rehabilitation. The lab evaluation helped resolve certain construction issues such as girder-to-deck connections and protecting the composites against wear at the abutment supports. Furthermore, the data measured during the testing provided baseline information by which to judge the bridge design and to compare later test data from the actual installed bridge.

- The deflection data from the lab testing indicates a serviceability ratio of L/195 with the impact factor (1.3) included, or L/255 without the impact factor. Data from the field testing was briefly presented, and that data indicated a response of L/450 (with impact factor). It is noted that the value of the impact factor has not yet been determined for this structure; 1.3 is derived from the traditional bridge design guidelines. Still, the bridge structure is relatively flexible compared to steel and concrete designs, and a more optimal design utilizing a different composite beam geometry or lay up would be more appropriate.

- The simple 1-D finite-difference model developed herein was shown to predict the response of the lab test structure fairly well, with a difference in maximum deflection of only 6 to 12% for the HS20 center loading. However, the predicted maximum deflection under the design case of HS20 side loading is less accurate; the difference was nearly 20%. This inability of the model to accurately predict deflections near the edges of the bridge is also evident in the center loading case, where edge deflections (away from the loads) differ by around 25%. This weakness may possibly be attributed to improper boundary conditions. Uplift of the outer composite beams changed the boundary conditions from the simple beam case (pin-roller) used in the model to a case where upward vertical displacements are possible. It may be more accurate to attempt to derive the Euler and Timoshenko equations for boundary equations that allow limited vertical displacement only in the positive *z*-direction (upward). However, relative to the response of the actual field structure, the model provides very conservative predictions.

- Although the model demonstrates only limited success, its usefulness lies in its simplicity. The computer code required to solve the 1-D problem is minimal, and the execution time small. The code is well suited for integration with other subroutines, such as the mechanics of laminated beam program utilized in this study. An additional merit of the bridge model is in exploring the influence of various parameters such as composite beam properties, girder spacing, and loading type. The author recommends that the model be used as a first approximation for design purposes. Consideration of loading away from the edges of the structure may yield more accurate predictions. A full three-dimensional finite element model may ultimately be necessary to guide serious bridge design utilizing this type of composite member.

- A first attempt at utilizing mechanics of laminated beam (MLB) theory to predict the response of the composite box I-beam was found to provide a very good estimate of the beam's flexural stiffness. The accuracy of the estimate for the shear stiffness *KGA* is still uncertain. The approach developed by the West Virginia University group may also prove useful as a simple design tool for customizing the composite section to meet different bridge designs. Further verification of this approach and the resulting shear properties is needed. Still, the MLB calculations indicate that the manufacturer should consider alternate designs (i.e. beam depth) for small, HS20 class bridges such as the Tom's Creek Bridge.

- The reader is also asked to consider a number of other factors while interpreting the results of this research: environmental effects, creep under dead load, long-term fatigue, etc. Further study of the shear and torsional properties, as well as lateral-torsional stability and local buckling, of this particular composite beam are also necessary.

- Finally, it was briefly noted the actual field structure acted much stiffer than the laboratory mock-up. The difference is likely due to the substantial rub rail/guard rail design and girder-abutment connections used in the field. The rail may act to tie the seven deck beams together and promote plate action. Although the investigation of Section 5.1.5 indicated that the addition of stiff outer beams (to simulate the rub rails) had little effect on the bridge response, those results are questionable considering the deficiency of the model in predicting deflections near the outer edges of the structure. Again, though, this deficiency may be related to the boundary conditions of the composite beams. The use of the girder-abutment connections in the field structure may increase the bending spring constant of each composite girder by enforcing "tighter" boundary conditions (i.e. clamped-clamped compared to pinned-pinned).

REFERENCES

1. "Composite Structural Shapes for Infrastructure," National Institute of Standards and Testing (NIST) Advanced Technology Program (ATP), 1994.
2. J. Mistretta, "Opening Remarks, USAF," *Presentation at the Midwestern Workshop for Fiber Reinforced Composite Infrastructure*, Hamilton, Ohio, August 27, 1997.
3. B. Brailsford, S.M. Milkovich, D.W. Prine, J.M. Fildes, "Definition of Infrastructure Specific Markets for Composite Materials: Topical Report," Northwestern University BIRL Project P93-121/A573, July 11, 1995.
4. A.H. Zureick, B. Shih, E. Munley, "Fiber-Reinforced Polymeric Bridge Decks," *Structural Engineering Review*, v7 n3 (Aug 1995), 257-266.
5. M. El-Mikawi and A.S. Mosallam, "A methodology for evaluation of the use of advanced composites in structural civil engineering applications," *Composites: Part B*, v27B (1996) 203-215.
6. Sotiropoulos, GangaRao, and Barbero, "Static Response of Bridge Superstructures Made of Fiber Reinforced Plastic," *Use of Composite Materials in Transportation Systems American Society of Mechanical Engineers, Applied Mechanics Division*, AMD, ASME: New York, NY, v129, 57-65.
7. R. Lopez-Anido and H.V.S. GangaRao, "Design and Construction of Composite Material Bridges," US-Canada-Europe Workshop on Bridge Engineering, Zurich, Switzerland, July 14-15, 1997, 1-8.
8. M.W. Hargrave, E. Munley, and T.J. Pasko, "FHWA's applied highway infrastructure research program on composite materials," *Public Roads*, v60 n4 (Spring 1997), 23 (9).
9. C.A. Ballinger, "Advanced Composites in the Construction Industry," *Materials Working for You in the 21st Century, International SAMPE Symposium and Exhibition*, SAMPE: Covina, CA., v37 (1992) 1-14.
10. L.H. Sperling, Introduction to Physical Polymer Science, 2nd edition, John Wiley and Sons: New York, 1992, 478-480.
11. Y. Weitsman, "Moisture in Composites: Sorption and Damage," Fatigue of Composite Materials, ed. K.L. Reifsnider, Elsevier Science Publishers: NY, NY, 1990, 385-427.
12. I. Ghorbel and D. Valentin, "Hydrothermal Effects on the Physico-Chemical Properties of Pure and Glass Fiber Reinforced Polyester and Vinylester Resins," *Polymer Composites*, v14 n4 (1993) 324-334.
13. C.L. Schutte, "Environmental durability of glass-fiber composites," *Materials Science and Engineering: Reports*, v13 n7 (Nov 15 1994) 265-324.
14. A. Chateauminois, L. Vincent, B. Chabert, and J.P. Soulier, "Study of the interfacial degradation of a glass-epoxy composite during hygrothermal ageing using water diffusion measurements and dynamic mechanical thermal analysis," *Polymer*, v35 n22 (1994) 4766-4774.
15. L.C. Bank, T.R. Gentry, and A. Barkatt, "Accelerated Test Methods to Determine the Long-Term Behavior of FRP Composites," *J. Reinforced Plastics and Composites*, v14 (1995) 559-587.

16. J. Gomez and B. Casto, “Freeze-Thaw Durability of Composite Materials,” *Fiber Composites in Infrastructure*, Proceedings of the First International Conference on Composites in Infrastructure 1996, ed. H. Saadatmanesh and M.R. Ehsani, 947-955.
17. P.K. Dutta and D. Hui, “Low-temperature and freeze-thaw durability of thick composites,” *Composites Part B: Engineering*, v27 n3-4 (1996) 371-379.
18. J.B. Kosmatka, F. Policelli, B. Hornbeck, and K. Bernetich, “An Overview of the Development of the ARPA/BIR Composite Assault Bridge,” *Technology Transfer in a Global Community*, International SAMPE Technical Conference, v28 (1996) 1228-1239.
19. K. Bernetich, D. Briggs, and S. Vickocil, “SCRIMP® Fabrication of Bridge Decks,” *Technology Transfer in a Global Community*, International SAMPE Technical Conference, v28 (1996) 1240-1248.
20. G. Mandigo, "Two Federal Agencies Experiment with Composite Bridges: Case Studies on the Acceptance of Composite Materials," *Proceedings of the 1997 International Composites Expo*, Nashville, Tennessee, (January 27-29, 1997) Section 3-A, 1-7.
21. "Lasalle Street Composite Bridge," Northwestern University Infrastructure Technology Institute web site: http://iti.acns.nwu.edu/composites/lasalle.html .
22. "Composite Materials Featured in Chicago's LaSalle Street Bridge," *BIRLprogress*, v6 n1 (Spring 1996), p. 1.
23. K. Liao, R.I. Altkorn, S.M. Milkovich, J. Gomez, C.R. Schultheisz, L.C. Brinson, J.M. Fildes, and B. Brailsford, “Long-Term Durability of Composites in Secondary Infrastructure Applications,” *Technology Transfer in a Global Community*, International SAMPE Technical Conference, v28 (1996) 1278-1289.
24. "Antioch Composite Pedestrian Bridge," Northwestern University Infrastructure Technology Institute web site: http://iti.acns.nwu.edu/composites/antioch.html.
25. G.E. Johansen, R.J. Wilson, F. Roll, and G.Gaudini, “Design and Construction of Long Span FRP Pedestrian Bridges,” *Building to Last Structures Congress Proceeding*, ASCE: New York, NY, v1 (1997) 46-50.
26. I.E. Harik, P.J. Szak, B.N. Robson, T.H. Hopwood, D. Witcher, and B. Brailsford, “Hybrid Composite I-Girder Pedestrian Bridge,” *Technology Transfer in a Global Community International SAMPE Technical Conference*, SAMPE: Covina, CA v28 (November 4-7, 1996) 1270-1277.
27. P. Rosta, “Plastics Becoming Heavy Players in Lightweight Span Construction,” *ENR*, (July 1, 1996) 32-33.
28. F. Seible and R. Burgueno, “Advanced Composites in Pedestrian Bridge Design,” *Building to Last Structures Congress Proceedings*, ASCE: New York, NY, v1 (1997) 378-382.
29. F. Seible, “US Perspective of Advanced Composite Bridge Technology in Europe and Japan,” *Proceedings of the Second International Conference on Composites in Infrastructure*, v1, (January 5-7, 1998) 645-650.
30. R. Lopez-Anido, H.V.S. Gangarao, J. Trovillion, and J. Busel, "Development and Demonstration of a Modular FRP Deck for Bridge Construction and Replacement," *Proceedings of the 1997 International Composites Expo*, Nashville, Tennessee, (January 27-29, 1997) Section 16-D, 1-6.

31. D. Richards, “Lockheed Corporation – Bridge Design,” Presentation at the Midwestern Workshop for Fiber Reinforced Composite Infrastructure, Hamilton, Ohio, August 27, 1997.
32. "Composite Bridge Demonstration Project," Idaho National Engineering and Environmental Laboratory (INEEL) web site: http://www.inel.gov/capabilities/transportation/bridge1.html.
33. D. Richards, C. Dumlao, M. Henderson, and D. Foster, “Methods of Installation and the Structural Analysis of Two Short Span Composite Highway Bridges,” *Proceedings of 1998International Composite Expo*, Nashville, TN, (January 19-21, 1998) Session 4-E, 1-6.
34. D. Foster, “Butler County Bridge Installation,” Presentation at the Midwestern Workshop for Fiber Reinforced Composite Infrastructure, Hamilton, Ohio, August 27, 1997.
35. M. Chajes, J. Gillespie, D. Mertz, and H. Shenton, “Advanced Composite Bridges in Deleware,” *Proceedings of the Second International Conference on Composites in Infrastructure*, Tuscon, Arizona, v1 (January 5-7, 1998) 645-650.
36. R. Lopez-Anido, H.V.S. Gangarao, V. Vedam, and N. Overby, "Design and Evaluation of a Modular FRP Bridge Deck," *Proceedings of the 1997 International Composites Expo*, Nashville, Tennessee, (January 27-29, 1997) Section 3-E, 1-6.
37. R. Lopez-Anido, p.A. Howdyshell, L.D. Stephenson, and H.V.S. GangaRao, “Fatigue and Failure Evaluation of Modular FRP Composite Bridge Deck,” *Proceedings of the 1998 International Composites Expo*, Nashville, Tennessee, (January 19-21, 1998) Session 4-B, 1-6.
38. V.M. Karbhari, F. Seible, G.A. Hegemier, and L. Zhao, “Fiber Reinforced Composite Decks for Infrastructure Renewal – Results and Issues,” *Proceedings of the 1997 International Composites Expo*, Nashville, Tennessee, (January 27-29, 1997) Section 3-C, 1-6.
39. M.D. Hayes, J.J. Lesko, T. Cousins, and D. Ohanehi, "Static and Fatigue Performance of a Square Tube and Plate Type Fiberglass Composite Bridge Deck System,” *Proceedings of the 1998 International Composites Expo*, Nashville, Tennessee, (January 19-21, 1998) Session 7, 1-7.
40. L.C. Bank, “Shear Coefficients for Thin-Walled Composite Beams,” *Composite Structures*, v8 (1987) 47-61.
41. L.C. Bank, T.R. Gentry, and M. Nadipelli, “Careful design can optimize performance of pultruded beams” *Modern Plastics* (September 1994) 105-107.
42. E.J. Barbero, R. Lopez-Anido, and J.F. Davalos, “On the Mechanics of Thin-Walled Laminated Composite Beams,” *Journal of Composite Materials*, v27 n8 (1993), 806-829.
43. S. Ohseop, “Modeling and Response Analysis of Thin-Walled Beam Structures Constructed of Advanced Composite Materials,” *Ph.D. Dissertation*, Virginia Polytechnic Institute and State University, 1990, 1-6.
44. M.D. Gilchrist, A.J. Kinloch, F.L. Matthews, and S.O. Osiyemi, “Mechanical Performance of Carbon-Fibre- and Glass-Fibre-Reinforced Epoxy I-Beams: I. Mechanical Behaviour,” *Composite Science and Technology*, v56 n1 (1996) 37-53.
45. Barbero, Fu, and Raftoyiannis, “Ultimate Bending Strength of Composite Beams,” *Journal of Materials in Civil Engineering*, v3 n4 (November 1991) 292-306.

46. G.D. Sims, A.F. Johnson, and R.D. Hill, "Mechanical and Structural Properties of a GRP Pultruded Section," *Composite Structures*, v8 (1987) 173-187.
47. E. Cosenza, F. Lazzaro, M. Peece, "Experimental Evaluation of Bending and Torsional Deformability of FRP Pultruded Beams," *Advanced Composite Materials in Bridges and Structures*, Montreal, Quebec, (1996) 117-124.
48. L.C. Bank, "Flexural and Shear Moduli of Full-Section Fiber Reinforced Plastic (FRP) Pultruded Beams," *Journal of Testing and Evaluation*, v17 n1 (1989), 40-45.
49. J.F. Davalos, H.A. Salim, P. Qiao, R. Lopez-Anido, and E.J. Barbero, "Analysis and Design of Pultruded FRP Shapes Under Bending," *Composites Part B: Engineering*, v27 n3-4 (1996) 295-305.
50. J.T. Mottram, "Evaluation of design analysis for pultruded fiber-reinforced polymeric box beams," *Structural Enigineering*, v69 n11 (June 4 1991) 211-220.
51. J.T. Mottram, "Lateral-torsional buckling of a pultruded I-beam," *Composites*, v23 n2 (1992), 81-92.
52. E.J. Barbero and I.G. Raftoyiannis, "Lateral and Distortional Buckling of Pultruded I-Beams," *Composite Structures*, v27 (1994), 261-268.
53. M.D. Pandey, M.Z. Kabir, and A.N. Sherbourne, "Flexural-Torsional Stability of Thin-Walled Composite I-Section Beams," *Composites Engineering*, v5 n3 (1995), 321-342.
54. Z. Razzaq, R. Prabhakaran, and M.M. Sirjani, "Load and resistance factor design (LRFD) approach for reinforced-plastic channel beam buckling," *Composites Part B: Engineering*, v27 n3-4 (1996) 361-369
55. F.C. McCormick, "Laboratory Fatigue Investigation of a GRP Bridge," *Serviceability and Durability of Construction Materials, Proceedings of the First Materials Engineering Congress,* ASCE: Boston, MA (1990) 996-1005.
56. L.C. Bank and A.S. Mosallam, "Creep and Failure of a Full-Size Fiber Reinforced Plastic Pultruded Frame," *American Society of Mechanical Engineers, Petroleum Division (Publication) PD*, ASME: New York, NY, v32 (1990) 49-56.
57. <u>ASCE Structural Plastics Design Manual</u>, ASCE Manual of Engineering Practice No. 63, American Society of Civil Engineers, NY, 1984.
58. S.V. Hoa, "Creep of a Composite Box Beam with Design Implications," *Journal of Reinforced Plastics and Composites*, v14 (February 1995), 128-142.
59. J.T. Mottram, "Short- and long-term stuctural properties of pultruded beam assemblies fabricated using adhesive bonding," *Composite Structures*, v25 n1-4 (1993) 387-395.
60. "Proposed Bridge on Tom's Creek Road Over Tom's Creek Bridge, Town of Blacksburg," Tom's Creek Bridge design plans, Commonwealth of Virginia Department of Transportation, May 8, 1997.
61. Meeting with Dan Witcher and Glen Barefoot, Strongwell Inc., at Virginia Tech, August 21, 1997.
62. B. Moser, M. Hyer, and J.J. Lesko, "Computer Modeling of the Mechanical Response of Composite Structural Beams in the Tom's Creek Bridge," Research Report submitted to the *National Science Foundation Science and Technology Center for High Performance Polymeric Adhesives and Composites*, Virginia Tech, Summer 1996.

63. J. Lesko, M. Hayes, J. Haramis, J. Hou, T. Cousins, J. Gomez, and P. Massarelli, "Laboratory and Field Characterization of the Tom's Creek Bridge Composite Superstructure," *Proceedings of the Second International Conference on Composites in Infrastructure*, Tuscon, Arizona, v1 (January 5-7, 1998) 634-644.
64. J.N. Howard, "Investigation of the Structural Behavior of Asphalt/Wood Deck Systems for Girder Bridges," *M.S. Thesis*, Virginia Polytechnic Institute and State University, 1997.
65. F.P. Beer and E.R. Johnston, <u>Mechanics of Materials</u>, 2nd edition, McGraw-Hill, Inc: New York, 1992.
66. <u>MMFG EXTREN® Design Manual</u>, Morrison Molded Fiber Glass Company, Bristol, VA, 1989.
67. C.L. Dym and I.H. Shames, <u>Solid Mechanics: A Variational Approach</u>, McGraw-Hill, Inc.: New York, 1973.
68. G.R. Cowper, "The Shear Coefficient in Timoshenko's Beam Theory," *Journal of Applied Mechanics*, June 1966, 335-340.
69. A.P. Boresi, R.J. Schmidt, and O.M. Sidebottom, <u>Advanced Mechanics of Materials</u>, 5th edition, John Wiley and Sons: New York, 1993.
70. Personal correspondence with Dan Witcher, Strongwell Inc, July 1997.

Appendices

Appendix A: Weibull Statistics Calculations

- Mean:

$$\mu = \beta \cdot \Gamma\left(\frac{\alpha+1}{\alpha}\right) \quad \text{(A1)}$$

  where Γ is the gamma function.

- Standard deviation:

$$\sigma = \beta^2 \cdot \left[\Gamma\left(\frac{\alpha+2}{\alpha}\right) - \Gamma^2\left(\frac{\alpha+1}{\alpha}\right)\right]^{1/2} \quad \text{(A2)}$$

- A allowable:

$$\tilde{\beta}_{lower}\left[\ln\left(\frac{1}{0.99}\right)\right]^{1/\alpha} \quad \text{(A3)}$$

- B allowable:

$$\tilde{\beta}_{upper}\left[\ln\left(\frac{1}{0.90}\right)\right]^{1/\alpha} \quad \text{(A4)}$$

  where $$\tilde{\beta}_{lower} = \beta\left[\frac{2n}{\mathrm{X}^2{}_{0.05}}\right]^{1/\alpha},\ \tilde{\beta}_{upper} = \beta\left[\frac{2n}{\mathrm{X}^2{}_{0.95}}\right]^{1/\alpha} \quad \text{(A5)}$$

- Weibull density function: $f(x) = \frac{\alpha}{\beta}\left(\frac{x}{\beta}\right)^{\alpha-1} \exp\left[-\left(\frac{x}{\beta}\right)^{\alpha}\right]$ (A6)
- Weibull cumulative distribution: $F(x) = \int_0^\infty f(x)dx = 1 - \exp\left[-\left(\frac{x}{\beta}\right)\right]^{\alpha}$ (A7)
- reliability: $R = \exp\left[1 - \left(\frac{x}{\tilde{\beta}}\right)^{\alpha}\right]$

  where x is the allowable design value (A8)

Vita

Michael D. Hayes was born in Nashville, Tennessee on October 26, 1972 to Jimmy and Sharon Hayes. He grew up in the small town of Farragut outside of Knoxville, Tennessee. Michael graduated from Farragut High School as a valedictorian in 1991, and then enrolled in Virginia Tech. While at Tech, he studied Engineering Science and Mechanics and as a senior, Michael worked in the area of biomaterials, characterizing and testing polymers for orthopedic applications. After completing his B.S. in 1995, Michael continued his education in Engineering Mechanics, working on various aspects of fiber-reinforced composite materials research. Upon completion of this Master's degree December 1997, Michael plans to find employment in industry.